Doctoral Dissertation

Development of Cell Scaffolds Capable of Controlled Oxygen Release by Surface Modification of Calcium Peroxide

(過酸化カルシウムの表面修飾により酸素徐放を制御可能な細胞足場材料の創製)

DAISUKE TOMIOKA

January 2025

Department of Applied Chemistry

Graduate School of Engineering

Osaka University

Content

General Introduction

In 1993, Langer and Vacanti advocated “Tissue engineering” for the construction of three-dimensional (3D) engineering tissues *in vitro* using three essential factors: cells, scaffolds and signaling molecules.[1] Based on tissue engineering, regenerative medicine has attracted much attention as a new medical technique for recovering tissue function by transplanting cells and tissues to the disease sites. Treatments using cell suspensions and two-dimensional cell sheets are currently in practical use.[2] To utilize 3D tissues for regenerative medicine, researchers have been working to construct 3D tissues using a broad range of materials, cells and techniques in tissue engineering field. However, *in vitro* construction of thick 3D tissues (>200 μm) with high cell density is still a major challenge because limited diffusion of oxygen inside these tissues causes cell death (**Figure 1a**).[3-5] For example, oxygen consumption in monolayers of adult rat hepatocytes cultured at confluence is 40-90 pmol s^{-1} cm^{-2}, while oxygen diffusion from cell culture medium is only 17 pmol s^{-1} cm^{-2}.[6] As a result, oxygen shortage causes cell death in 3D tissues thicker than around 200 μm. In addition, before the angiogenesis to the transplanted tissues, insufficient oxygen supply results in cell death, preventing efficient tissue regeneration *in vivo*.[7] Solving these oxygen shortage problems are therefore considered important for the development of regenerative medicine and tissue engineering.

To address the problem of cell death due to oxygen shortage, oxygen releasing materials have attracted much attention in recent years.[5,8,9] Heme proteins such as hemoglobin[10,11] and myoglobin[12,13] are some of the most common oxygen sources for these materials because they supply oxygen in our body. However, low payload of oxygen and protein stability are challenges, which prevent sustained oxygen supply.[5] Although perfluorocarbons (PFC) have also attracted much attention as an artificial oxygen carrier because of their high oxygen solubility, low payload of oxygen and short duration of oxygen release are also challenges.[5,14] To overcome these limitations, calcium peroxide (CaO_2) is often used for oxygen releasing materials because CaO_2 can theoretically achieve a higher oxygen payload compared to heme proteins and PFC.[5] CaO_2 is an inorganic solid and it generates oxygen, hydrogen peroxide and calcium hydroxide by the reaction with water.[15-17] Therefore, many researchers reported oxygen releasing hydrogels by mixing CaO_2 into the hydrogels.[18-20] However, the initial burst release of oxygen from CaO_2 is a major issue because of the uncontrollability of oxygen release after immersion in water, which prevent sustained oxygen supply from materials (**Figure 1b**).

Recently, hydrophobic synthetic polymers such as polydimethylsiloxane,[21,22] poly(lactide-co-glycolide)[23] and polycaprolactone[24,25] have been used for the sustained oxygen release from CaO_2 by suppressing the reaction with water. Although sustained oxygen release of around two weeks was achieved in these reports, CaO_2 is simply mixed in the polymer materials and thus the distribution of CaO_2 particles is totally random. As a result, some of the CaO_2 particles are exposed at the surface of the polymer materials. Since direct contact between CaO_2 and cells may cause cell death due to toxic byproducts, these hydrophobic oxygen releasing materials were incorporated in hydrogels together with cells for tissue engineering applications. However, obtained tissues are far from real tissue in our body since most part of constructs are hydrogels, not cells.[24,25] Therefore, even with oxygen releasing materials, the construction of thick living 3D tissue with high cell density is still challenging.

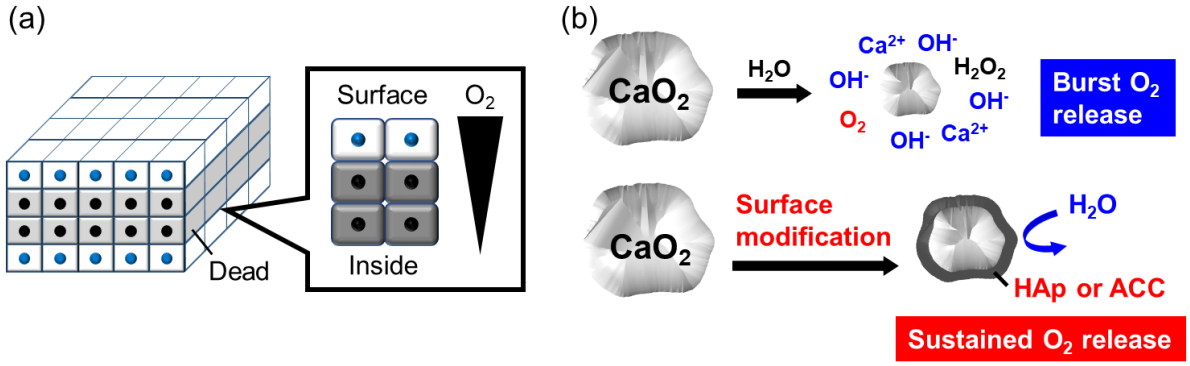

Figure 1. Schematic illustration of (a) the oxygen shortage in 3D tissues and (b) the burst release of oxygen from CaO_2 and sustained oxygen release from surface modified CaO_2.

Outline of this thesis

In this thesis, the author introduces the surface modification of CaO_2 as a new strategy for the controlled release of oxygen from CaO_2 (**Figure 1b**). In addition, oxygen releasing materials were fabricated using surface modified CaO_2 for the cell culture and construction of thick living 3D tissue with high cell density.

Chapter 1

Surface Modification of Calcium Peroxide by Hydroxyapatite for Sustained Oxygen Release

In Chapter 1, sustained oxygen release from CaO_2 was achieved by suppressing the reaction with water through the formation of hydroxyapatite (HAp) on the surface (HAp-CaO_2).

This coating can be applied by simple immersion of CaO_2 in phosphate buffer (PB) solution. Since HAp is a main component of teeth and bone, this biocompatible surface modification will be preferable for tissue engineering application.[26] For general tissue engineering application, oxygen releasable gelatin hydrogels were fabricated using HAp-CaO_2 as an oxygen source. Catalase has also been incorporated in oxygen releasable gelatin hydrogels because it is an enzyme that decomposes toxic hydrogen peroxide into oxygen and water.[27] The effects of sustained oxygen supply from the hydrogels to cells and 3D tissues were investigated. Since HAp-CaO_2 can be incorporated in a broad range of biomaterials, HAp-CaO_2 is expected to provide sustained oxygen releasing properties to existing and yet-to-be-developed biomaterials.

Chapter 2

Controlled Release of Oxygen from Calcium Peroxide in a Weak Acidic Condition by Stabilized Amorphous Calcium Carbonate Coating

In Chapter 2, stabilized amorphous calcium carbonate (ACC) coating on CaO_2 (ACC-CaO_2) was performed using sodium hydrogen carbonate ($NaHCO_3$) solution including phosphate ions for pH dependent oxygen release. Oxygen release from ACC-CaO_2 was suppressed in a neutral cell culture medium because ACC formation on CaO_2 acts as a diffusion barrier to water. On the other hand, since ACC dissolves in weak acidic aqueous solutions, pH-dependent oxygen release bahavior of ACC-CaO_2 was evaluated in a cell culture medium.[28] It is reported that the environments in ischemic tissues and cancer are weakly acidic.[29,30] Therefore, selective oxygen release from ACC-CaO_2 at these environments are highly expected.

Chapter 3

Construction of Thick Living 3D Tissue with High Cell Density Using Oxygen Releasing Micro-Cell Scaffold

In Chapter 3, oxygen releasing micro-cell scaffold was fabricated by Layer-by-Layer (LbL) nanofilm assembly on HAp-CaO_2 (LbL-HAp-CaO_2) for the construction of 3D tissues. LbL nanofilm was fabricated by electostatic intercations between anionic catalase and cationic poly-L-lysine (PLL). Since catalase in LbL nanofilm decomposes toxic hydrogen peroxide into oxygen, hydrogen peroxide release from LbL-HAp-CaO_2 was suppressed in this system. On the other hand, PLL improves cell adhesion on LbL-HAp-CaO_2 because of the absorption of the cell adhesion proteins. Thick living 3D tissue with high cell density was constructed using LbL-HAp-CaO_2 since oxygen supply suppressed cell apoptosis due to oxygen shortage. LbL-HAp-CaO_2 would be a strong tool for the alleviation of hypoxia in 3D tissues, which will enable

the construction of a broad range of 3D tissues.

Chapter 4

Microfluidic Synthesis of Oxygen Releasing Microgels

In Chapter 4, oxygen-releasing microgels were fabricated via a droplet-based microfluidic system. Homogeneous, monodisperse and stable oxygen-releasing microgels were obtained by photo-crosslinking of droplets composed of biocompatible dextran modified with methacrylate groups and CaO_2 nanoparticles as an oxygen source. This microfluidic system was also applied for the in situ ACC formation on CaO_2 nanoparticles to achieve the controlled release of oxygen from the microgel depending on pH changes. By taking advantage of oxygen-releasing materials and microgels, fabricated oxygen-releasing microgels are expected to be a very useful biomaterial for tissue engineering applications.

References

[1] R. Langer, J. P. Vacanti, *Science* **1993**, *260*, 920.

[2] J. Kobayashi, A. Kikuchi, T. Aoyagi, T. Okano, *J. Biomed. Mater. Res. Part A* **2019**, *107*, 955.

[3] M. Radisic, J. Malda, E. Epping, W. Geng, R. Langer, G. V. Novakovic, *Biotechnol. Bioeng.* **2006**, *93*, 332.

[4] A. I. Neto, C. R. Correia, M. B. Oliveira, M. I. R. Hermida, C. A. Lorenzo, R. L. Reis, J. F. Mano, *Biomater. Sci.* **2015**, *3*, 581.

[5] N. G. A. Willemen, S. Hassan, M. Gurian, J. Li, I. E. Allijn, S. R. Shin, J. Leijten, *Trends Biotechnol*. **2021**, *39*, 1144.

[6] Y. Sakai, M. Nishikawa, F. Evenou, M. Hamon, H. Huang, K. P. Montagne, N. Kojima, T. Fujii, T. Niino, *Methods Mol. Biol.* **2012**, *826*, 189.

[7] T. Shimizu, H. Sekine, J. Yang, Y. Isoi, M. Yamato, A. Kikuchi, E. Kobayashi, T. Okano, *FASEB.J.* **2006**, *6*, 708.

[8] A. L. Farris, A. N. Rindone, W. L. Grayson, *J. Mater. Chem. B* **2016**, *4*, 3442.

[9] T. Agarwal, S. Kazemi, M. Costantini, F. Perfeito, C. R. Correia, V. Gaspa, L. Montazeri, C. D. Maria, J. F. Mano, M. Vosough, P. Makvandi, T. K. Maiti, *Mater. Sci. Eng. C* **2021**, *122*, 111896.

[10] A. Paciello, G. Amalfitano, A. Garziano, F. Urciuolo, P. A. Netti, *Adv. Healthcare Mater.* **2016***, 5,* 2655.

[11] S. Ohta, K. Hashimoto, X. Fu, M. Kamihira, Y. Sakai, T. Ito, *J. Biosci. Bioeng.* **2018**, *126*, 533.

[12] D. Tomioka, H. Nakatsuji, S. Miyagawa, Y. Sawa, M. Matsusaki, *Chem. Commun.* **2021**, *57*, 5131.

[13] A. Kishimura, A. Koide, K.Osada, Y. Yamasaki, K. Kataoka, *Angew. Chem. Int. Ed*. **2007**, *46*, 6085.

[14] H. Y. Lee, H. W. Kim, J. H. Lee, S. H. Oh, *Biomaterials* **2015***, 53,* 583.

[15] Y. Ma, B. T. Zhang, L. Zhao, G. Guo, J. M. Lin, *Luminescence* **2007**, *22*, 575.

[16] A. Northup, D. Cassidy, *J. Hazard. Mater.* **2008**, *152*, 1164.

[17] H. Wang, Y. Zhao, T. Li, Z. Chen, Y. Wang, C. Qin, *Chem. Eng. J.* **2016**, *303*, 450.

[18] S. Park, K. Min Park, *Biomaterials* **2018***, 182,* 234.

[19] B. Newland, M. Baeger, D. Eigel, H. Newland, C. Werner, *ACS Biomater. Sci. Eng.* **2017***, 3,* 787.

[20] N. Alemdar, J. Leijten, G. C. Unal, J. Hjortnaes, J. Ribas, A. Paul, P. Mostafalu, A. K. Gaharwar, Y. Qiu, S. Sonkusale, R. Liao, A. Khademhosseini, *ACS Biomater. Sci. Eng.* **2017**, *3*, 1964.

[21] E. Pedraza, M. M. Coronel, C. A. Fraker, C. Ricordi, C. L. Stabler, *Proc. Natl. Acad. Sci. U. S. A.* **2012***, 109,* 4245.

[22] J. P. Liang, R. P. Accolla, M. Soundirarajan, A. Emerson, M. M. Coronel, C. L. Stabler, *Acta. Biomater.* **2021***, 130,* 268.

[23] L. Daneshmandi, C. T. Laurencin, *J. Biomed. Mater. Res. Part A* **2020***, 108,* 1045.

[24] A. Farzin, S. Hassan, L. S. M. Teixeira, M. Gurian, J. F. Crispim, V. Manhas, A. Carlier, H. Bae, L. Geris, I. Noshadi, S. R. Shin, J. Leijten, *Adv. Funct. Mater.* **2021***, 31*, 2100850.

[25] N. G. A. Willemen, S. Hassan, M. Gurian, M. F. J. Salazar, K. Fan, H. Wang, M. Becker, I. E. Allijn, A. B. Öztürk, J. Leijten, S. R. Shin, *Adv. Healthcare Mater.* **2022**, *11*, 2102697.
[26] S. Bhat, U. T. Uthappa, T. Altalhi, H. Y. Jung, M. D. Kurkuri, *ACS Biomater. Sci. Eng.* **2022**, *8*, 4039.
[27] M. A. Prieto, X. Biarnés, P. Vidossich, C. Rovira, *J. Am. Chem. Soc.* **2009**, *131*, 11751.
[28] M. Wang, B. Zhou, L. Wang, F. Zhou, N. Smith, D. Saunders, R. A. Towner, J. Song, J. Qu, W. R. Chen, *J. Mater. Chem. B* **2020**, *8*, 8261.
[29] G. X. Yan, A. G. Kléber, *Circ. Res.* **1992**, *71*, 460.
[30] I. F. Tannock, D. Rotin, *Cancer Res.* **1989**, *49*, 4373.

Chapter 1

Surface Modification of Calcium Peroxide by Hydroxyapatite for Sustained Oxygen Release

1.1 Introduction

In the tissue engineering field, cell death due to an oxygen shortage is still a major challenge for the construction and transplantation of 3D tissues.[1,2] To address this problem, oxygen releasing materials have attracted much attention in recent years.[3] Although calcium peroxide (CaO_2) is one of the most common oxygen sources for these types of materials, limitations have also been reported concerning the burst release of oxygen after immersion in water.[4]

As a new strategy for the sustained oxygen release from CaO_2, the surface modification of CaO_2 itself was considered in this chapter. Herein, the author has achieved sustained oxygen release from CaO_2 by suppressing the reaction with water through the formation of hydroxyapatite (HAp) on the surface using a phosphate buffer (PB) (**Figure 1-1a**). It is known that the reaction between calcium hydroxide and phosphoric acid yields HAp which has poor solubility.[5,6] Thus, calcium hydroxide produced by CaO_2 reaction is expected to react with phosphoric acid in PB to form HAp on the surface of CaO_2. Since HAp is a main component of teeth and bone, this biocompatible surface modification will be preferable for tissue engineering application especially for hard tissues.[7] Furthermore, the HAp coating method consists of simply immersing CaO_2 in the PB, indicating its applicability to existing and yet to be developed oxygen releasing materials.

For general tissue engineering application beyond hard tissue, oxygen releasable gelatin hydrogels enzymatically crosslinked by transglutaminase (TG) were fabricated using catalase and CaO_2 coated with HAp (HAp-CaO_2). TG is an enzyme that crosslinks the carboxamide groups of glutamine residue side chains with the primary amine of lysine residue side chains.[8] It is reported that TG-crosslinked gelatin hydrogels show excellent biocompatibility and they have been applied to scaffolds for 3D cell culture,[9] 3D bioprinting[10] and microsphere fabrication.[11] In addition, catalase has been incorporated in oxygen releasable gelatin

hydrogels because it is an enzyme that decomposes hydrogen peroxide into oxygen and water.[12] Therefore, the suppression of cytotoxicity derived from hydrogen peroxide which is the byproduct of CaO_2 reaction is expected. The author's results demonstrated that the sustained oxygen release from hydrogels including HAp-CaO_2 improved cell proliferation of various cell types under a hypoxic condition (**Figure 1-1b**). The developed oxygen releasing hydrogels including HAp-CaO_2 therefore show great potential for solving the oxygen shortage problem in regenerative medicine and tissue engineering fields. In addition, HAp-CaO_2 is expected to be applied for a broad range of biomaterials as a new oxygen source capable of sustained oxygen release.

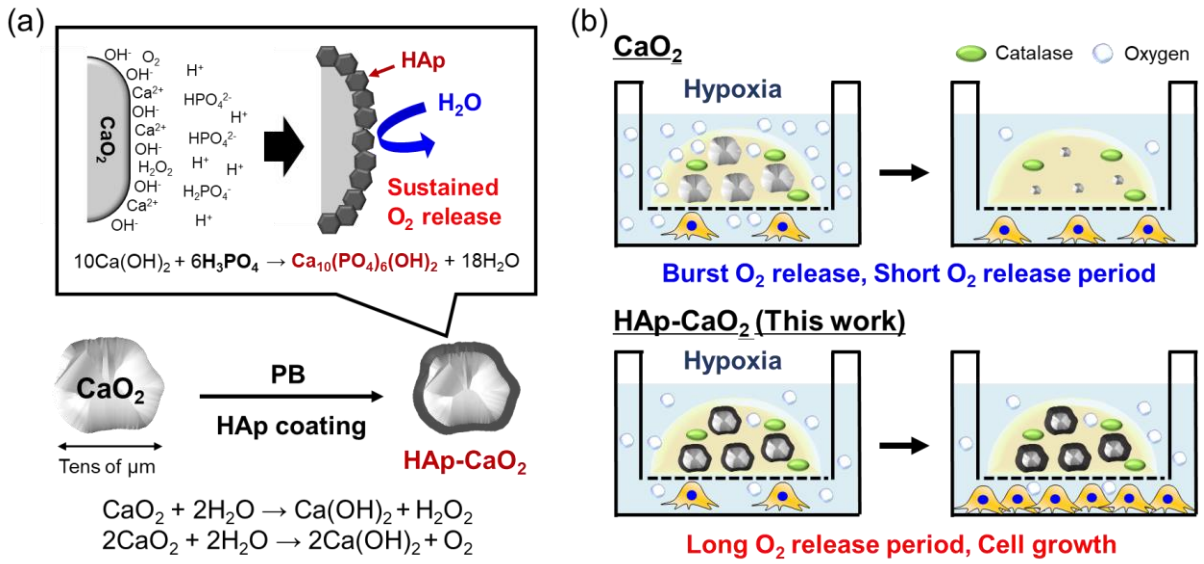

Figure 1-1. Schematic illustration of (a) the sustained oxygen release from CaO_2 through the HAp coating by PB treatment and (b) the sustained oxygen supply from the hydrogel including HAp-CaO_2 and catalase, which improved cell proliferation under a hypoxic condition.

1.2 Experiments

1.2.1 Materials

Calcium peroxide (CaO_2) (particle size < 200 mesh (74 μm)), HEPES sodium salt, catalase from bovine liver, bovine serum albumin (BSA, A3294), collagenase from Clostridium histolyticum (Type I, C0130), fibronectin human plasma and Triton-X 100 were purchased from Sigma-Aldrich (Missouri, USA). Sodium dihydrogenphosphate, disodium hydrogenphosphate 12-water, gelatin (077-03155), calcium chloride anhydrous, 5 mol L^{-1} hydrochloric acid (HCl), sulfuric acid and trypsin from porcine pancreas were purchased from FUJIFILM Wako Pure

Chemical Corporation (Osaka, Japan). Mineral Oil High sensitivity (oxygen barrier oil) and Phalloidin-iFluor 594 Reagent was purchased from Abcam (Cambridge, UK). *L*(+)-ascorbic acid, potassium dihydrogenphosphate, Dulbecco's modified Eagle medium (DMEM) (transparent; 08489-45, cell culture; 08458–16), ethanol, Dulbecco's phosphate buffered saline (PBS) and 10% formaldehyde neutral buffer solution were purchased from Nacalai Tesque (Kyoto, Japan). Ammonium molybdate 4-hydrate was purchased from KISHIDA CHEMICAL CO., LTD. (Osaka, Japan). Transglutaminase (TG) was kindly donated by Ajinomoto Co., Inc. (Tokyo, Japan). Tert-butyl alcohol was purchased from Tokyo Chemical Industry Co., Ltd. (Tokyo, Japan). Fetal bovine serum (FBS) (10270), antibiotics (50 U mL^{-1} penicillin and 50 μg mL^{-1} streptomycin) and 4′,6-diamidino-2-phenylindole (DAPI) were purchased from Thermo Fisher Scientific (MA, USA). Normal human dermal fibroblasts (NHDF, CC-2509) and human mesenchymal stem cells (MSC, PT-2501) were purchased from LONZA (Basel, Switzerland). HepG2 hepatocellular carcinoma cells (Human) were purchased from Cellular Engineering Technologies (HEPG2-500, Iowa, USA). Normal Goat serum was purchased from Jackson Immuno Research Laboratories Inc. (PA, USA).

1.2.2 Oxygen and hydrogen peroxide release behavior of CaO_2

PB was prepared by mixing same concentration of sodium dihydrogenphosphate solution and disodium hydrogenphosphate solution to adjust solution pH as 7.0. Oxygen release behavior of CaO_2 was determined by measuring the dissolved oxygen concentration in several buffers using a multiparameter DO Meter (HANNA, Woonsocket, USA). 10 mg of CaO_2 was dispersed in 10 mL of HEPES (100 mM) and PB (25, 100 and 500 mM) in a sample tube. Next, the DO meter was immersed in the solution. To suppress the diffusion of oxygen to the air, the sample solution and DO meter were fully covered by oxygen barrier oil. Dissolved oxygen concentration was measured at 37°C every 2 min while stirring the solution.

5 mg of CaO_2 was dispersed in 5 mL of HEPES (100 mM) and PB (100 mM). After 1 h incubation at 37ºC, hydrogen peroxide concentration in each solution was quantified using an Oxiselect Hydrogen Peroxide/Peroxidase Assay Kit (Fluorometric) (STA-344, Cell Biolabs Inc., San Diego, USA) according to the manufacturer's protocol. Due to the limitation of detection range for this assay kit, supernatants of each sample were diluted 1,000 times using an assay buffer. 50 μL of sample solution was mixed with 50 μL of working solution of the assay kit in a black 96-well plate (3603, Corning, NY, USA). After 30 min incubation at room temperature, fluorescent intensity was measured by microplate reader (SYNERGY/HTX multi-mode reader,

BioTek Instruments, Winooski, USA) using λ_{ex}=540 nm for excitation wavelengths and λ_{em}=590 nm for emission wavelengths. Hydrogen peroxide concentration was calculated from a standard curve obtained from the fluorescent intensities of the known concentrations of hydrogen peroxide (0-12.5 μM).

1.2.3 Analysis of surface structural changes of CaO_2 after phosphate buffer treatment

Surface structure of uncoated CaO_2 and CaO_2 immersed in PB were analyzed by SEM and EDX measurements. CaO_2 was immersed in 100 and 500 mM PB at a concentration of 5 mg mL^{-1} for 1 h at 37°C. The resulting samples were collected by centrifugation at 4,000 rpm for 3 min and then washed three times by MilliQ. Samples were then dried under reduced pressure at 80°C. For the high-resolution SEM, uncoated CaO_2 and CaO_2 immersed in PB were sputter-coated with osmium using an HPC-30 Plasma Coater (Vacuum Device, Ibaraki, Japan) and their surface morphologies were observed by a JSM-6701F instrument (JEOL Ltd., Tokyo, Japan). For the elemental analysis on their surface, SEM-EDX measurements were performed by a Miniscope TM 3000 equipped with Swift ED 3000 (Hitachi Ltd., Tokyo, Japan) without sputtering. Crystal structures of each sample were evaluated by XRD (AERIS, Malvern Panalytical, Malvern, UK) and chemical structures were evaluated by FT-IR (FT-720, HORIBA, Kyoto, Japan).

For the cross-section analysis of HAp-CaO_2, a CaO_2 plate was prepared by compressing CaO_2 microparticles at 30 MPa in a silicon sheet mold with 6 mm diameter using a high pressure jack (1-1187-01, As one, Osaka, Japan). The prepared CaO_2 plate was immersed in 500 mM PB for 1 h at 37ºC. After washing three times by MilliQ, the plate was dried under reduced pressure at 80°C. Cross-sections of the prepared plate were analyzed by SEM-EDX measurement.

Phosphorus amount on HAp-CaO_2 was quantitatively evaluated using the molybdenum blue method as previously reported.[13,14] HAp-CaO_2 was prepared by immersing 3 mg of CaO_2 in 3 mL of 100 and 500 mM PB (1 mg mL^{-1}) for 1 h at 37°C. After washing three times by MilliQ, HAp-CaO_2 was completely dissolved in 3 mL of 1 N HCl for 1 h. As a control sample, 3 mg of uncoated CaO_2 was also dissolved in 3 mL of 1 N HCl. To adjust the HCl concentration to 0.5 N, 3 mL of MilliQ was added to each sample. Due to the limitation of detection range for this molybdenum blue method, the prepared samples were diluted 10 times using 0.5 N HCl. 250 μL of diluted sample solutions were mixed with 750 μL of coloring reagent, consisting of

1 part of 10 % ascorbic acid solution and 6 parts of 0.42 % ammonium molybdate solution in 1 N H_2SO_4. Coloring reagent needs to be freshly prepared immediately before use. After 20 min incubation in a water bath at 45 °C, the absorbance at 820 nm was measured using a UV-vis spectrophotometer (V-670M, JASCO, Tokyo, Japan). The standard curves were prepared using potassium dihydrogenphosphate in the same way. HAp concentrations were calculated assuming that all detected phosphorus was derived from HAp.

1.2.4 Fabrication of oxygen releasing hydrogels

For the hydrogel preparation, 100 U mL^{-1} TG solution and 10,000 U mL^{-1} catalase solution were prepared using transparent DMEM and 0.5 M $CaCl_2$ solution was prepared using MilliQ. To prepare gelatin stock solution, 2500 mg of gelatin was dissolved in 10 mL of transparent DMEM (20 wt%) by heating. HAp-CaO_2 was prepared by immersing 1 mg mL^{-1} CaO_2 in 100 and 500 mM PB for 1 h at 37°C. The resulting HAp-CaO_2 were collected by centrifugation at 4,000 rpm for 3 min. Uncoated CaO_2 or HAp-CaO_2 were dispersed in gelatin stock solution and then 10,000 U mL^{-1} catalase, 100 U mL^{-1} TG, 0.5 M $CaCl_2$ and transparent DMEM were mixed so that the final concentrations were 2.5, 10 mg mL^{-1} CaO_2, 16 wt% gelatin, 10 U mL^{-1} TG, 100 U mL^{-1} catalase, and 2.5 mM $CaCl_2$, respectively. HAp-CaO_2 concentration was defined from the CaO_2 concentration before the HAp coating. The samples without catalase were prepared in the same way. For the evaluation of hydrogel formation, 800 μL of the prepared solutions were added to the sample tube. After 1 h incubation at 37°C, gelation was checked by tilting the sample tube.

1.2.5 Characterization of oxygen releasing hydrogels

Porous structures of hydrogels were characterized by SEM. 200 μL of hydrogels with catalase including 2.5 mg mL^{-1} of different types of CaO_2 (uncoated CaO_2, HAp-CaO_2 (100 and 500 mM PB)) were prepared in a 24-well plate insert (3470, Corning, NY, USA). As a control, hydrogel without CaO_2 was fabricated in the same way. To suppress the shrinkage of the hydrogels during the lyophilization procedure, t-butyl alcohol substitution was performed before the lyophilization. Briefly, the prepared hydrogels were immersed in ethanol for 1 h and then immersed in t-butyl alcohol 3 times for 1 h. After lyophilization and cutting the samples, surface morphologies of each of the samples sputter-coated with osmium were observed by SEM.

Mechanical properties of hydrogels were characterized by compression test using

EZTest (SHIMADZU, Kyoto, Japan). 200 μL of hydrogels with catalase including 0 and 2.5 mg mL^{-1} of HAp-CaO_2 (500 mM PB) were prepared in a 24-well plate insert. Hydrogels were taken out from the insert and compression test was performed at a constant test speed of 0.5 mm min^{-1}. Young modulus of hydrogels were calculated from the slope of stress-strain curve between 10 to 20% strain.

Rheological properties of hydrogels were characterized by rheometer (MCR302, Anton Paar, Graz, Austria). 200 μL of hydrogels with catalase including 0 and 2.5 mg mL^{-1} of HAp-CaO_2 (500 mM PB) were prepared in a 24-well plate insert. Hydrogels were taken out from the insert and then dynamic frequency sweeps were performed from 0.1 to 10 rad s^{-1} at 1.0 % strain amplitude. The starting axial force for all measurements was 0.2 N.

Swelling behavior of oxygen releasing hydrogels was evaluated from weight changes. 200 μL of hydrogels with catalase including 0 and 2.5 mg mL^{-1} of HAp-CaO_2 (500 mM PB) were prepared in a 24-well plate insert. To study the swelling behaviors of hydrogels, hydrogels were incubated in 2 mL of DMEM for 1 day at 37°C. After measuring the swollen weight, hydrogels were freeze dried and then dry weights were also measured. The weight-swelling ratio was calculated as the ratio of swollen weight to dry weight of hydrogels.

Degradation behavior of oxygen releasing hydrogels was evaluated in DMEM. 200 μL of hydrogels with catalase including 0 and 2.5 mg mL^{-1} of HAp-CaO_2 (500 mM PB) were prepared in a 24-well plate insert. Prepared hydrogels were freeze dried and then dry weights (W_0) were measured. To study the degradation behaviors of hydrogels, prepared hydrogels were incubated in 2 mL of DMEM at 37°C. After 7 and 14 days incubation, hydrogels were freeze dried and then dry weights (W_t) were measured. The remaining mass ratio of hydrogels were calculated as W_t/W_0.

Hydrogen peroxide release from oxygen releasing hydrogel was evaluated in DMEM. Hydrogen peroxide concentrations in transparent DMEM including hydrogels were evaluated using an Oxiselect Hydrogen Peroxide/Peroxidase Assay Kit. 200 μL of hydrogels with or without catalase including different concentrations of HAp-CaO_2 (100 mM PB) (0, 2.5, 5, 10 mg mL^{-1}) were incubated with 2 mL of transparent DMEM in a 24-well plate (3820-024, IWAKI, Shizuoka, Japan) at 37°C in a 5 % CO_2 incubator. After 3 days incubation, 100 μL of supernatant of each sample was collected. Due to the limitation of detection range for the hydrogen peroxide assay kit, supernatant derived from hydrogel including 10 mg mL^{-1} HAp-

CaO_2 without catalase was diluted 100 times and hydrogel including 5 mg mL^{-1} HAp-CaO_2 without catalase was diluted 10 times. Hydrogen peroxide concentration of each sample was evaluated as mentioned above.

To evaluate the oxygen release behavior of hydrogels, the dissolved oxygen amount in DMEM including hydrogels was measured under a hypoxic condition using an SDR SensorDish Reader (SDRSensorDish®Reader, PreSens, Regensburg, Germany). 200 µL of hydrogels with catalase including different concentrations and types of CaO_2 (2.5 mg mL^{-1} uncoated CaO_2, 2.5 mg mL^{-1} HAp-CaO_2 (100 mM PB), 2.5, 5, 10 mg mL^{-1} HAp-CaO_2 (500 mM PB)) were fabricated in a 24-well plate insert as mentioned above. As a control, hydrogel without CaO_2 was fabricated in the same way. 24-well plate inserts were put in a 24-well sensor dish (OxoDish®OD24, PreSens, Regensburg, Germany) and then 2 mL of transparent DMEM was added to each sample. As a control, DMEM without hydrogels were also prepared. The SensorDish Reader and the 24-well sensor dish were placed in a hypoxia cell culture airtight bag (6-8669-03, As one, Osaka, Japan). To create a hypoxic condition, three anaeropack O_2 absorbers (MITSUBISHI GAS CHEMICAL COMPANY INC., Tokyo, Japan) were added to the bag and it was then completely sealed using parafilm. The dissolved oxygen amount in the DMEM was then monitored at 37°C after the first 6 hours and for each of the 24 hours.

1.2.6 Cell culture with oxygen releasing hydrogels under a hypoxic condition

Adipose-derived stem cells (ADSC) was isolated from adipose tissues using a previously reported method.[15] Abdominal human adipose tissues from patients were isolated at the Kyoto Prefectural University of Medicine Hospital and kept on an ice pack during transportation to Osaka University. The tissues were first washed in PBS containing 5 % of antibiotics. Then, 8-10 g of tissue were separated into fragments to fill the 6 wells of a 6-well plate and then minced to obtain a size of around 1mm^3 using autoclaved scissors and tweezers, directly in 2 mL of collagenase solution at 2 mg mL^{-1} in DMEM 0 % FBS, 5 % BSA and 1 % antibiotics (sterilized by filtration). After 1 h of incubation at 37°C with 250 rpm rotation, DMEM medium was added and the lysate was filtrated using a 500 µm filter, before being centrifuged for 3 min at 80g. The cells pellet was washed twice in PBS with 5 % BSA and 1 % antibiotics and once in complete DMEM, with 3 min of centrifugation at 80g between each wash. Then, the final pellet was resuspended in DMEM for ADSC expansion by changing the medium every day for three days and then passaging the cells when they reached 80 % of confluency.

Ethics statement: The adipose tissues were collected from Kyoto Prefectural University of Medicine Hospital (Kyoto, Japan) after abdominal adipose tissues or liposuction isolation of human female donors. All use was approved by the Human Ethics Committee (Approval number: ERB-C-1317-1) of the Kyoto Prefectural University of Medicine Institutional Review Board and conformed to the principles outlined in the Declaration of Helsinki.

Cell proliferation under a hypoxic condition with oxygen releasing hydrogels was evaluated by WST-8 (CCK-8) kit assay. Briefly, 200 μL of hydrogels with catalase including different concentrations of HAp-CaO_2 (500 mM PB) (0, 2.5, 5, 10 mg mL^{-1}) were fabricated in a 24-well plate insert and washed 3 times by 2 mL of DMEM containing 10 % FBS and 1 % antibiotics. 2×10^4 cells of NHDF, MSC, ADSC and HepG2 were seeded on a 24-well plate using 1 mL of DMEM containing 10 % FBS and 1 % antibiotics. After 3 h incubation at 37°C in a 5 % CO_2 incubator, the 24-well plate inserts containing hydrogels were placed in the 24-well plate and then 1 mL of DMEM containing 10 % FBS and 1 % antibiotics was added. As a control, a cell culture without hydrogels was also prepared. The 24-well plates were incubated in a gas barrier box (As one, GB-3.0L, Osaka, Japan) with two anaeropack O_2 absorbers at 37°C to create a hypoxic condition. WST assay reagent was prepared by mixing transparent DMEM and cell count reagent SF (Nacalai Tesque, Kyoto, Japan) at a ratio of 9:1. After 7 days incubation under a hypoxic condition, cells were washed by 1 mL of PBS and then 200 μL of WST assay reagent was added. The cells were incubated in a 5 % CO_2 incubator for 1 h for NHDF and 45 min for MSC, ADSC and HepG2 at 37°C. Then, 100 μL of WST solutions from each well were collected in a 96-well plate Transwell (3860-096, IWAKI, Shizuoka, Japan) and absorbance at 450 nm was measured using a microplate reader. The mitochondrial activity of each sample was standardized from the relative values of absorbance at 450 nm as compared to 100 % for that of a cell culture without hydrogel. Phase contrast images of each sample were also taken using an EVOS™ XL Core Imaging System (Thermo Fisher Scientific, MA, USA) after 7 days cell culture.

Cell proliferation under a hypoxic condition using preincubated oxygen releasing hydrogels was also evaluated by WST-8 kit assay. 200 μL of hydrogels with catalase including different concentrations and types of CaO_2 (2.5 mg mL^{-1} uncoated CaO_2, 0, 2.5, 5, 10 mg mL^{-1} HAp-CaO_2 (500 mM PB)) were fabricated in a 24-well plate insert and then incubated in 2 mL of DMEM containing 10 % FBS and 1 % antibiotics for 3 days in a 5 % CO_2 incubator. Next, 2×10^4 cells of NHDF were cultured in a 24-well plate with hydrogels in the 24-well plate

insert under a hypoxic condition as mentioned above. After 7 days cell culture, wst assay was performed for 45 min incubation as mentioned above.

1.2.7 Construction of 3D tissue in the presence of oxygen releasing hydrogel

For the construction of 3D tissue in the presence of oxygen releasing hydrogel, 400 μL of 16 wt% gelatin solution (DMEM) containing 10 U mL^{-1} TG, 100 U mL^{-1} catalase, 2.5 mM $CaCl_2$ and 2.5 mg mL^{-1} HAp-CaO_2 (500 mM PB) was added in the 24-well plate. Before the gelation, 24-well insert containing 100 μL of 0.2 mg mL^{-1} fibronectin solution (50 mM Tris buffer at pH 7.4) was put on the gelatin solution. After 1 hour incubation at 37°C for the gelation, fibronectin solution was removed and the obtained hydrogel was washed by culture medium (DMEM containing 10 % FBS and 1% antibiotics). 5×10^6 cells of L929 were suspended in 200 μL of culture medium and added in the 24-well insert. After 15 minutes centrifuge of 24-well plate at 1100 g, 1 mL of culture medium was added. As a control sample, L929 tissue was constructed in the 24-well insert in the same procedure without hydrogels. Tissues were cultured in the 5 % CO_2 incubator and culture medium was exchanged every day. After 3 days culture, the L929 tissues were fixed by 10% formaldehyde neutral buffer solution. For histology staining and fluorescence imaging, the fixed 3D tissues were sent to the Applied Medical Research Company for paraffin embedding. Sectioned 3D tissues were stained with hematoxylin-eosin (HE) staining. The images were captured using an FL EVOS Auto microscope (Thermo Fisher Scientific, MA, USA). For the calculation of cell density in the HE staining images, cell number in the five areas (200 μm x 200μm) around the center area were counted per each tissue by ImageJ. For the fluorescence imaging, the nuclei were stained with DAPI and F-actin were detected by phalloidin. Sectioned 3D tissues were permeabilized with 0.3% Triton X-100 for 5 min and blocked with 1 % bovine serum albumin and 10 % normal goat serum in PBS. The tissues were then incubated with staining solution (Phalloidin-iFluor 594, DAPI, 1:500 dilution in PBS). After washing in the PBS, the 3D tissue was finally observed using confocal laser scanning microscope (CSLM) FluoView FV3000 (Olympus, Tokyo, Japan). The images were taken by keeping the same exposure time and excitation power for each sample.

1.3 Results and discussion

1.3.1 Oxygen and hydrogen peroxide release behavior of CaO_2 in several buffers

The chemical reaction between CaO_2 and water is as follows[16-18]:

$$CaO_2 + 2H_2O \rightarrow Ca(OH)_2 + H_2O_2$$

Ma and co-workers reported that hydroxyl radical and superoxide anion were detected when CaO_2 reacts with water.[16] Therefore, it is considered that produced hydrogen peroxide can readily undergo redox by obtaining a single electron in the suspension of alkaline earth metal peroxides to offer the hydroxyl radical.

$$H_2O_2 + e^- \rightarrow \bullet OH + {}^-OH$$

The following reactions can also occur in the system to produce superoxide anion.

$$\bullet OH + H_2O_2 \rightarrow H_2O + HO_2\bullet$$

$$HO_2\bullet \rightarrow \bullet O_2^- + H^+$$

Because of the short lifetime of these reactive oxygen species, they react quickly to produce oxygen.

$$\bullet OH + HO_2\bullet \rightarrow H_2O + O_2$$

$$\bullet O_2^- \rightarrow O_2 + e^-$$

From the above discussion, the sum reaction for CaO_2 with water was proposed as follows:

$$2CaO_2 + 2H_2O \rightarrow 2Ca(OH)_2 + O_2$$

As a result, CaO_2 generates oxygen, hydrogen peroxide and calcium hydroxide by the reaction with water.[16-18]

As shown in **Figure 1-1b**, the rapid reaction between CaO_2 and water results in burst release of oxygen in the solution. On the other hand, sustained oxygen release from CaO_2 is expected in a PB through the formation of HAp on the surface because the reaction between

calcium hydroxide and phosphoric acid provides HAp as follows[5,6]:

$$10Ca(OH)_2 + 6H_3PO_4 \rightarrow Ca_{10}(PO_4)_6(OH)_2 + 18H_2O$$

To confirm this hypothesis, oxygen release behaviors of CaO_2 microparticles (particle size < 74 μm) were evaluated in 4-(2-hydroxyethyl)piperazine-1-ethanesulfonic acid (HEPES) buffer (pH 7.4) and PB (pH 7.0). HEPES is known as an effective buffer for culturing tissues and cells in vitro and often used in the field of biochemistry as well. Dissolved oxygen (DO) concentration was measured by immersing a DO meter in each buffer after the addition of CaO_2 at a concentration of 1 mg mL^{-1}. To prevent the diffusion of oxygen to the air, the buffer and DO meter were fully covered by oxygen barrier oil. In the case of 100 mM HEPES, the dissolved oxygen concentration increased to 200 % within 6 min and then maintained the same value (**Figure 1-2a**). Furthermore, after the addition of CaO_2 in HEPES, CaO_2 disappeared within 3 min. These results suggest that the reaction between CaO_2 and water completed quickly in HEPES. On the other hand, the initial burst increase of dissolved oxygen concentration was dramatically suppressed in 100 mM PB (**Figure 1-2a**). Furthermore, white solids remained in the solution after the addition of CaO_2 in 100 mM PB. The author also evaluated hydrogen peroxide release from CaO_2 in each buffer (**Figure 1-2b**). As with the oxygen, hydrogen peroxide release from CaO_2 was dramatically suppressed in PB compared to HEPES. These results suggest that the reaction between CaO_2 and water was suppressed in PB, probably because HAp formation on CaO_2 delays this reaction. The author hypothesizes that the formed HAp layer acts as diffusion barrier to water, thus significantly slowing down the reaction of water with CaO_2 and thus also subsequent oxygen formation.

To evaluate the effect of PB concentration on the oxygen release behavior of CaO_2, the dissolved oxygen concentration was measured in 25, 100 and 500 mM PB in the same way (**Figure 1-2c**). Interestingly, as the PB concentration increased from 25 to 100 and 500 mM, the dissolved oxygen concentration after 1 h incubation decreased from 220 to 160 and 120 %. According to these results, the reaction between CaO_2 and water was suppressed especially at higher PB concentrations, probably because the amount of HAp on CaO_2 also increased with PB concentration. The observed behavior fits to the author's hypothesis, as the diffusion length of water through the HAp layer is increased with growing layer thickness, thus slowing down the oxygen production with increasing layer thickness. Since dissolved oxygen amount in 500 mM PB have plateaued within 1 hour at 37°C, HAp-CaO_2 were prepared by immersing CaO_2 in PB for 1 hour at 37°C for further studies.

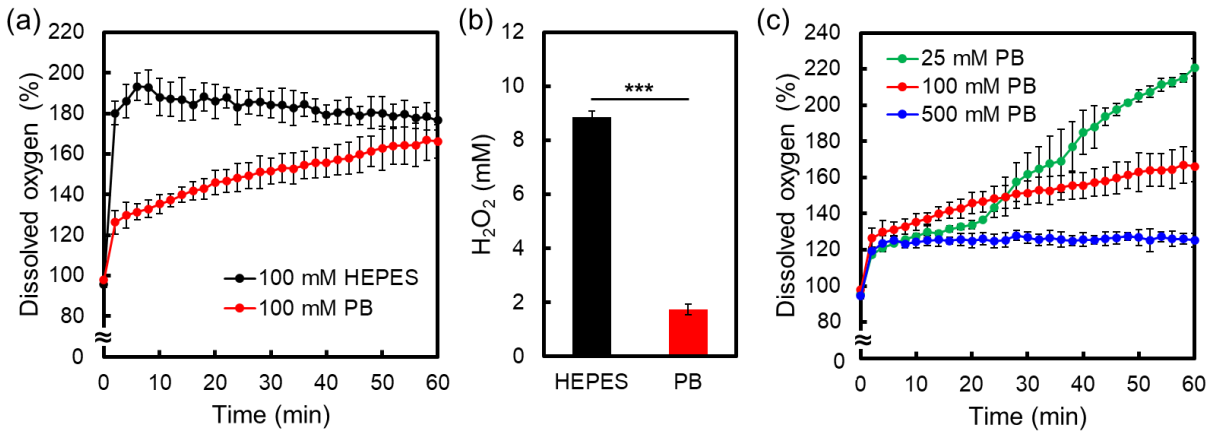

Figure 1-2. (a) Dissolved oxygen changes in 100 mM HEPES and 100 mM PB for 1 h at 37°C in a closed system after the addition of 1 mg mL^{-1} CaO_2. (b) Hydrogen peroxide concentration in 100 mM HEPES and 100 mM PB 1 h after the addition of 1 mg mL^{-1} CaO_2. (c) Dissolved oxygen changes in 25, 100 and 500 mM PB for 1 h at 37°C in a closed system after the addition of 1 mg mL^{-1} CaO_2. All data are representative of three independent experiments, mean ± SD. ***$p < 0.001$.

1.3.2 Characterization of the HAp coating on CaO_2

To confirm the HAp coating on CaO_2 by PB treatment, the surface morphology of CaO_2 was evaluated. **Figure 1-3a** shows scanning electron microscope (SEM) images of untreated CaO_2 and CaO_2 immersed in 100 and 500 mM PB for 1 h at 37°C. CaO_2 immersed in the PB showed a porous structure on the surface, suggesting structural surface changes and formation of HAp nanocrystal.[5] For the elemental analysis on the surface of CaO_2, SEM and energy dispersive X-ray spectroscopy (EDX) measurement were performed (**Figure 1-3b**). Elemental mapping of untreated CaO_2 showed calcium but no phosphorus at the same location of CaO_2 in the SEM image. On the other hand, CaO_2 immersed in 100 and 500 mM PB showed both calcium and phosphorus at the same location of CaO_2 in the SEM images. These results suggested that phosphorus-containing crystals were formed on the surface of CaO_2 by PB treatment. Furthermore, EDX spectra of each sample showed that the peak intensity derived from phosphorus increased with PB concentration (red arrow in the figure). Accordingly, it is also suggested that the amount of phosphorus-containing crystals on the surface of CaO_2 increased with PB concentration.

To clarify the crystal structure of phosphorus-containing crystals, X-ray diffraction

(XRD) was measured (**Figure 1-3c,d**). In both untreated CaO_2 and CaO_2 immersed in 500 mM PB, peaks at 30, 36, 48, 52 and 53° were observed, which were assigned to the (002), (110), (112), (200) and (103) reflections of CaO_2.[19,20] Peaks at 26, 29, 32, 34, 40, 47 and 50° were also observed in CaO_2 immersed in 500 mM PB, which were assigned to the (002), (210), (211), (202), (310), (222) and (213) reflections of HAp.[21, 22] According to the XRD data, phosphorus-containing crystals were identified as HAp. HAp formation was also confirmed using Fourier-transform infrared spectroscopy (FT-IR) (**Figure 1-3e**). The clear band at 1,020 cm^{-1} which was assigned to the P-O stretching vibration was observed in CaO_2 immersed in 500 mM PB, suggesting HAp formation.[22] According to these results, HAp coating on CaO_2 microparticles by PB treatment was confirmed, which enabled sustained oxygen release from CaO_2 in the PB.

For the cross-section analysis of HAp-CaO_2, a CaO_2 plate was prepared by compressing CaO_2 microparticles using a mold. After immersing the CaO_2 plate in 500 mM PB for 1 h, SEM-EDX measurements of the cross-section of the CaO_2 plate were taken. As shown in the merged image of SEM and elemental mapping**,** calcium was observed throughout the cross-sections (**Figure 1-3f**). On the other hand, phosphorus was observed mainly near the plate surface, suggesting that HAp is formed on the surface of the CaO_2 plate. A small amount of phosphorus was also observed inside the CaO_2 plate, probably because of the PB that penetrated through the voids of the CaO_2 plate to react with the CaO_2 inside. Furthermore, according to the enlarged merged image of SEM and elemental mapping, phosphorus was observed on the surface of the CaO_2 microparticles in the plate and the thickness of the HAp layer on these microparticles was estimated to be no more than a few micrometers.

Since SEM-EDX measurements suggested PB concentration-dependent HAp formation, the amount of phosphorus on the surface of CaO_2 was quantitatively evaluated using the molybdenum blue method[13,14] (**Figure 1-3g**). HAp-CaO_2 was dissolved in 1N-HCl [$Ca_{10}(PO_4)_6(OH)_2 + 8H^+ \rightarrow 10Ca^{2+} + 6HPO_4^{2-} + 2H_2O$] and then the amount of dissolved phosphorus ions was measured. As expected, no phosphorus ions were detected in the case of untreated CaO_2. When 1 mg mL^{-1} (13.84 mM) CaO_2 was immersed in 100 mM PB for 1 h, 1.92 mM of phosphorus ions was detected, which corresponds to 0.32 mg mL^{-1} HAp assuming that all the detected ions were derived from HAp. Furthermore, in the case of 500 mM PB, 4.10 mM of phosphorus ions was detected, which corresponds to 0.69 mg mL^{-1} HAp. These results confirmed that the HAp amount on CaO_2 increased with PB concentration, which enabled PB concentration-dependent oxygen release from CaO_2 (**Figure 1-2c)**.

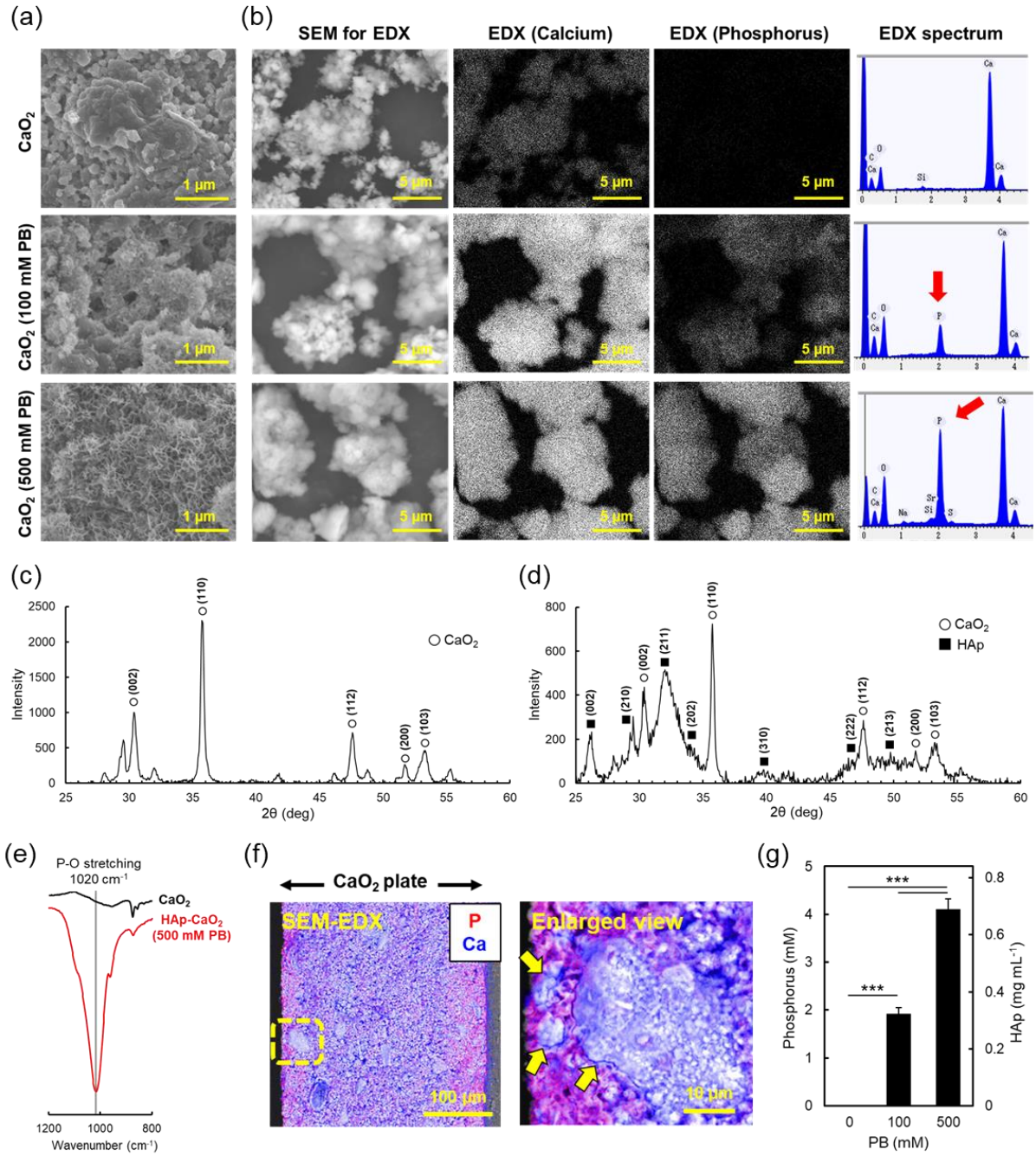

Figure 1-3. Characterization of the HAp coating on CaO_2. (a) SEM images and (b) SEM images, elemental mapping of calcium and phosphorus and EDX spectrum of CaO_2 (top) and CaO_2 immersed in 100 (middle) and 500 mM PB (bottom) for 1 h. XRD spectrum of (c) CaO_2 and (d) CaO_2 immersed in 500 mM PB. (e) FT-IR spectrum of CaO_2 and CaO_2 immersed in 500 mM PB. (f) SEM and elemental mapping of calcium (blue) and phosphorus (red) of the cross-section of CaO_2 plate after immersing CaO_2 plate in 500 mM PB and enlarged view of yellow area. (g) Phosphorus and HAp amount in CaO_2 and CaO_2 immersed in 100 and 500 mM PB. HAp concentrations were calculated assuming that all detected phosphorus was derived from HAp. The data are representative of three independent experiments, mean ± SD. ***$p < 0.001$.

1.3.3 Fabrication and characterization of oxygen releasing hydrogels

For the broader application of HAp-CaO_2 to tissue engineering, the author demonstrates that HAp-CaO_2 can be used as additive to hydrogels at the example of enzymatically crosslinked gelatin hydrogels. HAp-CaO_2 was prepared by immersing CaO_2 microparticles in 100 or 500 mM PB for 1 h at 37°C. After mixing gelatin, TG, catalase and CaO_2 or HAp-CaO_2 in Dulbecco's Modified Eagle Medium (DMEM), the sample solutions were incubated for 1 h at 37°C to gelate **(Figure 1-4a)**. Interestingly, in the case of uncoated CaO_2, gelation was not observed without catalase. It is reported that TG is deactivated by hydrogen peroxide due to conformational changes of the peptide main chain associated with disulfide bond formation.[23] Thus, it is suggested that crosslinking of gelatin by TG was suppressed without catalase because of the initial burst release of hydrogen peroxide from CaO_2. In addition, gelation was observed at 2.5 mg mL^{-1} CaO_2 but not at 10 mg mL^{-1} CaO_2 with catalase. This is probably because of the deactivation of TG by hydrogen peroxide prior to the decomposition by catalase at the higher concentration of uncoated CaO_2. On the other hand, gelation was observed in all samples using HAp-CaO_2 (100 mM PB) because the HAp coating on CaO_2 suppresses the burst release of hydrogen peroxide. These results clearly suggested that HAp-CaO_2 is applicable to the hydrogels obtained by enzymatic reactions, which are difficult to prepare using uncoated CaO_2. The morphology of freeze-dried hydrogels was analyzed by SEM (**Figure 1-4b**). Porous structures with pore sizes of around 5 to 10 μm were identified in all hydrogels, suggesting no marked differences in hydrogel structures. The compression tests and rheological tests showed that hydrogels with and without HAp-CaO_2 had similar strain-stress curve, young modulus and storage modulus (G'), suggesting that these hydrogels have similar mechanical properties (**Figure 1-4c-e**). Swelling behaviors and degradation behaviors also showed similar trends between hydrogels with and without HAp-CaO_2 (**Figure 1-4f,g**). These results suggested that incorporation of HAp-CaO_2 in the gelatin hydrogel enzymatically crosslinked by TG didn't affect hydrogel properties.

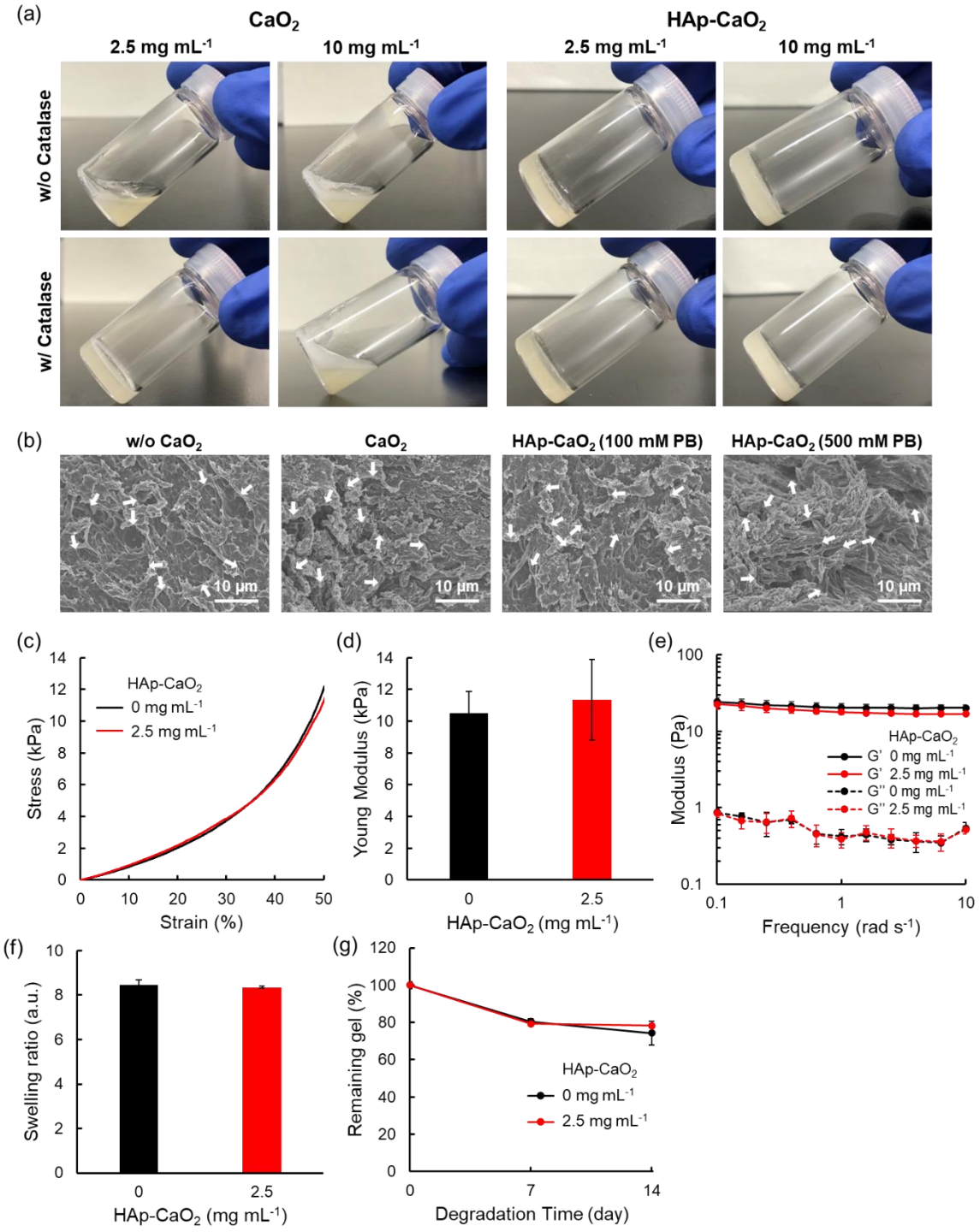

Figure 1-4. (a) Hydrogel formation after 1 h incubation at 37°C after mixing 16 wt% gelatin, 10 U mL^{-1} TG, 2.5 mM $CaCl_2$, 0 and 100 U mL^{-1} catalase and various concentrations of CaO_2 or HAp-CaO_2 (100 mM PB). (b) SEM images of the hydrogels including 100 U mL^{-1} catalase and 0 and 2.5 mg mL^{-1} of CaO_2 or HAp-CaO_2 (100 and 500 mM PB) (White arrows indicate pores for the estimation of pore size). (c) Compression stress-strain curves, (d) young modulus, (e) frequency scanning rheological properties, (f) swelling behaviors and (g) degradation behaviors of hydrogels including 100 U mL^{-1} catalase and 0 and 2.5 mg mL^{-1} of HAp-CaO_2

(500 mM PB). HAp-CaO_2 (100 and 500 mM PB) were prepared by immersing CaO_2 in 100 and 500 mM PB for 1 h. All data are representative of three independent experiments.

When CaO_2 reacts with water, hydrogen peroxide is also released as a by-product. Since this compound exhibits cytotoxic properties above certain concentrations, hydrogen peroxide release from hydrogels was evaluated in DMEM after 3 days incubation (**Figure 1-5a**). In the case of hydrogels without catalase, the concentration of hydrogen peroxide increased with HAp-CaO_2 (100 mM PB) concentration (HAp-CaO_2 5 mg mL^{-1}, 47 μM; 10 mg mL^{-1}, 139 μM). However, hydrogen peroxide was not detected in the hydrogel including 2.5 mg mL^{-1} HAp-CaO_2, probably because released hydrogen peroxide was decomposed by the components of DMEM such as methionine.[24] On the other hand, hydrogen peroxide was hardly detected in any of the hydrogels with catalase (H_2O_2 < 1.5 μM) because catalase is an enzyme that decomposes hydrogen peroxide into oxygen. These results clearly suggested that potentially cytotoxic hydrogen peroxide release from hydrogels is dramatically suppressed using catalase. Accordingly, the author used hydrogels including catalase for further characterization as preparation for cell culture experiments.

The time-span over which oxygen is released is one of the most important properties for oxygen releasing materials. To evaluate the oxygen release behavior of hydrogels, dissolved oxygen concentrations in DMEM with hydrogels were evaluated under a hypoxia condition (O_2 < 0.1 %). At first, the oxygen release behavior of hydrogels including 2.5 mg mL^{-1} uncoated CaO_2 or HAp-CaO_2 prepared by 100 and 500 mM PB was measured to evaluate the effect of the HAp coating on CaO_2 (**Figure 1-5b,c**). As expected, the hydrogel including uncoated CaO_2 showed an initial burst release of oxygen and short-term oxygen release for only 3 days due to the rapid reaction with water. On the other hand, in the case of the hydrogel including HAp-CaO_2 by 100 mM PB, the initial burst release of oxygen was suppressed compared to uncoated CaO_2 and the oxygen release period increased to 4 days. In addition, the hydrogel including HAp-CaO_2 by 500 mM PB showed a drastic suppression of the initial burst release of oxygen and long-term oxygen release of around 10 days. These results clearly confirmed that PB concentration-dependent HAp coating on CaO_2 suppressed the reaction with water, which enabled sustained oxygen release from the hydrogel. Furthermore, when HAp-CaO_2 (500 mM PB) concentration in the hydrogels increased from 0 to 10 mg mL^{-1}, the dissolved oxygen concentration also increased (**Figure 1-5d,e**). For example, dissolved oxygen concentrations

after 5 days incubation were 6.0 % (2.5 mg mL^{-1}), 8.8 % (5 mg mL^{-1}) and 15.2 % (10 mg mL^{-1}). Since the dissolved oxygen concentration in real tissue such as heart (9~18 %), skeletal muscle (9~18 %), brain (16 %) and liver (19~28 %) are similar to these values,[25] the oxygen releasing properties of these hydrogels should be sufficient for tissue engineering application.

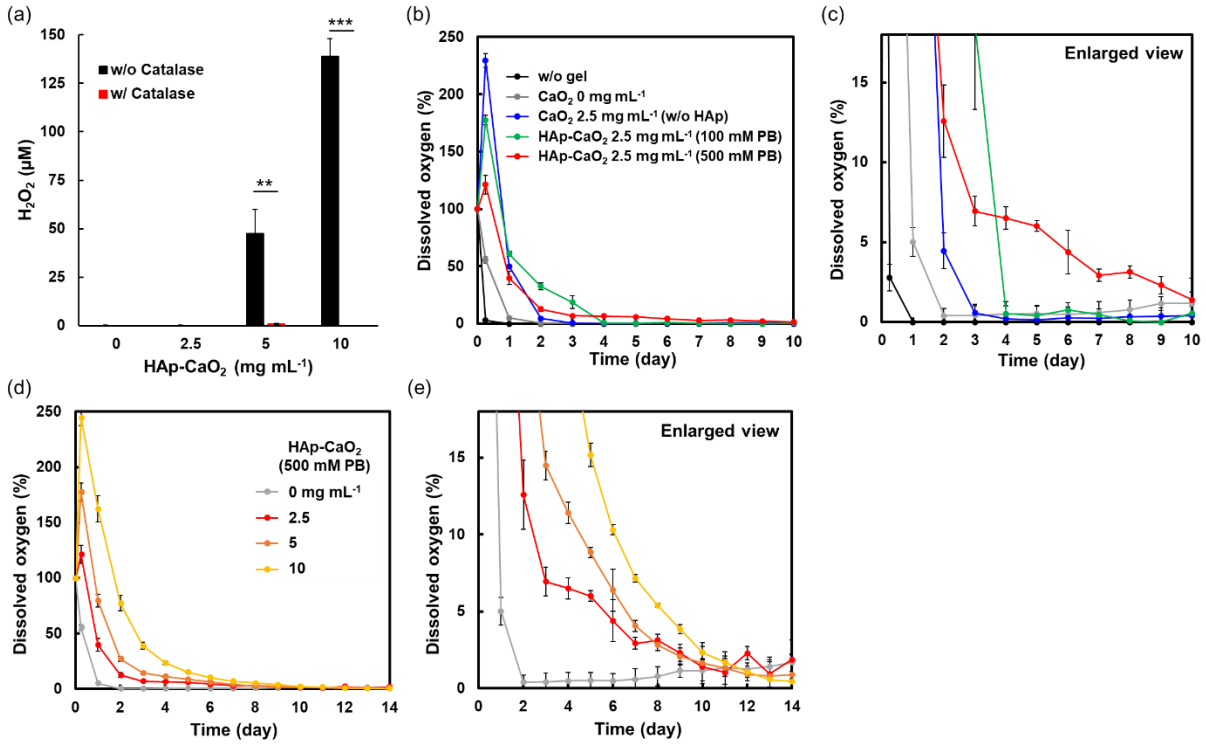

Figure 1-5. (a) Hydrogen peroxide concentrations in 2 mL of DMEM with 200 μL of hydrogels including 0 (black) and 100 U mL^{-1} (red) catalase and various concentrations of HAp-CaO_2 (100 mM PB) after 3 days incubation. Dissolved oxygen changes in 2 mL of DMEM with 200 μL of hydrogels including 100 U mL^{-1} catalase, (b,c) 0 and 2.5 mg mL^{-1} CaO_2 or HAp-CaO_2 (100 and 500 mM PB) and (d,e) 0, 2.5, 5 and 10 mg mL^{-1} HAp-CaO_2 (500 mM PB) under a hypoxic condition. Figures 1-5c and e show enlarged views of Figures 1-5b and d, respectively. All data are representative of three independent experiments, mean ± SD. $^{**}p < 0.01$ and $^{***}p < 0.001$.

1.3.4 Cell proliferation under a hypoxic condition using oxygen releasing hydrogels

To evaluate the effect of oxygen supply from the hydrogels on cell proliferation, normal

human dermal fibroblast (NHDF) was cultured with oxygen releasing hydrogels including HAp-CaO_2 (500 mM PB) under a hypoxic condition (O_2 < 0.1 %) (**Figure 1-6a**). After 7 days incubation, the mitochondrial activity of each sample was assessed by WST assay. To easily compare cell proliferation, the relative values of mitochondrial activity as compared to 100 % for that of a cell culture without hydrogel are shown in **Figure 1-6b**. In the case of the hydrogel without HAp-CaO_2, mitochondrial activity increased slightly, probably because the oxygen originally dissolving in the hydrogel was supplied to the cells in the early stages of incubation. On the other hand, the hydrogel including 2.5 mg mL^{-1} HAp-CaO_2 showed dramatically increased mitochondrial activity to 518 %. Furthermore, as the HAp-CaO_2 concentration in the hydrogels increased from 2.5 mg mL^{-1} to 5 and 10 mg mL^{-1}, mitochondrial activity also increased from 518 % to 567 and 657 %. This result is consistent with the trend that the amount of released oxygen increased with HAp-CaO_2 concentration in the hydrogels (**Figure 1-5d,e**). In addition to NHDF, mesenchymal stem cells (MSC) (**Figure 1-6c**), adipose derived stem cells (ADSC) (**Figure 1-6d**) and HepG2 (**Figure 1-6e**) cells were also cultured with oxygen releasing hydrogels under a hypoxic condition. Although ADSC often used for regenerative medicine of adipose tissue reconstruction, transplantation of adipose tissues is unsuitable for tissue reconstruction as the lack of blood vessels results in inadequate nutrient and oxygen delivery, leading to necrosis in situ.[26] The oxygen releasing hydrogel including 2.5 mg mL^{-1} HAp-CaO_2 showed increased mitochondrial activity to 563 % for MSC, 164 % for ADSC and 920 % for HepG2. These differences in mitochondrial activity are probably because of the differences in oxygen utilization for each cell.[27] Cell morphologies of each sample after 7 days incubation under a hypoxic condition are shown in phase contrast images (**Figure 1-6f**). The cells did not spread well without oxygen releasing hydrogels probably because the lack of oxygen affected cell function.[28] On the other hand, the cells spread and proliferated very well with oxygen releasing hydrogels. According to these results, it is confirmed that the oxygen supply from hydrogels improved cell proliferation of various cell types under a hypoxic condition.

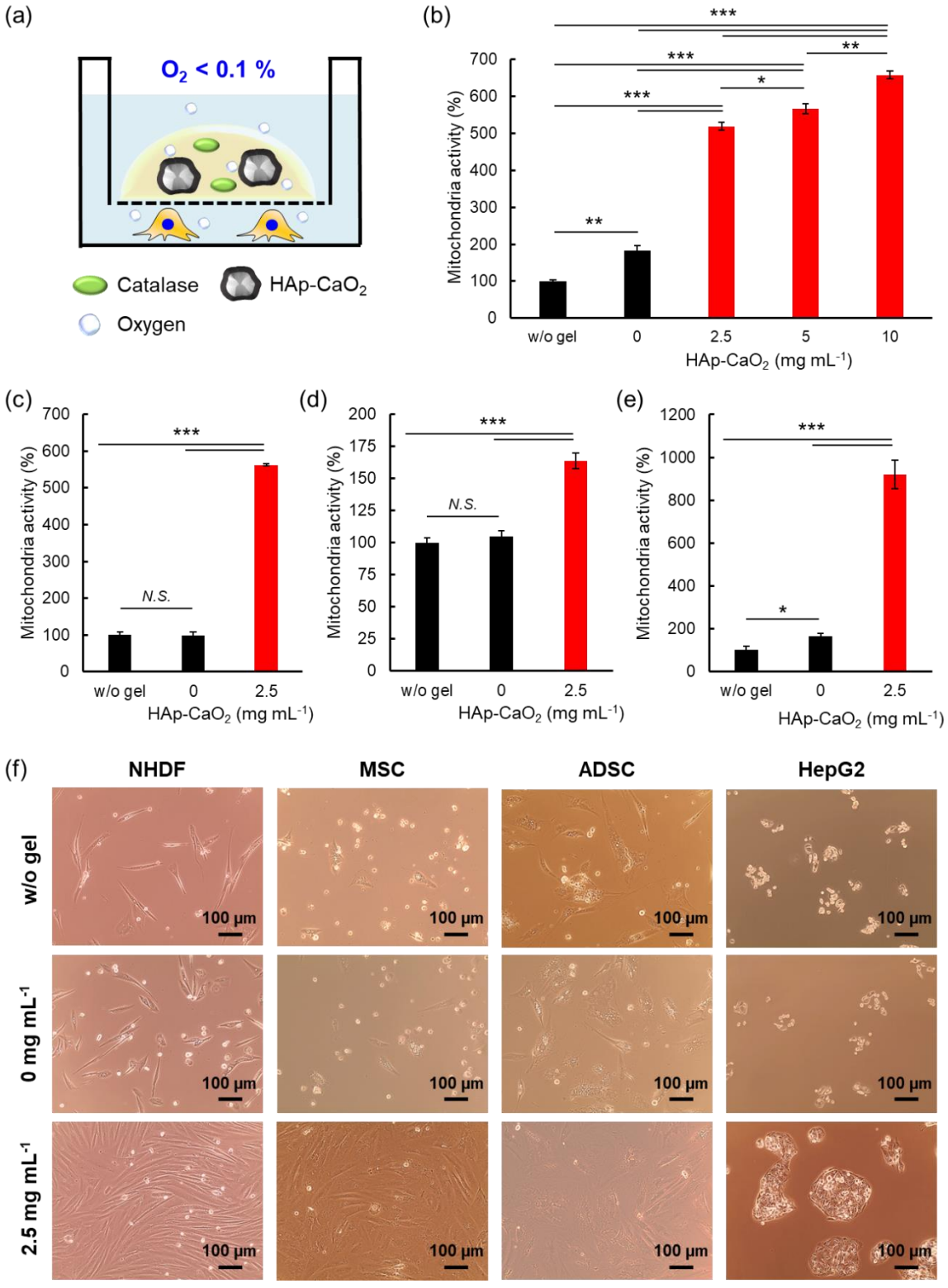

Figure 1-6. (a) Schematic illustration of the cell culture using an oxygen releasing hydrogel under a hypoxic condition. Mitochondrial activity of (b) NHDF (c) MSC (d) ADSC and (e) HepG2 and (f) phase contrast images of each sample after 7 days incubation with hydrogels including 100 U mL^{-1} catalase and various concentrations of HAp-CaO_2 (500 mM PB) under a hypoxic condition. Mitochondrial activity of each sample was standardized from the relative

values as compared to 100 % for that of a cell culture without hydrogel. All data are representative of three independent experiments, mean ± SD. *$p < 0.05$, **$p < 0.01$ and ***$p < 0.001$.

As shown in **Figure 1-5**, a HAp coating on CaO_2 dramatically increased the oxygen release periods of hydrogels. Thus, to evaluate the effects of the HAp coating on CaO_2 for cell proliferation, NHDF was cultured with preincubated hydrogels including uncoated CaO_2 or HAp-CaO_2 under a hypoxic condition. Since the oxygen release period of the hydrogel including uncoated CaO_2 is only 3 days (**Figure 1-5b,c**), oxygen release from the hydrogel should be completed within 3 days preincubation in DMEM. On the other hand, since the oxygen release period of the hydrogel including HAp-CaO_2 is 10 days, an additional 7 days oxygen release is expected even after 3 days preincubation, which is expected to improve cell proliferation under a hypoxic condition (**Figure 1-7a**). Hydrogels including 2.5 mg mL^{-1} HAp-CaO_2 dramatically increased mitochondrial activity to 369 %, while it was only 180 % for the hydrogel including 2.5 mg mL^{-1} uncoated CaO_2 (**Figure 1-7b**). In addition, phase contrast images after 7 days cell culture confirmed marked cell proliferation only in the hydrogel including HAp-CaO_2 (**Figure 1-7c**). These results clearly confirmed that the HAp coating on CaO_2 achieved sustained oxygen release from the hydrogel, which dramatically improved cell proliferation under a hypoxic condition compared to that of uncoated CaO_2. Furthermore, similar to the case shown in **Figure 1-6b**, as the HAp-CaO_2 concentration in the hydrogels increased from 2.5 mg mL^{-1} to 5 and 10 mg mL^{-1}, mitochondrial activity also increased from 369 % to 416 and 543 %. This is also probably because the amount of released oxygen increased with HAp-CaO_2 concentration in the hydrogels (**Figure 1-5d,e**).

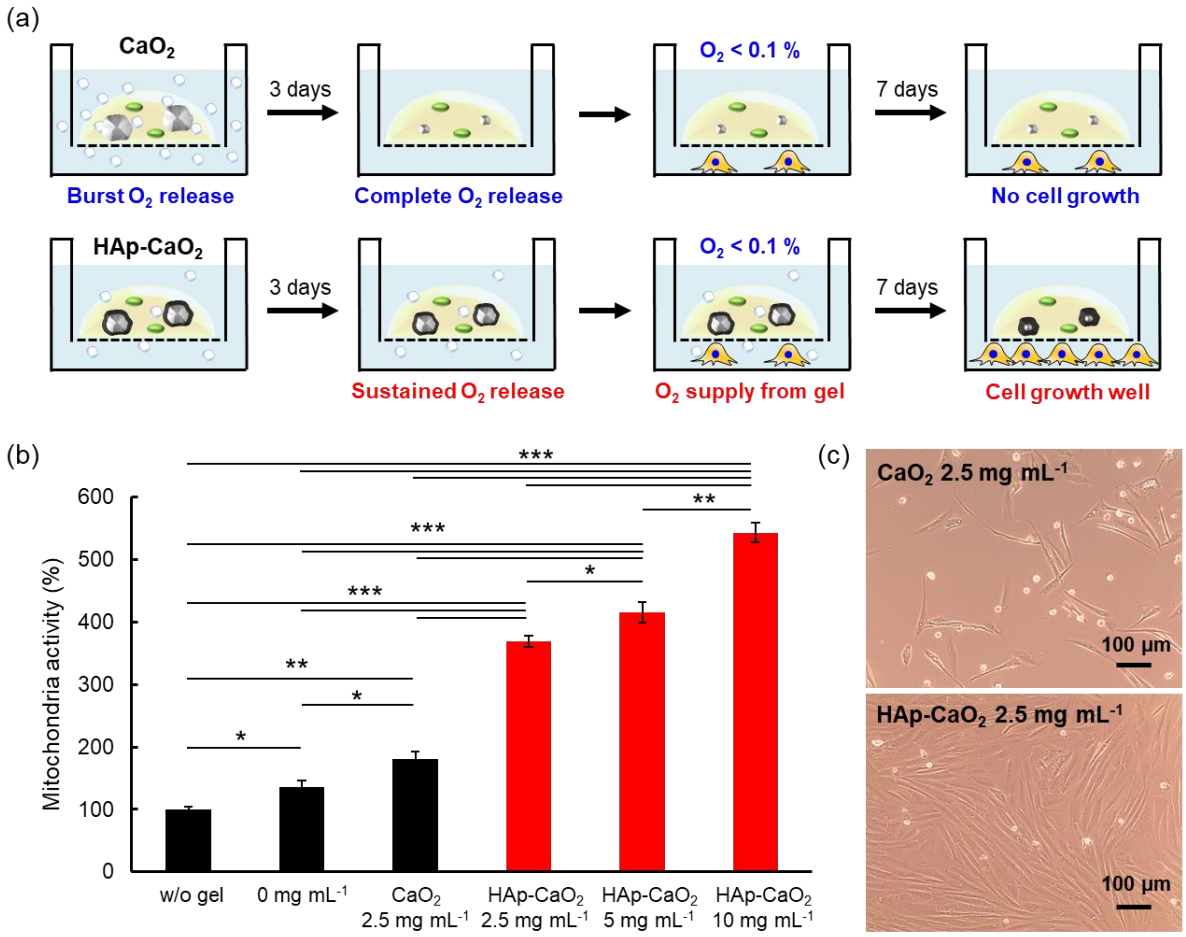

Figure 1-7. (a) Schematic illustration of the 7 days cell culture under a hypoxic condition using 3 days preincubated oxygen releasing hydrogels including CaO_2 or HAp-CaO_2. (b) Mitochondrial activity and (c) phase contrast images of NHDF after 7 days incubation under a hypoxic condition with 3 days preincubated hydrogels including 100 U mL^{-1} catalase and 2.5 mg mL^{-1} CaO_2 or various concentrations of HAp-CaO_2 (500 mM PB). Mitochondrial activity of each sample was standardized from the relative values as compared to 100 % for that of a cell culture without hydrogel. All data are representative of three independent experiments, mean ± SD. *$p < 0.05$, **$p < 0.01$ and ***$p < 0.001$.

1.3.5 Construction of 3D tissue in the presence of oxygen releasing hydrogel

To evaluate the effect of oxygen supply from the hydrogels on the construction of thick 3D tissue, 3D tissue was fabricated using mouse L929 fibroblast cells in the presence of oxygen releasing hydrogel as shown in **Figure 1-8a**. It is already reported that limited diffusion of oxygen causes cell death inside of the L929 tissues.[29] After 3 days tissue culture in the absence

or presence of oxygen releasing hydrogel, the morphology of the constructed 3D tissue was investigated by HE staining. In the absence of hydrogel, HE staining image showed many gaps in the 3D tissue (**Figure 1-8b**). On the other hand, in the presence of oxygen releasing hydrogel, HE staining image showed thick 3D tissue with high cell density (**Figure 1-8c**). For the quantitative evaluation, cell densities around the center area were calculated from HE staining images. Compared to the tissue culture in the absence of hydrogel, cell density was significantly higher in the presence of oxygen releasing hydrogel (**Figure 1-8d**). Furthermore, fluorescence images showed that the fluorescence derived from actin (red) is stronger in the presence of oxygen releasing hydrogel (**Figure 1-8e**). These results clearly suggested that oxygen supply from the hydrogels relieved oxygen shortage in the 3D tissue.

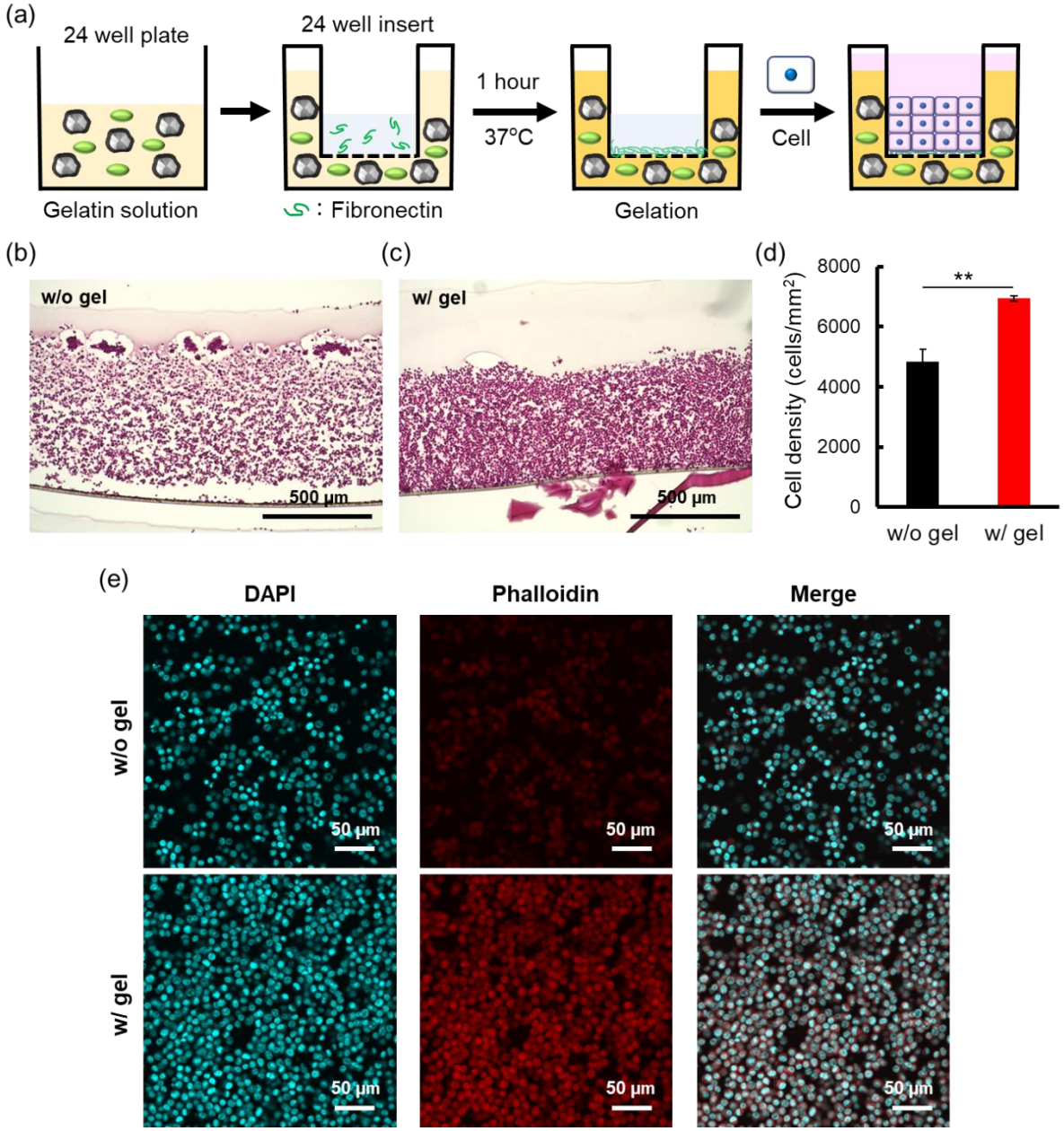

Figure 1-8. (a) Schematic illustration of the construction of 3D tissue in the presence of oxygen releasing hydrogels including HAp-CaO_2. Histological images of the 3D tissue constructed (b) in the absence of hydrogel and (c) in the presence of oxygen releasing hydrogel. Samples were stained hematoxylin (purple) and eosin (pink). (d) Cell densities around the center area of HE staining images analyzed by ImageJ. For the calculation of cell density in the HE staining images, cell number in the five areas were counted per each tissue. The data are representative of three independent tissues, mean ± SD. $^{**}p < 0.01$ (e) Fluorescence images of nuclei and actin in the 3D tissue stained with DAPI (blue) and phalloidin (red), respectively observed by CLSM.

1.4 Conclusion

In chapter 1, the author introduces a simple strategy to prepare HAp coated CaO_2 microparticles just by immersing CaO_2 in a PB. Since the HAp coating on CaO_2 acts as diffusion barrier and thus delays the reaction with water, both the usual initial burst release of oxygen was suppressed and a sustained oxygen release behavior were achieved. In addition, there was a clear relationship between the HAp amount on CaO_2 and PB concentration, which enabled PB concentration-dependent oxygen release from CaO_2. Since HAp coating on CaO_2 is a very simple procedure and highly effective for sustained oxygen release, application of this novel method to existing or yet to be developed oxygen releasing materials is greatly anticipated.

The author demonstrates this at the example of gelatin hydrogels, one of the most applied hydrogel materials in tissue engineering. Oxygen releasing gelatin hydrogels enzymatically crosslinked by TG were successfully fabricated using catalase and HAp-CaO_2 because the HAp coating on CaO_2 suppressed the burst release of hydrogen peroxide, which inactivated TG. Hydrogels crosslinked by enzymatic reactions are highly biocompatible and often applied for *in vitro*/*vivo* experiments. Thus, HAp-CaO_2 provides a broader range of material designs for oxygen releasing materials. Hydrogels including HAp-CaO_2 released oxygen for 10 days compared to only three days for the hydrogel including uncoated CaO_2. In the previous study, Leijten and co-workers reported 12 days of oxygen release from gelatin methacryloyl hydrogel containing polycaprolactone/CaO_2 composite microspheres with diameter around 5 μm.[30] Therefore, oxygen release period of this system is comparable to that of previously reported oxygen releasing materials using hydrophobic polymers. In addition, M.

Akashi and co-workers reported the transplantation of 3D artificial human vascular tissues with thickness around 50 μm and they showed that the implanted artificial human vascular networks were connected to the host blood vessel within two weeks after the transplantation.[31] Therefore, if 3D tissues with oxygen releasing scaffolds including HAp-CaO_2 are transplanted, suppression of the cell death due to oxygen shortage is expected by 10 days oxygen supply before the connection to the host blood vessel. In vitro experimanets confirmed that sustained oxygen supply from hydrogels improved proliferation of various cell types under a hypoxic condition. Therefore, the author proposes that HAp-CaO_2 and these oxygen releasing hydrogels show great potential for solving the oxygen shortage problem in regenerative medicine and tissue engineering fields.

1.5 References

[1] T. Shimizu, H. Sekine, J. Yang, Y. Isoi, M. Yamato, A. Kikuchi, E. Kobayashi, T. Okano, *FASEB.J.* **2006**, *6*, 708.
[2] D. Kouroupis, D. Correa, *Front. Bioeng. Biotechnol.* **2021**, *9*, 621748.
[3] N. G. A. Willemen, S. Hassan, M. Gurian, J. Li, I. E. Allijn, S. R. Shin, J. Leijten, *Trends Biotechnol*. **2021**, *39*, 1144.
[4] S. Park, K. M. Park, *Biomaterials* **2018***, 182,* 234.
[5] M. S. Shojai, M. T. Khorasani, E. D. Khoshdargi, A. Jamshidi, *Acta Biomater.* **2013**, *9*, 7591.
[6] K. H. Prakash, R. Kumar, C. P. Ooi, P. Cheang, K. A. Khor, *Langmuir* **2006**, *22*, 11002.
[7] S. Bhat, U. T. Uthappa, T. Altalhi, H. Y. Jung, M. D. Kurkuri, *ACS Biomater. Sci. Eng.* **2022**, *8*, 4039.
[8] L. Lorand, R. M. Graham, *Nat. Rev. Mol. Cell Biol.* **2003**, *4*, 140.
[9] G. Yang, Z. Xiao, X. Ren, H. Long, H. Qian, K. Ma, Y. Guo, *PeerJ* **2016**, *4*, e2497.
[10] Y. Zhou, S. Liao, Y. Chu, B. Yuan, X. Tao, X. Hu, Y. Wang, *Biofabrication* **2021**, *13*, 045026.
[11] C. A. Zbaraszczuk, H. Ozcelik, F. Meyerab, O. Galletc, P. Lavalleab, V. Ballab, C. M. Ghimbeu, P. Schaaf, H. K. Marques, *RSC Adv.* **2017**, *7*, 5528.
[12] M. A. Prieto, X. Biarnés, P. Vidossich, C. Rovira, *J. Am. Chem. Soc.* **2009**, *131*, 11751.
[13] E. A. Nagul, I. D. McKelvie, P. Worsfold, S. D. Kolev, *Anal. Chim. Acta.* **2015**, *890*, 60.
[14] T. J. Han, *J. Am. Oil*. *Chem. Soc*. **1995**, *72,* 881.
[15] F. Louis, Y. Sowa, S. Kitano, M. Matsusaki, *Bioact. Mater.* **2022**, *7*, 227.
[16] Y. Ma, B. T. Zhang, L. Zhao, G. Guo, J. M. Lin, *Luminescence* **2007**, *22*, 575.
[17] A. Northup, D. Cassidy, *J. Hazard. Mater.* **2008**, *152*, 1164.
[18] H. Wang, Y. Zhao, T. Li, Z. Chen, Y. Wang, C. Qin, *Chem. Eng. J.* **2016**, *303*, 450.
[19] X. Li, Y. Xie, F. Jiang, B. Wang, Q. Hu, Y. Tang, T. Luo, T. Wu, *Sci. Total Environ.* **2020**, *709*, 136123.

[20] X. Zhao, M. C. Nguyen, C. Z. Wang, K. M. Ho, *RSC Adv*. **2013**, *3*, 22135.
[21] A. Haider, S. Haider, S. S. Hanb, I. K. Kang, *RSC Adv.* **2017***, 7,* 7442.
[22] S. Koutsopoulos, *J. Biomed. Mater. Res.* **2002***, 62,* 600.
[23] M. C. Yi, A. V. Melkonian, J. A. Ousey, C. Khosla, *J. Biol. Chem.* **2018***, 293,* 2640.
[24] S. Boonvisut, A. Aksnes, L. R. NJAA, *Food Chem.* **1982***, 9,* 183.
[25] V. D. Santis, M. Singer, *Br. J. Anaesth.* **2015***, 115*, 357.
[26] A. S. Karanfil, F. Louis, M. Matsusaki, *Mater. Horiz.* **2023**, *10*, 1539.
[27] B. A. Wagner, S. Venkataraman, G. R. Buettner, *Free. Radic. Biol. Med.* **2011***, 51*, 700.
[28] A. Sendoel, M. O. Hengartner, *Physiology* **2014**, *29*, 168.
[29] A. I. Neto, C. R. Correia, M. B. Oliveira, M. I. R. Hermida, C. A. Lorenzo, R. L. Reis, J. F. Mano, *Biomater. Sci.* **2015**, *3*, 581.
[30] A. Farzin, S. Hassan, L. S. M. Teixeira, M. Gurian, J. F. Crispim, V. Manhas, A. Carlier, H. Bae, L. Geris, I. Noshadi, S. R. Shin, J. Leijten, *Adv. Funct. Mater.* **2021***, 31*, 2100850.
[31] Y. Asano, H. Shimoda, D. Okano, M. Matsusaki, M. Akashi, *J. Tissue Eng. Regen. Med.* **2017**, *11*, 1303.

Chapter 2

Controlled Release of Oxygen from Calcium Peroxide in a Weak Acidic Condition by Stabilized Amorphous Calcium Carbonate Coating

2.1 Introduction

In Chapter 1, the author found that HAp nanocrystals are formed on the CaO_2 surface in PB because $Ca(OH)_2$ derived from the CaO_2 reacts with phosphate to form HAp. Since the HAp coating on CaO_2 acts as a diffusion barrier, the reaction between CaO_2 and water was suppressed, which enabled sustained oxygen supply. On the other hand, it is well known that $Ca(OH)_2$ reacts with sodium hydrogen carbonate ($NaHCO_3$) to form calcium carbonate ($CaCO_3$).[1] Thus, $CaCO_3$ formation on CaO_2 is also expected in $NaHCO_3$ solution as with HAp formation in PB.

However, it is reported that formation of $CaCO_3$ crystals from calcium and carbonate ions goes through a complex pathway via a kinetically stabilized metastable phase, called amorphous calcium carbonate (ACC).[2,3] During the process of $CaCO_3$ crystal formation, ACC nanoparticles are formed by the reaction between calcium and carbonate ions initially, then ACC crystallizes to $CaCO_3$ crystals such as calcite and vaterite. However, it is reported that direct transformation from ACC to $CaCO_3$ crystals is less likely to progress due to the high energy barrier.[2,3] Therefore, a dissolution-reprecipitation process is now commonly considered for the crystallization mechanism of ACC.[3-7] In the dissolution-reprecipitation process, once $CaCO_3$ crystals form in solution, they consume ions as they grow, reducing the number of ions in the solution. When the ion concentrations drop to below the solubility of ACC, ACC starts to dissolve, which provides ions to $CaCO_3$ crystals. On the other hand, stabilization of ACC nanoparticles by additives has also been reported in recent years.[7-11] Although the mechanism is not yet fully understood, it is considered that additives such as Mg[7,8] and phosphates[9-11] suppress the crystal growth of calcite. As a result, the dissolution-reprecipitation process of ACC is suppressed and direct transformation from ACC to $CaCO_3$ crystals occurs over a longer period.

Based on the $CaCO_3$ chemistry, the author introduces a new surface chemistry of CaO_2

in a cell culture medium, which dramatically affects oxygen release behavior of CaO_2. In this chapter, stabilized ACC coating on CaO_2 in $NaHCO_3$ solution including phosphate ions which is a model solution for a cell culture medium is reported. Oxygen release from CaO_2 was suppressed because ACC formation on CaO_2 acts as a diffusion barrier to water. In $NaHCO_3$ solution without additives, $CaCO_3$ formation on CaO_2 did not occur because of the dissolution-reprecipitation process of ACC (**Figure 2-1**). On the other hand, in the presence of phosphate ions, ACC was stabilized by them, which suppressed the dissolution-reprecipitation of ACC. As a result, stabilized ACC nanocoating on CaO_2 suppressed the reaction with water (**Figure 2-1**). Since Dulbecco's Modified Eagle Medium (DMEM), which is one of the most common cell culture media, also includes $NaHCO_3$ and phosphate ions, the same phenomenon was also confirmed in DMEM. Furthermore, pH-dependent oxygen release from ACC-CaO_2 was also observed in DMEM because ACC nanoparticles easily dissolves in an acidic condition.[12] It is well known that the environments in ischemic tissue and cancer are weakly acidic.[13,14] Thus, pH-dependent oxygen release from ACC-CaO_2 in cell culture conditions is an attractive function for oxygen releasing materials and cancer drugs. This study provides the basis for the surface chemistry of CaO_2 in a cell culture medium, which is important for the application of CaO_2 to cells and tissues.

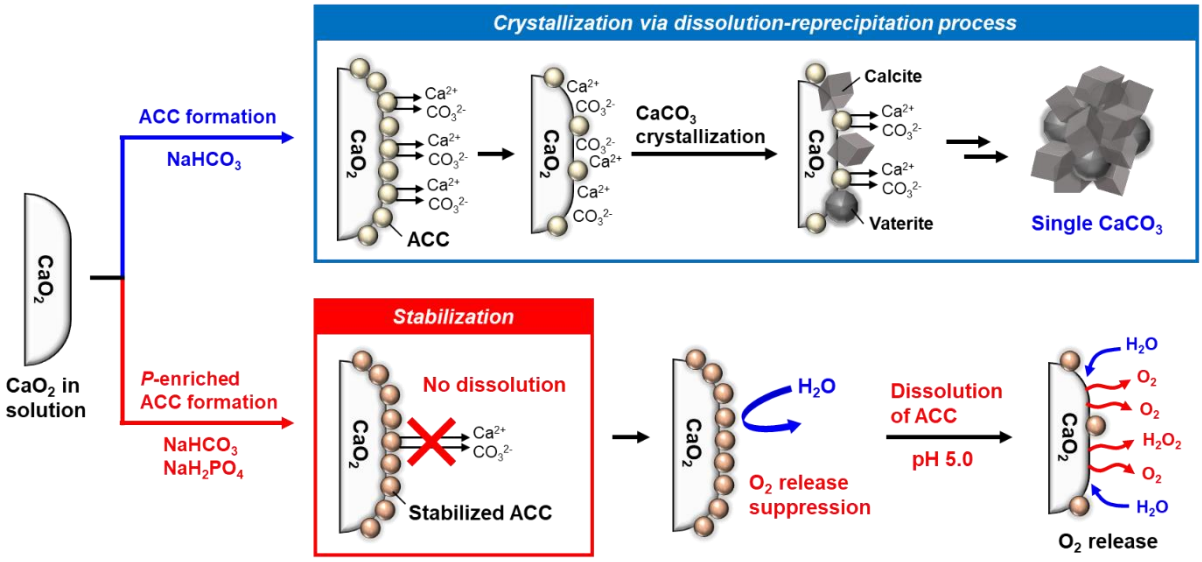

Figure 2-1. Schematic illustration of the suppression of oxygen release and pH-dependent oxygen release from CaO_2 by stabilized amorphous calcium carbonate (ACC) formation on CaO_2 using $NaHCO_3$ and NaH_2PO_4.

2.2 Experiments

2.2.1 Materials

Calcium peroxide (CaO_2) (particle size < 200 mesh (74 μm)) and HEPES sodium salt were purchased from Sigma-Aldrich (Missouri, USA). Sodium dihydrogen phosphate (NaH_2PO_4), disodium hydrogenphosphate 12-water and 5 mol L^{-1} hydrochloric acid (HCl) were purchased from FUJIFILM Wako Pure Chemical Corporation (Osaka, Japan). Dulbecco's modified Eagle medium (DMEM) (transparent; 08489-45), sodium hydrogen carbonate ($NaHCO_3$) and calcium hydroxide ($Ca(OH)_2$) were purchased from Nacalai Tesque (Kyoto, Japan).

2.2.2 Oxygen and hydrogen peroxide release behavior of CaO_2 in $NaHCO_3$ solutions

Oxygen and hydrogen peroxide release behavior of CaO_2 was measured as previously reported.[15] Ten milligrams of CaO_2 was dispersed in 10 mL of $NaHCO_3$ (44 mM) including 0, 0.01, 0.1 and 1 mg mL^{-1} NaH_2PO_4, 1 and 10 mM $NaHCO_3$, 44 mM HEPES (pH 7.4) and ultrapure water (MilliQ, Merck, Darmstadt, Germany) including 0 and 0.1 mg mL^{-1} NaH_2PO_4 in a sample tube. Multiparameter DO Meter (HANNA, Woonsocket, USA) was then immersed in the solution. The dissolved oxygen concentrations in several solutions were measured at room temperature.

Five milligrams of CaO_2 was dispersed in 5 mL of HEPES (44 mM) and $NaHCO_3$ (44 mM) including 0 and 0.1 mg mL^{-1} NaH_2PO_4. After 30 min incubation at room temperature, the hydrogen peroxide concentration in each solution was measured using an Oxiselect Hydrogen Peroxide/Peroxidase Assay Kit (Fluorometric) (STA-344, Cell Biolabs Inc., San Diego, USA) as previously reported.[15]

2.2.3 Analysis of surface structural changes of CaO_2 immersed in $NaHCO_3$ solutions

CaO_2 was immersed in 44 mM $NaHCO_3$ including 0, 0.1 and 1 mg mL^{-1} NaH_2PO_4 at a concentration of 1 mg mL^{-1} for 30 min at room temperature. The resulting samples were collected by centrifugation at 4,000 rpm for 3 min and then washed three times by ethanol. Washed samples were dried under reduced pressure at room temperature. Characterization of

samples by SEM (JSM-6701F, JEOL Ltd., Tokyo, Japan), SEM-EDX (Miniscope TM 3000 equipped with Swift ED 3000, Hitachi Ltd., Tokyo, Japan), XRD (AERIS, Malvern Panalytical, Malvern, UK) and FT-IR (FT-720, HORIBA, Kyoto, Japan) were performed. For the SEM, samples were sputter-coated with osmium (HPC-30 Plasma Coater,Vacuum Device, Ibaraki, Japan).

2.2.4 Characterization of the precipitates obtained by mixing $Ca(OH)_2$ and $NaHCO_3$ solutions

Five mL of $Ca(OH)_2$ solution (1 mg mL^{-1}) was mixed with 4.4 mL of $NaHCO_3$ solution (100 mM) and 600 μL of NaH_2PO_4 solution (0, 1.67 and 16.7 mg mL^{-1}) so that the final concentrations were 0.5 mg mL^{-1} $Ca(OH)_2$, 44 mM $NaHCO_3$ and 0, 0.1 and 1 mg mL^{-1} NaH_2PO_4, respectively. After 1 min incubation at room temperature, obtained precipitates were collected by centrifugation at 4,000 rpm for 3 min and then washed three times by ethanol. Washed samples were dried under reduced pressure at room temperature. SEM, EDX, XRD and FT-IR measurements of precipitates were performed as mentioned above.

2.2.5 Oxygen release behavior of CaO_2 in a cell culture medium at different pH

HAp-CaO_2 was prepared as previously reported.[15] Ten milligrams of CaO_2 was immersed in 500 mM phosphate buffer at a concentration of 1 mg mL^{-1}. After 1 h incubation at 37°C, the sample was collected by centrifugation at 4,000 rpm for 3 min. Collected HAp-CaO_2 or 10 mg of CaO_2 was dispersed in 10 mL of DMEM at neutral pH in a sample tube. A DO meter was immersed in DMEM and the dissolved oxygen concentration was measured at room temperature as mentioned above. After 30 min measurement, the sample was collected by centrifugation at 4,000 rpm for 3 min and then redispersed in 10 mL of DMEM at pH 5.0. Dissolved oxygen concentration in acidic DMEM was measured at room temperature for 30 min. HAp-CaO_2 immersed in an acidic cell culture medium was also characterized to understand oxygen release behavior. The resulting HAp-CaO_2 after the immersion in acidic DMEM were collected by centrifugation at 4,000 rpm for 3 min and then washed three times by ethanol. Washed samples were dried under reduced pressure at room temperature. SEM and XRD measurements of the sample were performed as mentioned above.

2.3 Results and discussion

2.3.1 Oxygen and hydrogen peroxide release behavior of CaO_2 in $NaHCO_3$ solutions

Oxygen release behaviors of CaO_2 in $NaHCO_3$ solutions including NaH_2PO_4 were evaluated by measuring the dissolved oxygen amount in the solutions after the addition of 1 mg mL^{-1} CaO_2. Herein, 100 % indicates equilibrium with oxygen in the atmosphere. Since DMEM contains 44 mM $NaHCO_3$ and 0.1 mg mL^{-1} NaH_2PO_4, 44 mM $NaHCO_3$ solutions with various concentrations of NaH_2PO_4 were evaluated initially (**Figure 2-2a**). Below 0.01 mg mL^{-1} NaH_2PO_4, CaO_2 showed burst release of oxygen and dissolved oxygen concentrations increased to around 180% after 30 min incubation probably because ACC or $CaCO_3$ crystals were not formed on the CaO_2 surface due to the dissolution-reprecipitation process as shown in **Figure 2-1**. On the other hand, dissolved oxygen concentrations were stable at around 100 % in 44 mM $NaHCO_3$ including 0.1 and 1 mg mL^{-1} NaH_2PO_4, indicating that oxygen release from CaO_2 was dramatically suppressed. This result suggested that formation of ACC stabilized by phosphate ions on CaO_2 suppressed the reaction with water above 0.1 mg mL^{-1} NaH_2PO_4. To evaluate the effect of $NaHCO_3$ concentrations on the oxygen release behavior of CaO_2, the dissolved oxygen concentration was measured in 10 and 1 mM $NaHCO_3$ including 0 and 0.1 mg mL^{-1} NaH_2PO_4 (**Figure 2-2b,c**). In the presence of 0.1 mg mL^{-1} NaH_2PO_4, oxygen release from CaO_2 was suppressed above 10 mM $NaHCO_3$, probably because ACC was not well formed at 1 mM $NaHCO_3$ due to the lack of carbonate ions. In the absence of NaH_2PO_4, the dissolved oxygen concentration after 30 min incubation increased from 139 to 164 and 180 % as the $NaHCO_3$ concentration increased from 1 to 10 and 44 mM. It has already been reported that the reaction speed of CaO_2 is slower in a basic condition.[16] Since $NaHCO_3$ has a buffering effect, it is suggested that this trend is derived from pH differences during the CaO_2 reaction in each of the $NaHCO_3$ solutions. As a control, dissolved oxygen concentrations were also measured in 44 mM 4-(2-hydroxyethyl)piperazine-1-ethanesulfonic acid (HEPES) buffer (pH 7.4) and ultrapure water (MilliQ) including 0 and 0.1 mg mL^{-1} NaH_2PO_4 (**Figure 2-2d,e**). Dissolved oxygen concentartions increased to around 180% for HEPES and 140% for MilliQ after 30 min incubation for both 0 and 0.1 mg mL^{-1} NaH_2PO_4. Since there is no surface structure change on CaO_2, oxygen release from CaO_2 was not suppressed in these conditions even in the presence of NaH_2PO_4. The author also evaluated hydrogen peroxide release from CaO_2 in 44 mM $NaHCO_3$ and HEPES including 0 and 0.1 mg mL^{-1} NaH_2PO_4 (**Figure 2-2f**). In 44 mM HEPES,

CaO_2 released 7.1 mM H_2O_2 without NaH_2PO_4 and 5.5 mM H_2O_2 in the presence of 0.1 mg mL^{-1} NaH_2PO_4. On the other hand, in 44 mM $NaHCO_3$ solution, CaO_2 released 6.2 mM H_2O_2 without NaH_2PO_4 while only 0.32 mM H_2O_2 in the presence of 0.1 mg mL^{-1} NaH_2PO_4. As with the oxygen, hydrogen peroxide release from CaO_2 was dramatically suppressed only in $NaHCO_3$ including phosphate ions. These results suggested that the reaction between CaO_2 and water was suppressed in $NaHCO_3$ including phosphate ions, probably because stabilized ACC nanocoating on CaO_2 delays this reaction.

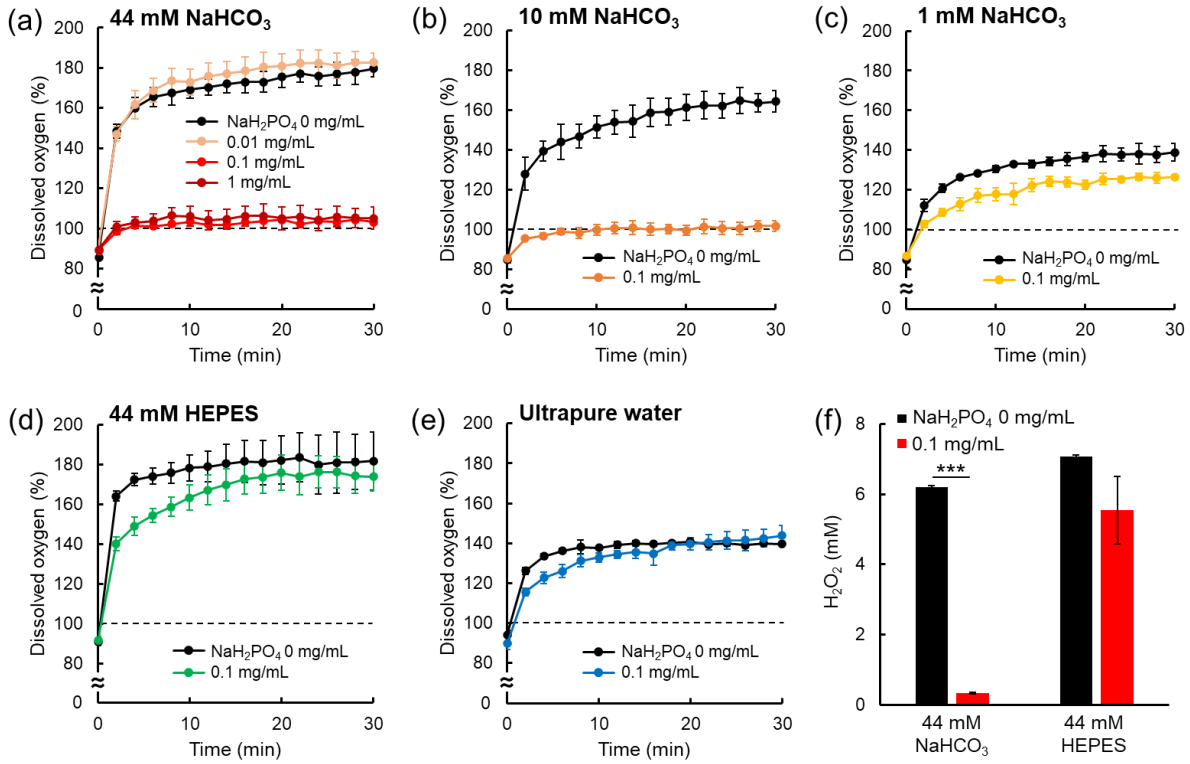

Figure 2-2. Dissolved oxygen changes in (a) 44 mM $NaHCO_3$ including 0, 0.01, 0.1 and 1 mg mL^{-1} NaH_2PO_4, (b) 10 mM and (c) 1 mM $NaHCO_3$, (d) 44 mM HEPES (pH 7.4) and (e) ultrapure water including 0 and 0.1 mg mL^{-1} NaH_2PO_4 for 30 min at room temperature after the addition of 1 mg mL^{-1} CaO_2. (f) Hydrogen peroxide concentration in 44 mM $NaHCO_3$ and 44 mM HEPES including 0 and 0.1 mg mL^{-1} NaH_2PO_4 30 min after the addition of 1 mg mL^{-1} CaO_2. All data are representative of three independent experiments, mean ± SD. ***$p < 0.001$.

2.3.2 Characterization of ACC-CaO_2

To confirm the ACC formation on CaO_2, the surface morphology of CaO_2 was evaluated. **Figure 2-3a** shows scanning electron microscope (SEM) images of untreated CaO_2 and CaO_2

immersed in 44 mM $NaHCO_3$ including 0, 0.1 and 1 mg mL^{-1} NaH_2PO_4 for 30 min at room temperature. In the case of 44 mM $NaHCO_3$ without NaH_2PO_4, cubic and spherical morphologies were observed, which are the specific morphologies of $CaCO_3$ crystals such as calcite (cubic) and vaterite (sphere).[1] On the other hand, SEM showed no cubic and spherical morphology in the presence of 0.1 and 1 mg mL^{-1} NaH_2PO_4. To clarify the crystal structures, X-ray diffraction (XRD) was measured. In the case of untreated CaO_2, the peaks at 30, 36, 48, 52 and 53° were observed, which were assigned to the (002), (110), (112), (200) and (103) reflections of CaO_2.[17,18] (**Figure 2-3b**). Unlike untreated CaO_2, CaO_2 immersed in 44 mM $NaHCO_3$ without NaH_2PO_4 showed the peaks only derived from calcite and vaterite (**Figure 2-3c**), suggesting that all CaO_2 were consumed to form calcium carbonate with calcite and vaterite crystal structures. On the other hand, CaO_2 immersed in 44 mM $NaHCO_3$ including 0.1 and 1 mg mL^{-1} NaH_2PO_4 showed almost same as the peaks of untreated CaO_2 (**Figure 2-3d,e**). Fourier-transform infrared spectroscopy (FT-IR) measurement showed a band derived from the P-O stretching vibration (yellow line) around 1,020 cm^{-1} in the case of 44 mM $NaHCO_3$ including NaH_2PO_4, suggesting the formation of a phosphorus-containing substrate on CaO_2. (**Figure 2-3f**). However, the bands derived from asymmetric vibration of carbonate in ACC such as at 880 and 1,400 cm^{-1} (blue line) were not clearly observed in these conditions because these bands overlapped the bands derived from O-Ca-O bending and O-O stretching of CaO_2 (green line).[19] In the FT-IR spectrum of 44 mM $NaHCO_3$ without NaH_2PO_4, the clear bands at 700, 880 and 1,400 cm^{-1} which were assigned to symmetric and asymmetric vibration of carbonate (blue line) were clearly observed because of the formation of calcite and vaterite. Herein, the band at 700 cm^{-1} is specific to $CaCO_3$ crystals.[20] For the elemental analysis, energy dispersive X-ray spectroscopy (EDX) measurements were performed (**Figure 2-3g**). EDX spectra showed a peak derived from phosphorus at CaO_2 immersed in 44 mM $NaHCO_3$ including NaH_2PO_4. In addition, the elemental mapping of CaO_2 immersed in 44 mM $NaHCO_3$ including 0.1 and 1 mg mL^{-1} NaH_2PO_4 showed phosphorus at the same location of CaO_2 in the SEM images, suggesting the formation of a phosphorus-containing substrate on CaO_2 (**Figure 2-3h**). From the results of dissolved oxygen measurement, SEM, XRD, EDX and FT-IR, it is suggested that a mixture of amorphous calcium phosphate and ACC was formed on the surface of CaO_2, which dramatically suppressed oxygen release from CaO_2 in $NaHCO_3$ solution including NaH_2PO_4.

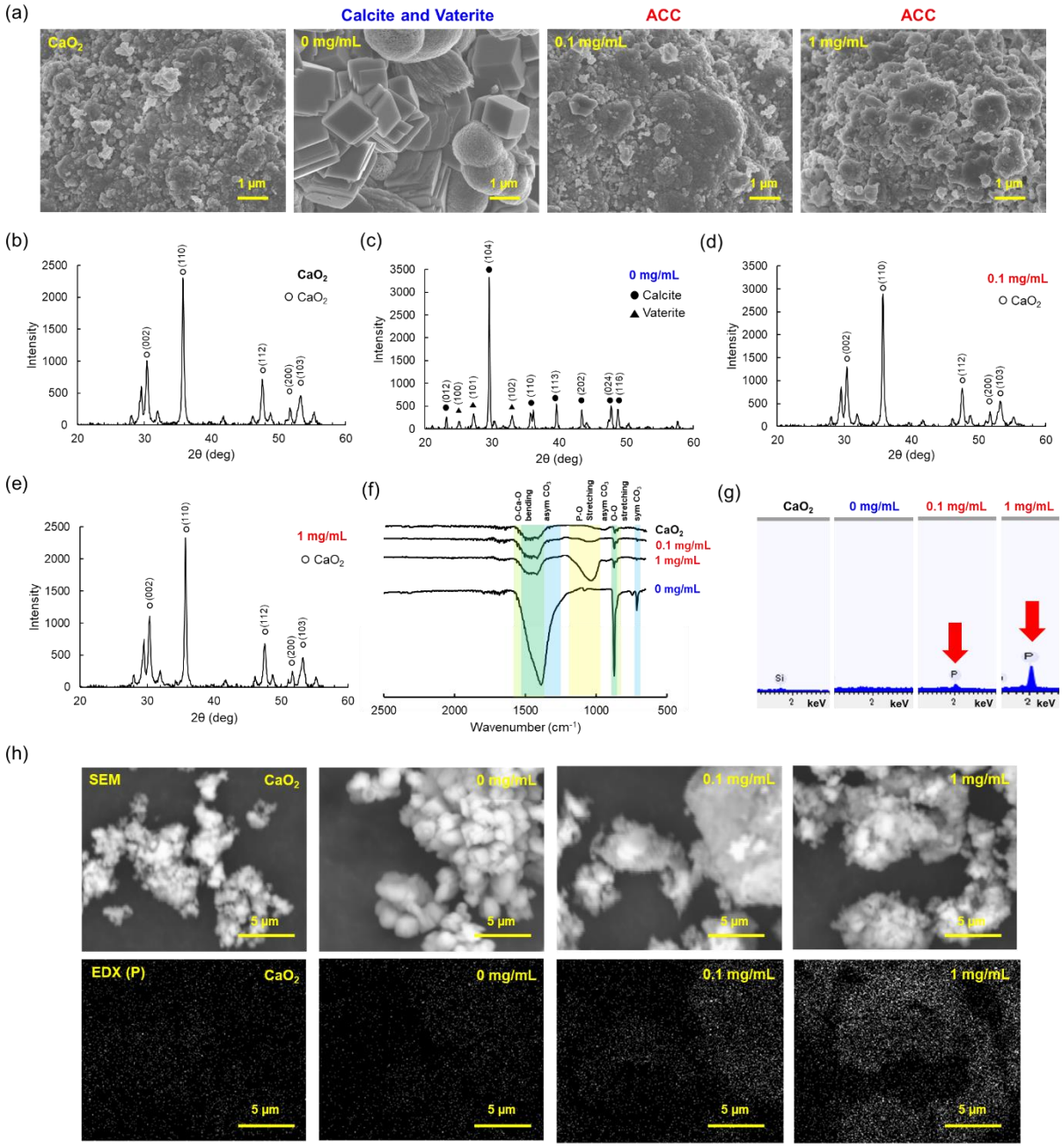

Figure 2-3. Characterization of CaO_2 immersed in 44 mM $NaHCO_3$ including 0, 0.1 and 1 mg mL^{-1} NaH_2PO_4. (a) SEM images, (b-e) XRD spectra (f) FT-IR spectra, (g) EDX spectra and (h) SEM images for EDX and elemental mapping of phosphorus of untreated CaO_2 and CaO_2 immersed in 44 mM $NaHCO_3$ including 0, 0.1 and 1 mg mL^{-1} NaH_2PO_4 for 30 min at room temperature.

2.3.3 ACC formation by the reaction of $Ca(OH)_2$ and $NaHCO_3$ solutions

In **Figure 2-3**, characterization of ACC on CaO_2 was confounded by the existence of solid CaO_2. Therefore, characterizations of the precipitates obtained by mixing $Ca(OH)_2$ solution and 44 mM $NaHCO_3$ solution including 0, 0.1 and 1 mg mL^{-1} NaH_2PO_4 were conducted because ACC and $CaCO_3$ crystals were produced by the reaction between $Ca(OH)_2$ derived from CaO_2 and $NaHCO_3$. The SEM image of precipitate obtained from $NaHCO_3$ without NaH_2PO_4 showed a cubic morphology, which is specific to calcite (**Figure 2-4a**). On the other hand, precipitates obtained from $NaHCO_3$ including NaH_2PO_4 did not show such a cubic morphology. In addition, elemental analysis by SEM-EDX confirmed that these precipitates contained phosphorus (**Figure 2-4b**). To clarify the crystal structure of precipitates, XRD was measured (**Figure 2-4c-e**). In both $NaHCO_3$ including 0 and 0.1 mg mL^{-1} NaH_2PO_4, the precipitates showed peaks derived from calcite. On the other hand, precipitates obtained from $NaHCO_3$ including 1 mg mL^{-1} NaH_2PO_4 did not show any peaks, suggesting that the obtained precipitate was in an amorphous phase. Interestingly, SEM images of precipitates obtained from 0.1 and 1 mg mL^{-1} NaH_2PO_4 showed a similar morphology while XRD results showed the peaks derived from calcite only in the case including 0.1 mg mL^{-1} NaH_2PO_4. These results suggested direct transformation from ACC to calcite at the precipitate as previsouly reported.[10,11] ACC formation was also confirmed using FT-IR (**Figure 2-4f**). It is reported that the band derived from carbonate at around 700 cm^{-1} is specific to $CaCO_3$ crystals while the band derived from OH at around 3,000 cm^{-1} is specific to ACC.[20] In the case including NaH_2PO_4, a broad band between 2,700 to 3,600 cm^{-1}, which was assigned to the OH stretching vibration, was observed in the precipitates (blue line). Furthermore, the band at 700 cm^{-1} derived from the symmetric vibration of carbonate in $CaCO_3$ crystals was not clearly observed in these precipitates (purple line). The remaining bands at 800 and 1,400 cm^{-1} were assigned to the asymmetric vibration of carbonate in both ACC and calcite (green line). These results confirmed that ACC stabilized by phosphate ions was formed by the reaction between $Ca(OH)_2$ and $NaHCO_3$ including NaH_2PO_4. Therefore, it is suggested that oxygen release from CaO_2 in $NaHCO_3$ solution including NaH_2PO_4 was suppressed because ACC stabilized by phosphate ions was formed on the CaO_2 surface.

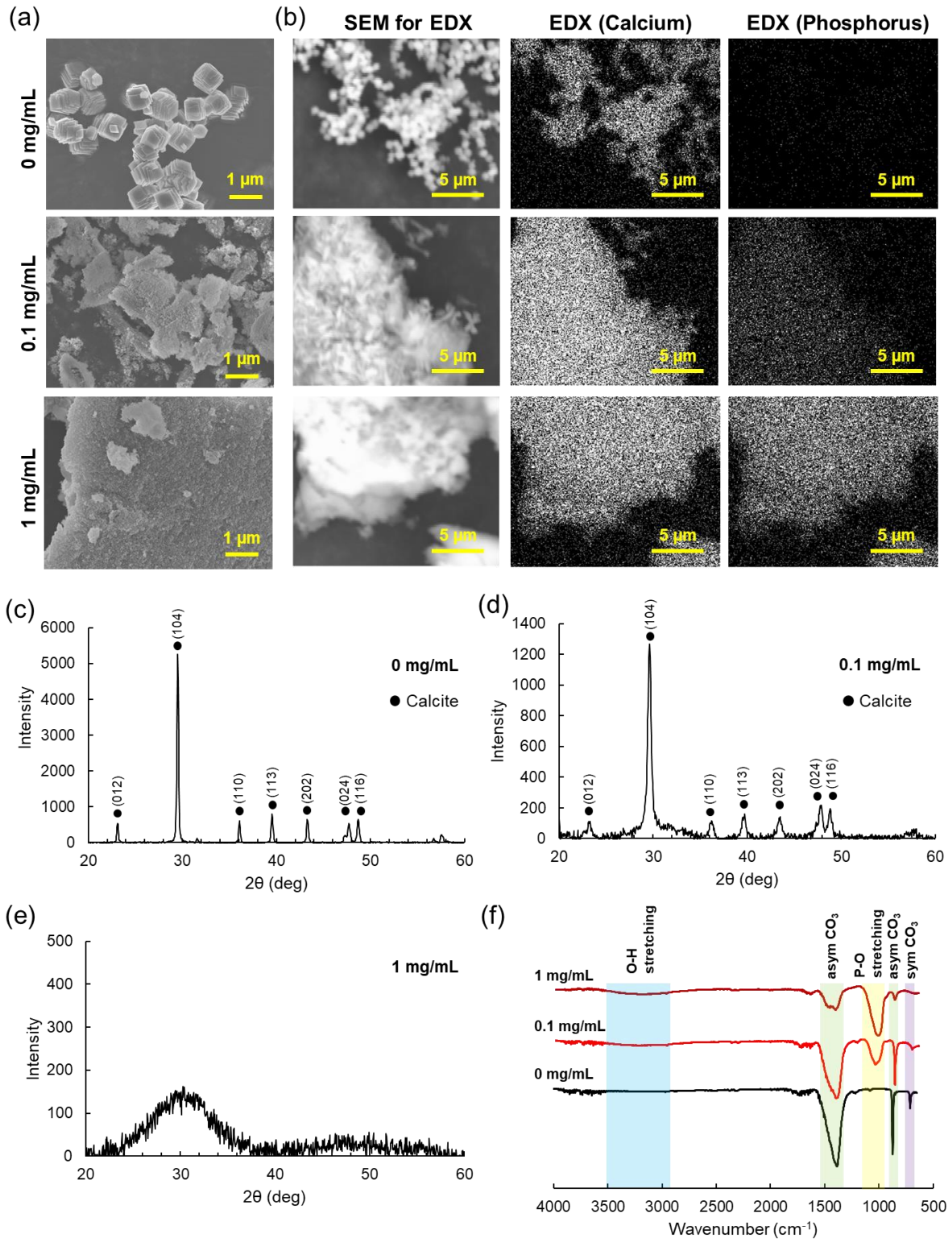

Figure 2-4. (a) SEM images, (b) SEM images for EDX, elemental mapping of calcium and phosphorus (c-e) XRD spectra and (f) FT-IR spectra of the precipitates obtained by mixing 0.5 mg mL^{-1} $Ca(OH)_2$ and 44 mM $NaHCO_3$ including 0, 0.1 and 1 mg mL^{-1} NaH_2PO_4 for 1 min at room temperature.

2.3.4 pH-dependent oxygen release behavior of ACC-CaO_2

It has been reported that the solubility of ACC nanoparticles increases in an acidic condition.[12] Thus, it is expected that ACC formed on CaO_2 dissolves in an acidic condition, which enables pH-dependent oxygen release in a cell culture medium. To evaluate this pH responsiveness, the oxygen release behavior of CaO_2 in DMEM at pH 5.0 was measured after measuring in DMEM at a neutral pH (**Figure 2-5a**). At a neutral pH, oxygen release from CaO_2 was suppressed in DMEM because DMEM contains 44 mM $NaHCO_3$ and 0.1 mg mL^{-1} NaH_2PO_4, which produced stabilized ACC on CaO_2. The ACC-CaO_2 in DMEM was then collected by centrifugation and dispersed in DMEM at pH 5.0. In acidic DMEM, oxygen release from ACC-CaO_2 was clearly observed, probably because ACC on CaO_2 dissolved in an acidic condition, which enabled the reaction between CaO_2 and water. pH-dependent oxygen release was also evaluated in CaO_2 coated with HAp (HAp-CaO_2). Compared to ACC-CaO_2, HAp-CaO_2 did not show active oxygen release in a weak acidic condition. An SEM image of HAp-CaO_2 immersed in acidic DMEM showed a porous structure and an XRD spectrum showed the peaks derived from HAp and CaO_2 (**Figure 2-5b,c**). Thus, pH-dependent oxygen release from HAp-CaO_2 was not achieved because HAp on CaO_2 did not dissolve in a weak acidic condition.

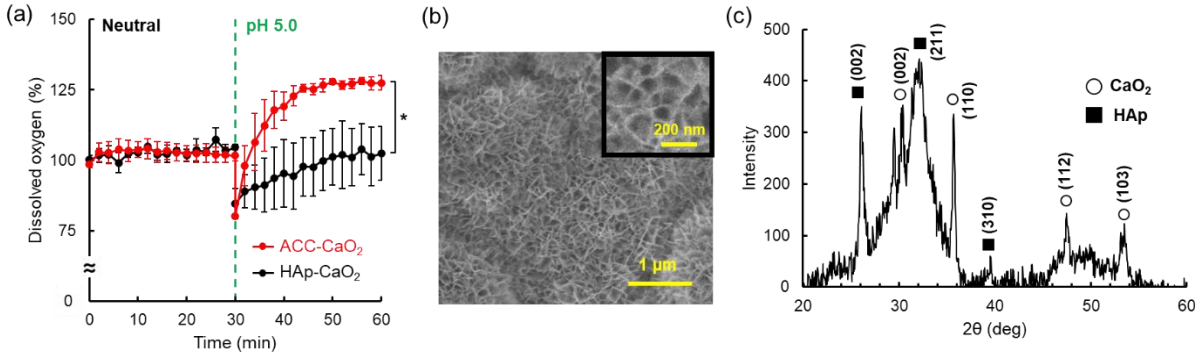

Figure 2-5. Controlled release of oxygen in a weak acidic condition from ACC-CaO_2 (a) Dissolved oxygen changes in DMEM at neutral and subsequent acidic pH after the addition of 1 mg mL^{-1} CaO_2 and HAp-CaO_2 for 60 min. After 30 min incubation in DMEM at neutral pH, the incubated CaO_2 was collected by centrifugation and then incubated in DMEM at pH 5.0 for an additional 30 min. HAp-CaO_2 was prepared by immersing CaO_2 in 500 mM phosphate buffer for 1 h at 37 °C. (b) SEM image and (c) XRD spectrum of HAp-CaO_2 immersed in acidic DMEM at pH 5.0 for 30 min at room temperature. The data are representative of three independent experiments, mean ± SD. *$p < 0.05$.

2.4 Conclusion

Based on the $CaCO_3$ chemistry, the author reported stabilized ACC coating on CaO_2 in a cell culture medium, which suppressed the reaction between CaO_2 and water. Stabilized ACC was produced by the reaction between $Ca(OH)_2$ derived from CaO_2 and $NaHCO_3$ including NaH_2PO_4 in a cell culture medium. In contrast, surface modification of CaO_2 by calcium carbonate crystals was difficult due to the crystallization process via dissolution-reprecipitation. To the best of the author's knowledge, there are no reports of such a surface chemistry of CaO_2 in cell culture conditions. In other words, many researchers used CaO_2 in cell culture conditions for tissue engineering and cancer therapies without noticing ACC formation on CaO_2. In addition, pH-dependent oxygen release from ACC-CaO_2 was also observed in DMEM probably because ACC on CaO_2 dissolved in a weak acidic condition. Although many researchers who used CaO_2 for cancer therapies have mentioned the specific dissolution behavior of CaO_2 in weak acidic cancer environments,[21,22] the detailed mechanism has not been widely discussed. In this research, the author found that CaO_2 easily dissolved even in the HEPES with neutral pH. Thus, it is suggested that nanoscale surface chemistry of CaO_2 is related to the previously reported dissolution behavior of CaO_2 in cancer drugs in the weak acidic cancer environment. Since ACC coating on CaO_2 dramatically affected the oxygen release behavior, these findings should be important for the application of CaO_2 in tissue engineering and cancer therapies.

2.5 References

[1] Y. Q. Niu, J. H. Liu, C. Aymonier, S. Fermani, D. Kralj, G. Falini, C. H. Zhou, *Chem. Soc. Rev.* **2022**, *51*, 7883.

[2] D. Gebauer, A. Völkel, H. Cölfen, *Science* **2008**, *322*, 1819.

[3] J. J. D. Yoreo, P. U. P. A. Gilbert, N. A. J. M. Sommerdijk, R. L.Penn, S. Whitelam, D. Joester, H. Zhang, J. D. Rimer, A. Navrotsky, J. F. Banfield, A. F. Wallace, F. M. Michel, F. C. Meldrum, H. Cölfen, P. M. Dove, *Science* **2015**, *349*, aaa6760.

[4] M. H. Nielsen, S. Aloni, J. J. D. Yoreo, *Science* **2014**, *345*, 1158.

[5] J. Ihli, W. C. Wong, E. H. Noel, Y. Y. Kim, A. N. Kulak, H. K. Christenson, M. J. Duer, Fi. C. Meldrum, *Nat. Commun*. **2014**, *5*, 3169.

[6] P. Bots, L. G. Benning, J. D. R. Blanco, T. R. Herrero, S. Shaw, *Cryst. Growth Des.* **2012**, *12*, 3806

[7] Z. Liu, Z. Zhang, Z. Wang, B. Jin, D. Li, J. J. D. Yoreo, *Proc. Natl. Acad. Sci. U. S. A.* **2020**, *117*, 3397.

[8] M. Albéric, L. Bertinetti, Z. Zou, P. Fratzl, W. Habraken, Y. Politi, *Adv. Sci*. **2018**, *5*, 1701000.
[9] Z. Zou, X. Yang, M. Albéric, T. Heil, Q. Wang, B. Pokroy, Y. Politi, L. Bertinetti, *Adv. Funct. Mater.* **2020**, *30*, 2000003.
[10] Z. Zou, J. Xie, E. M. Sánchez, Z. Fu, *Cryst. Growth Des.* **2021**, *21*, 414.
[11] S. Kababya, A. Gal, K. Kahil, S. Weiner, L. Addadi, A. Schmidt, *J. Am. Chem. Soc.* **2015**, *137*, 990
[12] M. Wang, B. Zhou, L. Wang, F. Zhou, N. Smith, D. Saunders, R. A. Towner, J. Song, J. Qu, W. R. Chen, *J. Mater. Chem. B* **2020**, *8*, 8261.
[13] G. X. Yan, A. G. Kléber, *Circ. Res.* **1992**, *71*, 460.
[14] I. F. Tannock, D. Rotin, *Cancer Res.* **1989**, *49*, 4373.
[15] D. Tomioka, S. Fujita, J. Groll, M. Matsusaki, *Chem. Mater.* **2023**, *35*, 5378.
[16] H. Wang, Y. Zhao, T. Li, Z. Chen, Y. Wang, C. Qin, *Chem. Eng. J.* **2016**, *303*, 450.
[17] X. Li, Y. Xie, F. Jiang, B. Wang, Q. Hu, Y. Tang, T. Luo, T. Wu, *Sci. Total Environ.* **2020**, *709*, 136123.
[18] X. Zhao, M. C. Nguyen, C. Z. Wang, K. M. Ho, *RSC Adv*. **2013**, *3*, 22135.
[19] A. Rastinfard, M. H. Nazarpak, F. Moztarzadeh, *RSC Adv.* **2018**, *8*, 91.
[20] J. D. R. Blanco, S. Shaw, L. G. Benning, *Nanoscale* **2011**, *3*, 265.
[21] B. Liu, Y. Bian, S. Liang, M. Yuan, S. Dong, F. He, S. Gai, P. Yang, Z. Cheng, J. Lin, *ACS Nano* **2022**, *16*, 617.
[22] S. Gao, Y. Jin, K. Ge, Z. Li, H. Li, X. Dai, Y. Zhang, S. Chen, X. Liang, J. Zhang, *Adv. Sci.* **2019**, *6*, 1902137.

Chapter 3

Construction of Thick Living 3D Tissue with High Cell Density Using Oxygen Releasing Micro-Cell Scaffold

3.1 Introduction

To prevent oxygen shortage problems in tissue engineering fields, a broad range of oxygen releasing materials have been reported in recent years.[1,2] Previsouly reported oxygen releasing materials were mainly applied for 3D cell culture in hydrogels. 3D cell culture in hydrogels can be combined with 3D bioprinting technology to create complex structures.[3] However, these constructs are far from real tissue in our body since most part of constructs are hydrogels, not cells. In other words, construction of thick livivng 3D tissue with high cell density has not yet been achieved even with oxygen releasing materials.

The author considered that there are two main reasons why the previously reported oxygen releasing materials were applied only to 3D cell culture in hydrogels. First, oxygen loading amount of these materials are not enough for the oxygen requirements of 3D tissue with high cell density. For example, theoretical oxygen loading amount of CaO_2 microparticle with a diameter around 50 μm is equivalent to the oxygen consumption amout of one thousand cells of iPS-derived cardiomyocyte per day.[4] Thus, it is expected that oxygen loading amount of CaO_2 itself is suitable for 3D tissue application. However, CaO_2 was finaly incorporated in hydorgels or hydrophobic polymer materials at concentrations of several tens mg mL^{-1} for tissue engineering applications.[2] As a result, oxygen loading amount of final product is low, which will not be able to supply enough oxygen to 3D tissue with high cell density. In addition, since oxygen loading amount of heme proteins and perfluocarbone are less than one-hundredth of CaO_2, oxygen releasing materials using these oxygen sources are even less suiatble for the alleviation of hypoxia in 3D tissues.[2] Second, cytotoxicity derived from byproducts of CaO_2 reaction such as hydrogen peroxide limits the material designs. In most cases, CaO_2-based oxygen releasing materials are incorporated in the hydrogel including catalase because catalase is an enzyme which decompose toxic hydrogen peroxide into oxygen and water.[2,5] As a result,

oxygen releasing materials are mainly used in 3D cell culture in hydrogels.

In chapter 1, the author reported HAp coating on CaO_2 microparticle for sustained oxygen release.[6] It is expected that HAp-CaO_2 itself can maintain high oxygen loading amount because it was obtained by simple surface modification of CaO_2. In this chapter, Layer-by-Layer (LbL) nanofilm composed of anionic catalase (pI=5.4) and cationic poly-L-lysine (PLL, pKa=10.6[7]) was fabricated on HAp-CaO_2 to obtain oxygen releasing micro-cell scaffold for the construction of thick living 3D tissue with high cell density (**Figure 3-1a**). LbL method is a popular and simple technique to create stable deposited nanoscale thin films on the substrate by alternate deposition of interacting polymers.[8] LbL-HAp-CaO_2 didn't release toxic hydrogen peroxide because catalase in the LbL nanofilm decomposed it into oxygen. In addition, since PLL improve cell adhesion on the material by the electrostatic absorption of cell adhesion proteins,[9] LbL-HAp-CaO_2 can be directly incorporated in the 3D tissue. Strikingly, thick living 3D tissue with high cell density was constructed using LbL-HAp-CaO_2 because oxygen supply from LbL-HAp-CaO_2 suppressed cell death due to oxygen shortage (**Figure 3-1b**). Therefore, LbL-HAp-CaO_2 would be a strong tool for the alleviation of hypoxia in 3D tissues, which will enable the construction of a broad range of thick 3D tissues with high cell density.

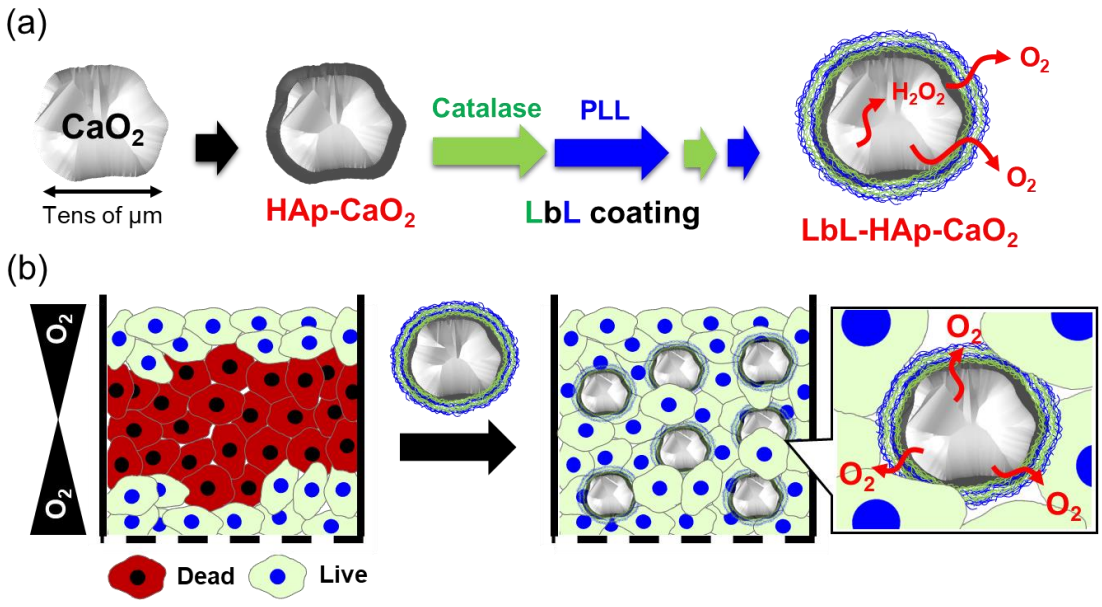

Figure 3-1. Schematic illustration of (a) the fabrication of oxygen releasing micro-cell scaffold (LbL-HAp-CaO_2) and (b) the construction of thick living 3D tissue with high cell density using LbL-HAp-CaO_2.

3.2 Experiments

3.2.1 Materials

Calcium peroxide (CaO_2) (particle size < 200 mesh), catalase from bovine liver, fluorescein isothiocyanate isomer I, fibrinogen from bovine plasma, thrombin from bovine plasma and fibronectin human plasma were purchased from Sigma-Aldrich (MO). Sulfuric acid (H_2SO_4, 95.0%), Sodium dihydrogenphosphate (NaH_2PO_4), disodium hydrogenphosphate 12-water (Na_2HPO_4) and dimethyl sulfoxide (DMSO) were purchased from FUJIFILM Wako Pure Chemical Corporation (Osaka, Japan). Poly-L-lysine hydrobromide (Mw 15000-30000) (PLL) was purchased from Sigma-Aldrich and FUJIFILM Wako Pure Chemical Corporation. Dulbecco's phosphate buffered saline (PBS), Dulbecco's modified Eagle medium (DMEM), Hoechst 33342 solution (1 mg mL^{-1}) and 4% paraformaldehyde phosphate buffer solution were purchased from Nacalai Tesque (Kyoto, Japan). Fetal bovine serum (FBS), antibiotics, calcein-AM and ethidium homodimer-1 were purchased from Thermo Fisher Scientific (MA, USA). Hydrogen peroxide (35%) was purchased from Kishida Chemical Co., Ltd. (Osaka, Japan). Mouse myoblast (C2C12) was purchased from ATCC (Virginia, USA).

3.2.2 Fabrication of catalase/PLL LbL nanofilm

The LbL nanofilm fabrication was monitored by 27 MHz quartz crystal microbalance (QCM) (AFFINIX Q8, ULVAC). QCM sensors coated with gold (QCM01S, ULVAC) were treated with Piranha solution (H_2SO_4:35% H_2O_2 = 3:1) for 10 min and repeated 3 times. After rinsing the sensor with Milli-Q water 3 times, 90 μL of 10, 100 and 500 mM phosphate buffer (PB, pH 7.0) at room temperature were added into the cells until the frequency reached a steady state. 10 μL of catalase solutions (10 mg mL^{-1}, PB) were added to the cells, and frequency changes were monitored. After 15 min of deposition, sensors were rinsed with PB 3 times and equilibrated in 90 μL of PB. 10 μL of PLL solutions (10 mg mL^{-1}, PB) were injected into the cells for the second layer deposition. By alternately changing the polymer solutions in cells, nanofilms via LbL assembly were fabricated. Zeta potential of catalase and PLL (1 mg mL^{-1}, 10 mM PB, pH7.0) was measured using a Zetasizer Nano ZS (Malvern, U.S.A).

The deposited mass (Δm) was calculated with the Sauerbrey equation.[10] Since frequency changes include water interacting with polymers, a frequency change in dry state (ΔF_{dry}) was calculated from a frequency change in wet state (ΔF_{wet}) as previously reported.

ΔF_{wet} is 2.5 times higher than ΔF_{dry} for catalase[11] while 3.6 times higher for polymer (22kDa).[12] A frequency change of 1 Hz corresponded to a mass change of 0.62 ng cm^{-2} in the QCM system used here (Equation 1-1).[13]

$$-\Delta m_{dry}\left(\mathrm{ng/cm^2}\right) = 0.62\Delta F_{dry}(\mathrm{Hz}) \qquad (1-1)$$

Based on the depostied dry mass (Δm), an assumed protein density of 1.3 g cm^{-3} and polymer density of 1.2 g cm^{-3},[14] the dry thickness of the resultant nanofilm was calculated according to the equation 1-2.

$$Thickness(nm) = \frac{\Delta m_{catalase}(ng/cm^2)}{1.3 \times 10^2} + \frac{\Delta m_{PLL}(ng/cm^2)}{1.2 \times 10^2} \qquad (1-2)$$

3.2.3 Characterization of LbL nanofilm

Nanofilms for AFM observation was fabricated on silicon wafers as previously reported.[15] Before the film fabrication, silicon wafers were treated with plasma for 1 min and then immersed in PLL solution (1 mg mL^{-1}) for 15 min to make the surface positive-charged. Substrates were alternately immersed into catalase solution (1 mg mL^{-1}, 10 mM PB, pH 7.0) and PLL solution (1 mg mL^{-1}, 10 mM PB, pH 7.0) for 15 min. Between each step, substrates were washed by 10 mM PB three times. After scratching the surface with tweezers, surface morphologies and roughness of LbL nanofilm in PBS was observed at room temperature by AFM (SHIMADZU, SPM-Nanoa). After that, nanofilm on silicon wafer was incubated in PBS for 1 day at 37°C and then AFM observation was performed. Nanofilms used for AFM measurement was assembled into 5 cycle layers.

To evaluate the decomposition of hydrogen peroxide by nanofilm, LbL nanofilm was fabricated on 24-well plate (3820-024, IWAKI, Shizuoka, Japan) as mentioned above. Briefly, 400 μL of catalase solution (1 mg mL^{-1}, 10 mM PB, pH 7.0) and PLL solution (1 mg mL^{-1}, 10 mM PB, pH 7.0) were alternately added in 24-well plate for 15 min at room temperature. Between each step, 24-well plate was washed by 10 mM PB three times. After 5 cycle LbL (10 layers), 1 mL of 1 mM hydrogen peroxide solution in PBS was added. Time dependent changes of hydrogen peroxide concentration was quantified using an Oxiselect Hydrogen Peroxide/Peroxidase Assay Kit (Fluorometric) (STA-344, Cell Biolabs Inc., San Diego, USA) according to the manufacturer's protocol. Every 20 min until after 60 min, 5 μL of supernatant was collected and mixed with 495 μL of assay buffer. 50 μL of sample solution was mixed with

50 μL of working solution of the assay kit in a black 96-well plate (3603, Corning, NY, USA). After 30 min incubation at room temperature, fluorescent intensity was measured by microplate reader (SYNERGY/HTX multi-mode reader, BioTek Instruments, Winooski, USA) using λ_{ex}=540 nm for excitation wavelengths and λ_{em}=590 nm for emission wavelengths. Hydrogen peroxide concentration was calculated from a standard curve obtained from the fluorescent intensities of the known concentrations of hydrogen peroxide. Decomposition of hydrogen peroxide by LbL nanofilm was also evaluated after 4, 7 and 14 days incubation in PBS at 37 °C in the same way.

L929 cells were culture on LbL nanofilm to evaluate the cytocompatibility. As mentioned above, 3 and 5 cycle LbL nanofilms were fabricated on 24-well plate. 5×10^4 cells of L929 were cultured on LbL nanofilms in 24-well plate using 1 mL of DMEM containing 10 % FBS and 1 % antibiotics. WST assay reagent was prepared by mixing transparent DMEM and cell count reagent SF (Nacalai Tesque, Kyoto, Japan) at a ratio of 9:1. After 1 day incubation in a 5 % CO_2 incubator, cells were washed by 1 mL of PBS and then 400 μL of WST assay reagent was added. The cells were incubated in a 5 % CO_2 incubator for 30 min. Then, 100 μL of WST solutions from each well were collected in a 96-well plate Transwell (3860-096, IWAKI, Shizuoka, Japan) and absorbance at 450 nm was measured using a microplate reader. The cell proliferation of each sample was standardized from the relative values of absorbance at 450 nm as compared to 100 % for that of a cell culture without LbL nanofilm.

3.2.4 Fabrication of LbL nanofilm on HAp-CaO_2

HAp-CaO_2 was prepared as previously reported.[6] Briefly, 10 mg of CaO_2 was immersed in 10 mL of 500 mM PB (pH 7.0) for 1 hour at 37°C. The resulting HAp-CaO_2 was collected by centrifugation at 1,000 rpm for 3 min. After washing 3 times by 100 % ethanol, HAp-CaO_2 was dried under reduced pressure at 80°C.

To visualize LbL nanofilm formation on HAp-CaO_2, fluorescein isothiocyanate labeled catalase (FITC-catalase) was synthesized as previously reported.[16] 20 mL of 1 mg mL^{-1} catalase solution in 50 mM PB (pH8.0) was mixed with 1.5 mL of 1 mg mL^{-1} FITC/DMSO for 45 min at room temperature. The solution was then dialyzed against 50 mM PB (pH7.4) for 48 hours at 4 °C and then freeze dried.

LbL nanofilm formation on HAp-CaO_2 was evaluated using FITC-catalase. 1 mg mL^{-1} HAp-CaO_2 was immersed in 1 mg mL^{-1} catalase solution (10 mM PB, pH 7.0) including 20%

FITC-catalase for 15 min. HAp-CaO_2 was collected by centrifugation at 1,000 rpm for 3 min and then dispersed in 10 mM PB. After washing, HAp-CaO_2 was collected by centrifugation at 1,000 rpm for 3 min and then dispersed in 1 mg mL^{-1} PLL solution (10 mM PB, pH 7.0) for 15 min. After 1, 2, 3 and 5 cycle LbL on HAp-CaO_2, fluorescent images of LbL-HAp-CaO_2 were captured in PBS at room temperature using a benchtop CQ1 confocal quantitative image cytometer (CellVoyager CQ1 System Highlights, Yokogawa, Japan). Fluorescent intensities derived from FITC-catalase on LbL-HAp-CaO_2 were analyzed using CellPathfinder software (Yokogawa, Japan). Fluorescent images of LbL-HAp-CaO_2 were also captured after 1, 4 and 7 days incubation in PBS at 37°C to analyze time dependent changes of fluorescent intensities on LbL-HAp-CaO_2 as mentioned above.

Surface structure of LbL-HAp-CaO_2 were analyzed by Scanning electron microscope (SEM) and energy dispersive X-ray spectrometry (EDX) measurements. LbL-HAp-CaO_2 (0, 1, 2, 3 and 5 cycle LbL) were fabricated as mentioned above without using FITC-catalase. After washing fabricated LbL-HAp-CaO_2 by MilliQ, LbL-HAp-CaO_2 was freeze dried. SEM and EDX measurements of LbL-HAp-CaO_2 were performed by Phenom ProX Desktop SEM (Thermo Fisher Scientific, MA) for the morphology and elemental analysis after sputter-coating with osmium using an HPC-30 Plasma Coater (Vacuum Device, Ibaraki, Japan).

3.2.5 Oxygen and hydrogen peroxide release behavior of LbL-HAp-CaO_2

Hydrogen peroxide concentrations in PBS including LbL-HAp-CaO_2 were evaluated using an Oxiselect Hydrogen Peroxide/Peroxidase Assay Kit. 3 mg of LbL-HAp-CaO_2 (0, 1, 2, 3, 5 cycle LbL) were dispersed in 3 mL of PBS. After 2 h, 1, 4, 7 and 14 days incubation at 37°C, hydrogen peroxide concentrations in PBS were evaluated. Briefly, 10 μL of supernatants were diluted 10 times for LbL-HAp-CaO_2 (1, 2, 3 and 5 cycle LbL) and 100 times for HAp-CaO_2 (0 cycle LbL) using PBS and then hydrogen peroxide concentrations were measured as mentioned above. LbL-HAp-CaO_2 amount was defined from the HAp-CaO_2 amount before LbL nanocoating.

To evaluate the oxygen release behavior of LbL-HAp-CaO_2, the dissolved oxygen amount in DMEM including LbL-HAp-CaO_2 was measured under a hypoxic condition using an SDR SensorDish Reader (SDRSensorDish®Reader, PreSens, Regensburg, Germany). 5 mg of LbL-HAp-CaO_2 after 0, 1, 2, 3 and 5 cycle LbL were dispersed in 500 μL of DMEM containing 1% antibiotics. For HAp-CaO_2 (0 cycle LbL), DMEM including 100 unit mL^{-1}

catalase was used to convert hydrogen peroxide into oxygen. LbL-HAp-CaO_2 suspensions were added in a 24-well sensor dish (OxoDish®OD24, PreSens, Regensburg, Germany). The SensorDish Reader and the 24-well sensor dish were placed in a hypoxia cell culture airtight bag (6-8669-03, As one, Osaka, Japan). To create a hypoxic condition, three anaeropack O_2 absorbers (MITSUBISHI GAS CHEMICAL COMPANY INC., Tokyo, Japan) were added to the bag and it was then completely sealed using parafilm. The dissolved oxygen amount in the DMEM was then monitored at 37°C.

3.2.6 Cytocompatibility assessment of LbL-HAp-CaO_2

Cytocompatibility of LbL-HAp-CaO_2 was evaluated by WST-8 kit assay. Briefly, 5×10^4 cells of C2C12 were cultured in a 24-well plate using 1 mL of DMEM containing 10 % FBS and 1 % antibiotics. After 1 day incubation in 5 % CO_2 incubator, cell culture medium was changed to 800 µL of fresh DMEM containing 10 % FBS and 1 % antibiotics. 5 mg of LbL-HAp-CaO_2 after 0, 1, 2 cycle LbL were dispersed in 200 µL of DMEM containing 10 % FBS and 1 % antibiotics. 24-well insert (3470, Corning, NY, USA) containing 200 µL of LbL-HAp-CaO_2 suspensions were placed into 24-well plate with cells. After 2 h incubation in 5 % CO_2 incubator, cells were washed by 1 mL of PBS and then 200 µL of WST assay reagent was added. The cells were incubated in a 5 % CO_2 incubator for 30 min. Then, 100 µL WST solutions from each well were collected in a 96-well plate Transwell and absorbance at 450 nm was measured using a microplate reader as mentioned above.

3.2.7 3D cell culture in fibrin hydrogel containing LbL-HAp-CaO_2

C2C12 cells were culture in fibrin hydrogel containing LbL-HAp-CaO_2 under hypoxic environment. 24-well insert was treated with plasma for 1 min. 5 mg of LbL-HAp-CaO_2 after 2 cycle LbL and 2 x 10^6 cells of C2C12 were dispersed in 50 µL of 6.6 unit mL^{-1} thrombin in DMEM, respectively. Each thrombin solutions and 100 µL of 24 mg mL^{-1} fibrinogen solution in DMEM were mixed and then 100 µL of solution was quickly added in 24-well insert. After 20 min incubation at room temperature and subsequent 40 min incubation at 37°C, 24-well insert was put in 6-well plate (3810-006N, IWAKI, Shizuoka, Japan) using adjuster. 12 mL of DMEM containing 10 % FBS and 1 % antibiotics was added in 6-well plate. The 6-well plates were incubated in a gas barrier box (A-110, MITSUBISHI GAS CHEMICAL COMPANY INC., Tokyo, Japan) with one anaeropack O_2 absorbers at 37°C to create a hypoxic condition. As a control sample, 3D cell culture without LbL-HAp-CaO_2 was also performed in the same way.

Live-dead assay solution was prepared by mixing 2.5 μL of calcein-AM, 10 μL of ethidium homodimer I and 25 μL of Hoechst in 5 mL of DMEM. After 7 days incubation under a hypoxic condition, 24-well insert was moved to 24-well plate and hydrogels were washed by PBS twice. 200 and 500 μL of live-dead assay solutions were added in 24-well insert and 24-well plate, respectively. After 2 h incubation at 37°C in 5 % CO_2 incubator, hydrogels were washed by PBS twice and then DMEM was added. Fluorescent images of 3D cell culture in hydrogels were captured using a benchtop CQ1 confocal quantitative image cytometer. Viability was analyzed from fluorescent images using CellPathfinder software.

3.2.8 3D tissue construction using LbL-HAp-CaO_2

3D tissue of C2C12 was constructed in 24-well insert by incorporating LbL-HAp-CaO_2 inside the tissue. 100 μL of 0.2 mg mL^{-1} fibronectin solution (50 mM Tris buffer at pH 7.4) was added in 24-well insert for fibronectin coating. 5 mg of LbL-HAp-CaO_2 (2 cycle LbL) was immersed in 0.1 mg mL^{-1} fibronectin solution for 30 min and then washed by DMEM containing 10 % FBS and 1 % antibiotics. 2 x 10^6 cells of C2C12 and 5 mg of LbL-HAp-CaO_2 were dispersed in 100 μL of DMEM containing 10 % FBS and 1 % antibiotics. 24-well insert containing 100 μL of cells and LbL-HAp-CaO_2 suspension was placed in 24-well plate with 800 μL of DMEM containing 10 % FBS and 1 % antibiotics. After 7 minutes centrifuge of 24-well plate at 1100 g, 100 μL of cell culture medium containing 2 x 10^6 cells of C2C12 and 5 mg of LbL-HAp-CaO_2 was slowly added in 24-well insert. After additional 7 minutes centrifuge of 24-well plate at 1100 g, 24-well insert was put in 6-well plate using adjuster. 12 mL of DMEM containing 10 % FBS and 1 % antibiotics was added in 6-well plate. Final tissue includes 10 mg of LbL-HAp-CaO_2 and 4 x 10^6 cells of C2C12 in 24-well insert. The 6-well plates were incubated in 5 % CO_2 incubator and cell culture medium was changed every day. As a control sample, C2C12 tissue without LbL-HAp-CaO_2 was fabricated in the same way. After 2 days culture, the C2C12 tissues were fixed by 4% paraformaldehyde phosphate buffer solution. For histology staining, the fixed 3D tissues were sent to the Applied Medical Research Company for paraffin embedding. Sectioned 3D tissues were stained with hematoxylin-eosin (HE) staining and TUNEL staining. The images were captured using an FL EVOS Auto microscope (Thermo Fisher Scientific, MA, USA). Apoptosis cell ratio in the TUNEL staining images were analyzed by ImageJ.

3.3 Results and discussion

3.3.1 Characterization of LbL nanofilm

Catalase is an anionic protein in a neutral solution since pI is 5.4. On the other hand, PLL is cationic polymer in a neutral solution since pKa is 10.6.[7] Therefore, catalase/PLL LbL nanofilm formation via electrostatic interaction is expected in a neutral buffer solution. The stepwise LbL assembly of the nanofilms composed of catalase and PLL was monitored by a quartz crystal microbalance (QCM) (**Figure 3-2a**). In 10 mM PB (pH7.0), stepwise decrease of frequency was observed as with the increase of LbL assembling, suggesting the successful formation of LbL nanofilm. On the other hand, frequency shift was small in 100 and 500 mM PB (pH7.0). This is probably because electrostatic interaction between catalase and PLL was suppressed in 100 and 500 mM PB due to high ion concentrations. Accordingly, the author used 10 mM PB for further experiments of LbL nanofilm assembly. The dry thickness of LbL nanofilms were calculated from frequency shift using Sauerbrey equation (**Figure 3-2b**).[10] After 5 cycle LbL assembly using 10 mM PB, the dry thickness of LbL nanofilm was estimated to be 33 nm. Zeta potentials in 10 mM PB were -10.9mV for catalase and +10.6 mV for PLL. According to these results, catalase/PLL LbL nanofilm formation by electrostatic interaction was confirmed in 10 mM PB. The thickness of LbL nanofilm in wet condition was evaluated by AFM at room temperature (**Figure 3-2c**). After 5 cycle LbL nanofilm assembly on silicon wafer, the thickness in PBS was 30 ± 1.9 nm and the surface roughness R_a (arithmetic mean deviation) was 5.5 ± 0.34 nm. Interestingly, after 1 day incubation of LbL nanofilm in PBS at 37°C, the thickness and R_a increased to 37 ± 3.3 nm and 17 ± 0.99 nm, respectively (**Figure 3-2d**). The author assumed that conformational changes of polymers in the LbL nanofilm between room temperature and 37°C affected nanofilm structure. Although the thickness and roughness changed, the LbL nanofilm was stable after 1 day incubation in PBS.

Decomposition of hydrogen peroxide is the main function of this LbL nanofilm. Therefore, decomposition of hydrogen peroxide by catalase/PLL LbL nanofilm (5 cycle) was evaluated in PBS (**Figure 3-2e**). Soon after the nanofilm preparation, hydrogen peroxide was quickly decomposed in the presence of LbL nanofilm (Brown line). After 4 and 7 days incubation of LbL nanofilm in PBS at 37°C, the kinetics of the decomposition of hydrogen peroxide decreased probably because of the deactivation of catalase in LbL nanofilm (red and pink line). Moreover, hydrogen peroxide was not decomposed after 14 days incubation of LbL nanofilm (orange line). These results suggested that LbL nanofilm can decompose hydrogen

peroxide at least for 7 days at 37°C. As shown in **Figure 3-1**, cytocompatibility of LbL nanofilm is essential for the application of LbL-HAp-CaO_2 to 3D tissue construction. Therefore, cells were cultured on the LbL nanofilm (3 and 5 cycle) for 1 day to evaluate cytocompatibility. Compared to the case without LbL nanofilm, cells on LbL nanofilms didn't change their proliferation behaviors, suggesting good cytocompatibility of LbL nanofilms (**Figure 3-2f**).

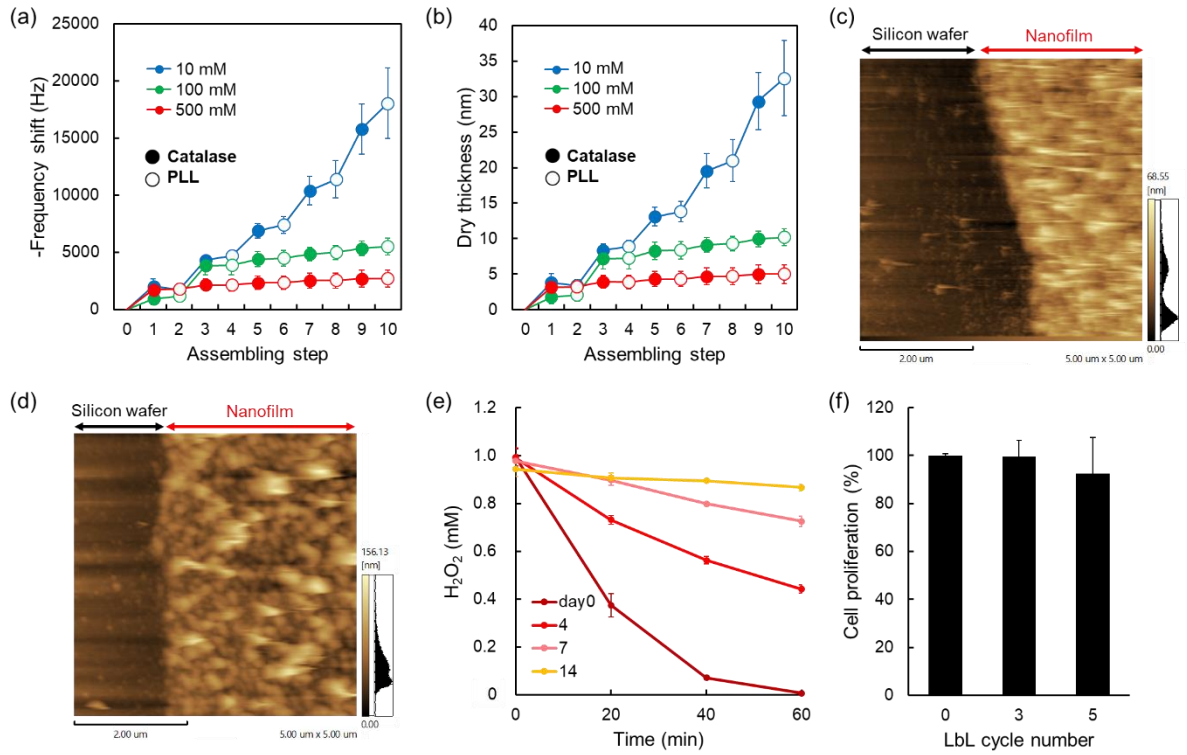

Figure 3-2. (a) Frequency shift and (b) calculated dry thickness of the catalase/PLL LbL nanofilm assembly using 10 (n=3), 100 (n=4) and 500 mM PB (pH 7.0) (n=4) , mean ± SD. AFM images of LbL nanofilms (5 cycle) in wet condition (c) soon after the nanofilm preparation and (d) after 1 day incubation in PBS at 37°C. (e) Time dependent changes of hydrogen peroxide concentrations in PBS in the presence of LbL nanofilm (5 cycle) soon after the nanofilm preparation and after 4, 7 and 14 days incubation of nanofilms in PBS at 37°C. (f) Cell proliferation on LbL nanofilms (3 and 5 cycle LbL). Data in (e) and (f) are representative of three independent experiments, mean ± SD.

3.3.2 Characterization of LbL-HAp-CaO_2

LbL nanofilm formation on HAp-CaO_2 was evaluated using FITC-labeled catalase. **Figure 3-3a** shows merged image of fluorescent and phase contrast images of LbL-HAp-CaO_2

after 5 cycle LbL nanofilm assembly. Fluorescence derived from FITC-catalase was observed over the entire surface of LbL-HAp-CaO_2. In addition, nanofilms with different numbers of LbL cycles were fabricated on a HAp-CaO_2 (**Figure 3-3b**). The fluorescent intensities derived from FITC-catalase on LbL-HAp-CaO_2 increased with LbL cycle number, suggesting the increase of catalase amount on LbL-HAp-CaO_2. These results confirmed the formation of catalase/PLL LbL nanofilm on HAp-CaO_2. Furthermore, fluorescence derived from FITC-catalase was clearly observed on LbL-HAp-CaO_2 even after 7 days incubation of LbL-HAp-CaO_2 (5 cycle) in PBS at 37°C (**Figure 3-3c**). **Figure 3-3d** shows time dependent changes of fluorescent intensities derived from FITC-catalase on LbL-HAp-CaO_2 with different numbers of LbL cycles. From day0 to day1, fluorescent intensities increased at all LbL cycle numbers. As shown in **Figure 3-2c,d**, the thickness and roughness of LbL nanofilm also increased after 1 day incubation in PBS at 37°C probably because of the conformational changes of polymers in the LbL nanofilm. Therefore, the author assumed that these conformational changes of polymers affected concentration quenching, local charge, pH and hydrophobic/hydrophilic environment around FITC, which increased fluorescent intensity. From day1 to day7, the fluorescent intensities were stable at all LbL cycle numbers, suggesting that LbL nanofilms on HAp-CaO_2 are stable.

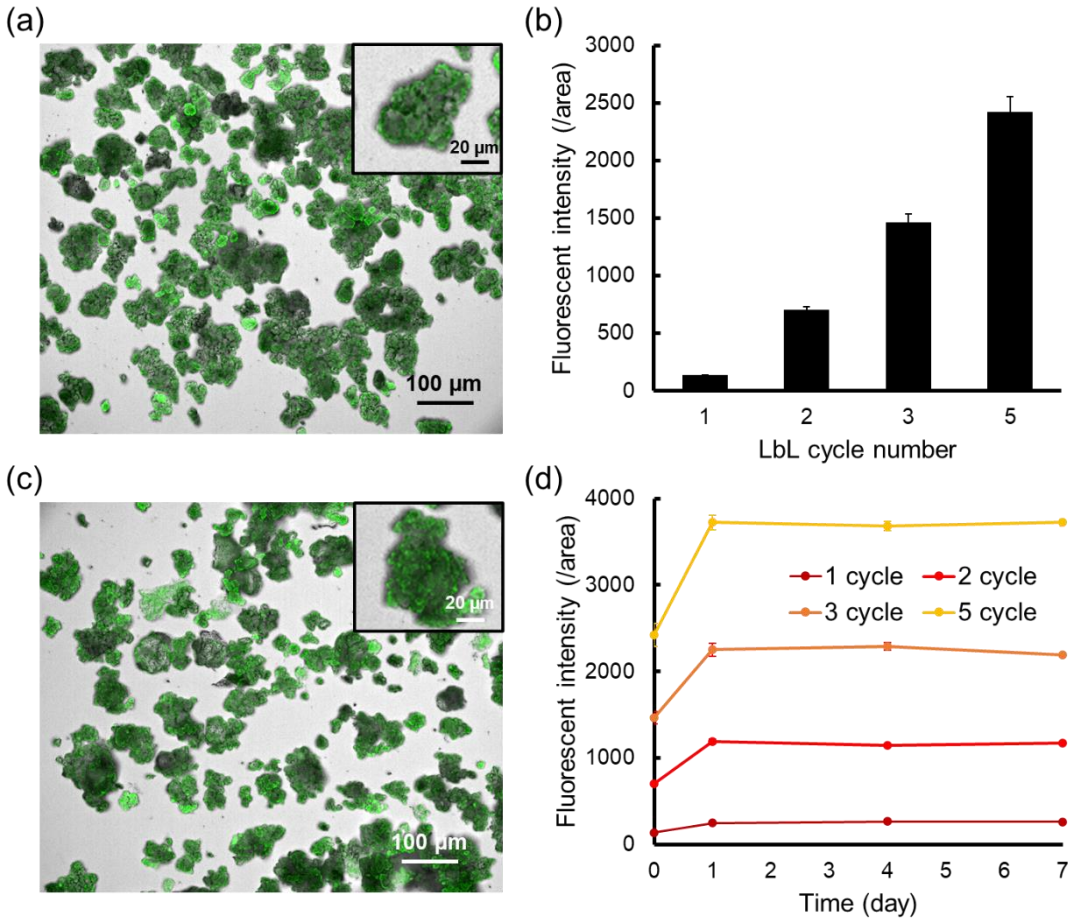

Figure 3-3. (a) Merge image of fluorescent and phase contrast images of LbL-HAp-CaO_2 after 5 cycle LbL assembly of catalase (20 % FITC-catalase) and PLL. (b) Fluorescent intensities on LbL-HAp-CaO_2 derived from FITC-catalase with different numbers of LbL cycles. (c) Merge image of fluorescent and phase contrast images of LbL-HAp-CaO_2 (5 cycle) after 7 days incubation in PBS at 37°C. (d) Time dependent changes of fluorescent intensities derived from FITC-catalase on LbL-HAp-CaO_2 with different numbers of LbL cycles. All data are representative of three independent experiments, mean ± SD.

LbL nanofilm formation on HAp-CaO_2 was also evaluated by elemental analysis using SEM-EDX. It is expected that nitrogen is newly detected on LbL-HAp-CaO_2 since catalase and PLL in LbL nanofilm include nitrogen in their chemical structure. **Figure 3-4a** shows EDX spectra of LbL-HAp-CaO_2 with different numbers of LbL cycles. Nitrogen was detected on LbL-HAp-CaO_2 after 1, 2, 3 and 5 cycle LbL nanofilm assembly as shown by yellow arrows while no nitrogen was detected on HAp-CaO_2 without LbL nanofilm. **Figure 3-4b-e** show SEM image for EDX and elemental mapping of nitrogen of LbL-HAp-CaO_2 (2 and 5 cycle). Nitrogen

was observed at the same location of LbL-HAp-CaO_2 in SEM image in both LbL cycle numbers. These results also confirmed LbL nanofilm formation on HAp-CaO_2.

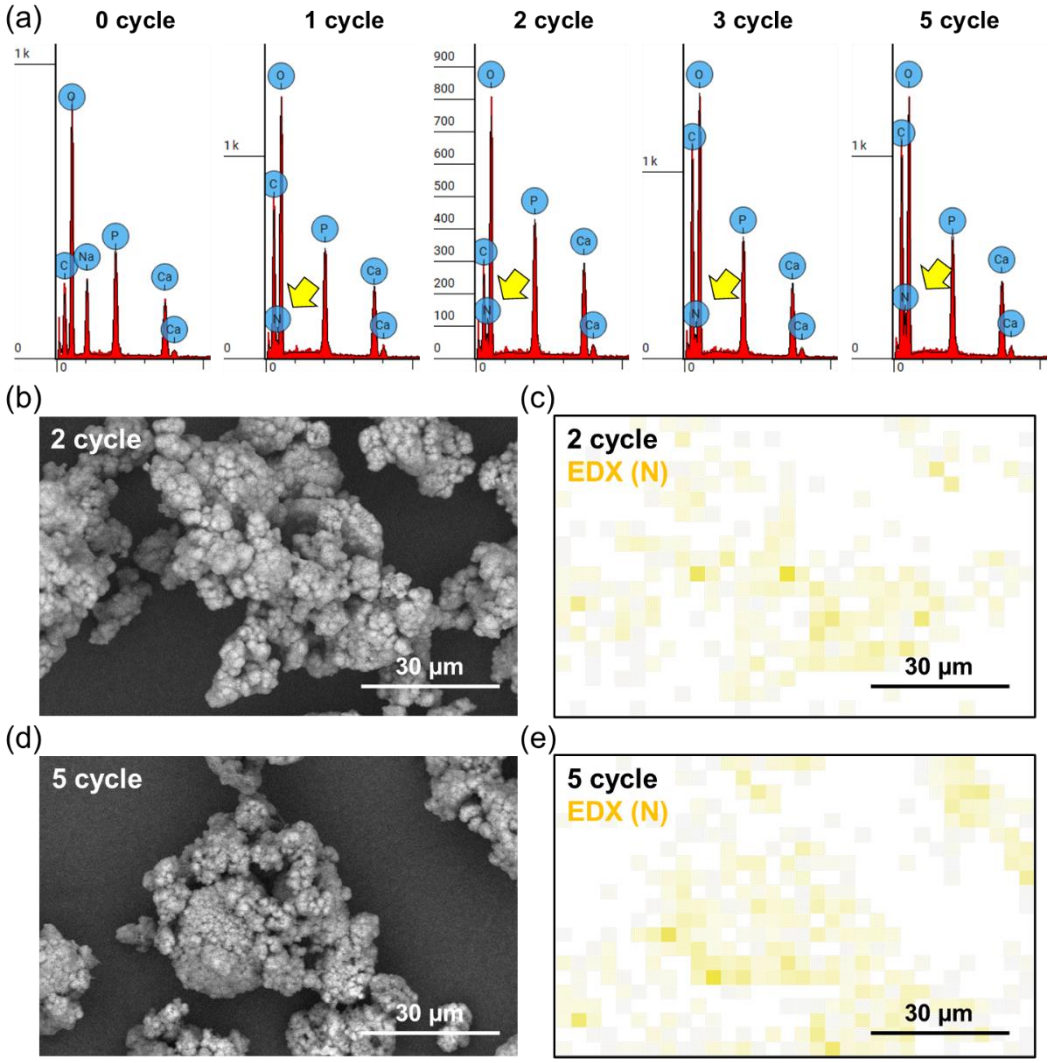

Figure 3-4. (a) EDX spectra of LbL-HAp-CaO_2 with different numbers of LbL cycles. (b,d) SEM image for EDX and (c,e) elemental mapping of nitrogen of LbL-HAp-CaO_2 after (b,c) 2 and (d,e) 5 cycle LbL nanofilm assembly.

Surface structure of LbL-HAp-CaO_2 was observed by SEM (**Figure 3-5**). Porous structure derived from HAp nanocrystal was observed on HAp-CaO_2 without LbL nanofilm as previously reported.[6] After 1 and 2 cycle LbL nanofilm assembly on HAp-CaO_2, this porous structure was still observed because the thickness of these LbL nanofilms were below 10 nm according to the QCM results (**Figure 3-2b**). On the other hand, less porous structure was observed on HAp-CaO_2 after 5 cycle LbL nanofilm assembly because the thickness of LbL

nanofilms increased at higher LbL cycle number (**Figure 3-2b**). These surface structure changes also suggested the formation of LbL nanofilm on HAp-CaO_2.

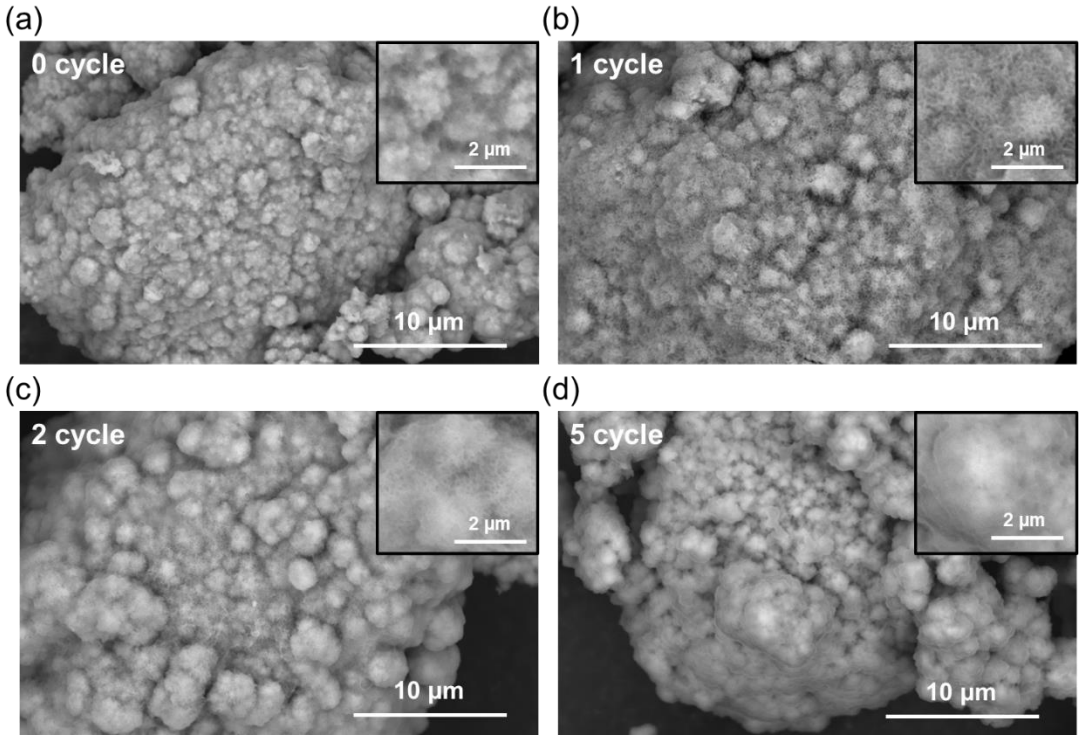

Figure 3-5. SEM images of HAp-CaO_2 (a) without LbL nanofilm and after (b) 1, (c) 2 and (d) 5 cycle LbL nanofilm assembly.

Since LbL nanofilm includes catalase which decompose toxic hydrogen peroxide derived from CaO_2 reaction, hydrogen peroxide release behaviors of LbL-HAp-CaO_2 with different numbers of LbL cycles were evaluated in PBS (**Figure 3-6a,b**). Without LbL nanofilm, 1 mg mL^{-1} HAp-CaO_2 released 360 μM hydrogen peroxide after 1 day incubation in PBS. After that, the hydrogen peroxide concentration slightly decreased probably because the autolysis of hydrogen peroxide was higher than the amount of hydrogen peroxide released from HAp-CaO_2. For 1 cycle LbL-HAp-CaO_2, hydrogen peroxide concentration decreased dramatically because catalase in LbL nanofilm decomposed hydrogen peroxide. However, 5 μM hydrogen peroxide was detected soon after the immersion of LbL-HAp-CaO_2 in PBS. On the other hand, hydrogen peroxide was hardly detected for LbL-HAp-CaO_2 higher than 2 cycle LbL cycle numbers. Therefore, it is suggested that at least 2 cycle LbL nanofilm assembly is necessary to suppress hydrogen peroxide release from HAp-CaO_2.

The time-span over which oxygen is released is one of the most important properties for oxygen releasing materials. To evaluate the oxygen release behavior of LbL-HAp-CaO_2, dissolved oxygen concentrations in DMEM including LbL-HAp-CaO_2 with different numbers of LbL cycles were evaluated under a hypoxia condition (O_2 < 0.1 %) (**Figure 3-6c,d**). Dissolved oxygen concentrations decreased as with the increase of LbL cycle numbers probably because the fabrication process of LbL nanofilm consumed CaO_2. Compared to HAp-CaO_2 without LbL nanofilm, dissolved oxygen concentration in DMEM including 1 cycle LbL-HAp-CaO_2 was lower at initial period while it became higher later. These results suggested that LbL nanofilm formation on HAp-CaO_2 suppressed the reaction between CaO_2 and water. Since oxygen concentration in DMEM including LbL-HAp-CaO_2 was stable at around 0 % after 6 days, it is suggested that the oxygen release period of LbL-HAp-CaO_2 was around 6 days.

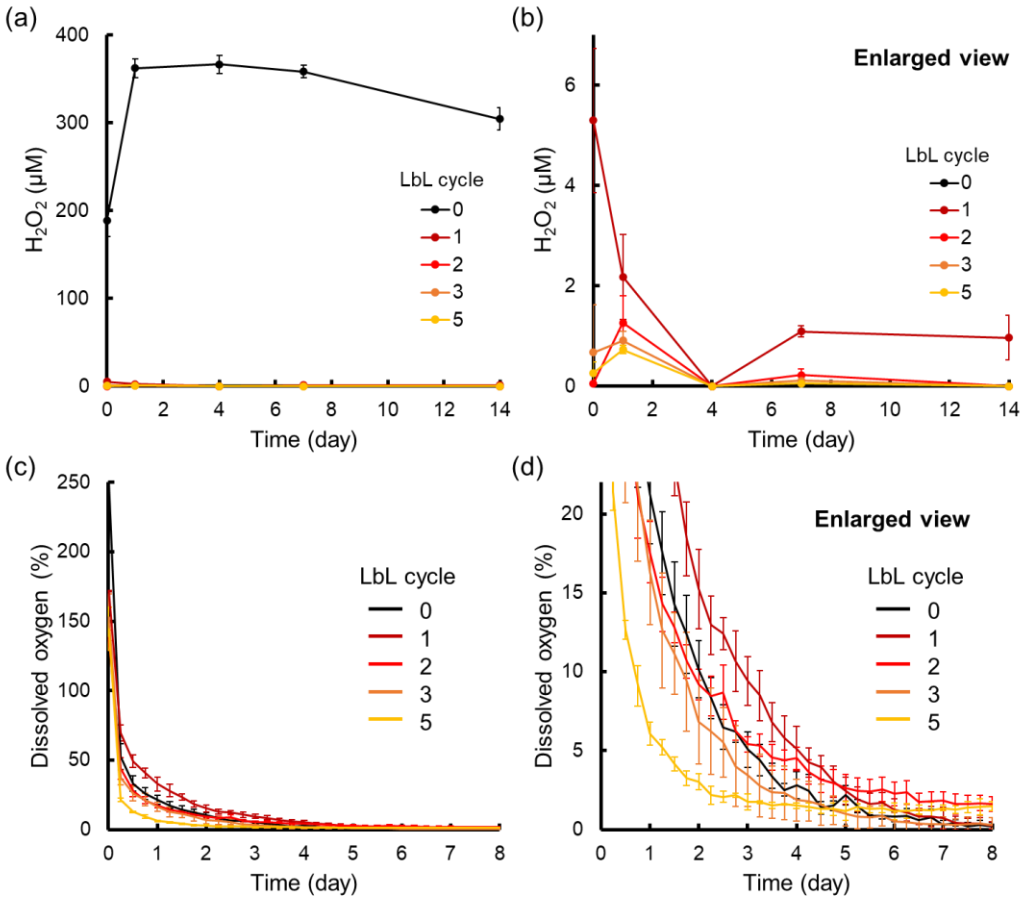

Figure 3-6. (a) Time dependent changes of hydrogen peroxide concentrations in PBS including 1 mg mL^{-1} LbL-HAp-CaO_2 with different numbers of LbL cycles. (c) Time dependent changes of dissolved oxygen concentrations in DMEM including 10 mg mL^{-1} LbL-HAp-CaO_2 with different numbers of LbL cycles under a hypoxic condition. For 0 cycle LbL, DMEM including 100 unit mL^{-1} catalase was used. Panels (b) and (d) show enlarged views of panels (a) and (c), respectively. All data are representative of three independent experiments, mean ± SD.

3.3.3 3D cell culture in fibrin hydrogel containing LbL-HAp-CaO_2

Before 3D cell culture application of LbL-HAp-CaO_2, C2C12 cells were cultured on 24-well plate in the presence of LbL-HAp-CaO_2 to evaluate its cytocompatibility (**Figure 3-7a**). Without LbL nanofilm, cell viability decreased to 80 % only after 2 hours incubation in the presence of 5 mg mL^{-1} HAp-CaO_2, suggesting that hydrogen peroxide released from HAp-CaO_2 showed cytotoxicity. On the other hand, LbL-HAp-CaO_2 (1 and 2 cycle) didn't decrease cell viability, suggesting cytocompatibility of LbL-HAp-CaO_2. For 1 cycle LbL-HAp-CaO_2, 5 μM hydrogen peroxide was detected in PBS including 1 mg mL^{-1} LbL-HAp-CaO_2 after 2 hours incubation (**Figure 3-6a,b**). It is reported that cell viability of C2C12 cells decreased in the presence of hydrogen peroxide above 500 μM.[17] Thus, it is considered that 25 μM hydrogen peroxide released from 5 mg mL^{-1} 1 cycle LbL-HAp-CaO_2 was low enough to show the cytotoxicity. However, when 1 cycle LbL-HAp-CaO_2 is incorporated in 3D tissues, the local hydrogen peroxide concentration around cells adherent to LbL-HAp-CaO_2 is expected to be very high. Therefore, HAp-CaO_2 after 2 cycle LbL nanofilm assembly was used for further experiments of 3D tissue constructions.

3D cell culture in hydrogels is one of the most common strategies of tissue engineering for clinical applications.[18] Thus, it is expected that oxygen supply in 3D cell culture in hydrogels is important to suppress cell death due to oxygen shortage.[2] To confirm the effect of oxygen supply from LbL-HAp-CaO_2, C2C12 cells were cultured in fibrin hydrogels including LbL-HAp-CaO_2 (2 cycle LbL) under a hypoxic condition (**Figure 3-7b-d**). Without LbL-HAp-CaO_2, cell viability was only 27 % after 7 days incubation because oxygen shortage caused cell death in hydrogels. On the other hand, cell viability improved to 82% in the presence of LbL-HAp-CaO_2. These results confirmed that sustained oxygen supply from LbL-HAp-CaO_2 improved cell viability in 3D hydrogels under a hypoxic condition. In this study, the author used fibrin hydrogels for 3D cell culture. However, since LbL-HAp-CaO_2 can be incorporated in any bulk hydrogels, application of LbL-HAp-CaO_2 for tissue engineering is highly expected. In addition, previously reported CaO_2-based oxygen releasing materials were used in hydrogels and cell culture medium containing catalase to reduce toxicity derived from hydrogen peroxide.[19,20] Thus, there is a concern about the toxicity of hydrogen peroxide on cells before it is decomposed by catalase. On the other hand, hydrogen peroxide is decomposed at LbL nanofilm on HAp-CaO_2 in this system, suggesting the usefulness of LbL-HAp-CaO_2.

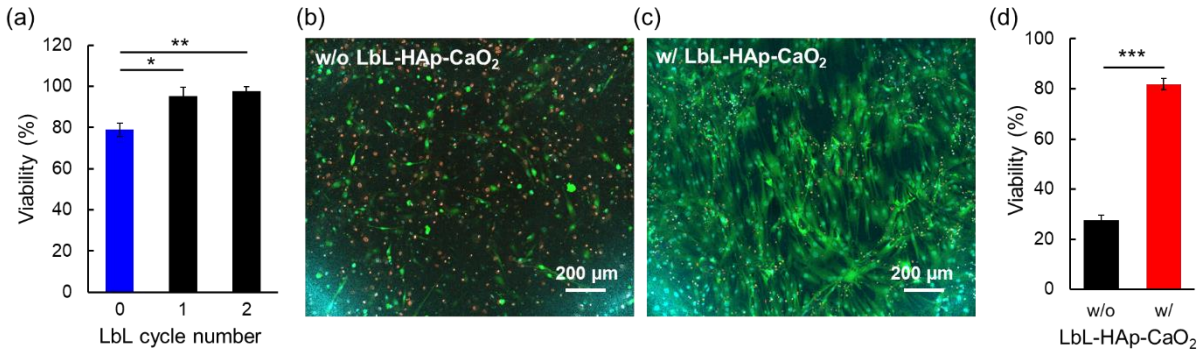

Figure 3-7. (a) Cell viability of C2C12 in the presence of 5 mg mL^{-1} LbL-HAp-CaO_2 (0, 1 and 2 cycle LbL) after 2 hours incubation. Viability of each sample was standardized from the relative values as compared to 100 % for that of a cell culture without LbL-HAp-CaO_2. Fluorescent images of live-dead assay of 3D cell culture in fibrin hydrogels (b) without LbL-HAp-CaO_2 and (c) with 25 mg mL^{-1} LbL-HAp-CaO_2 (2 cycle LbL) after 7 days incubation under a hypoxic condition. (d) Cell viability was analyzed from fluorescent images by ImageJ. All data are representative of three independent experiments, mean ± SD. *$p < 0.05$, **$p < 0.01$ and ***$p < 0.001$.

3.3.4 Construction of thick living 3D tissue with high cell density using LbL-HAp-CaO_2

In the previous research, oxygen releasing materials are mainly applied to 3D cell culture in hydrogels. However, these constructs are far from real tissue in our body since small number of cells are just dispersed in hydrogels. For example, Willemen and co-workers reported 3D cell culture of C2C12 cells in catalase-laden hydrogel containing hydrophobic oxygen generating microparticles and the cell density in hydrogels was only 2 x 10^6 cells cm^{-3}.[20] On the other hand, cell density of C2C12 spheroid was around 3 x 10^8 cells cm^{-3} estimated from the spheroid size and seeding cell numbers.[21] Thus, most part of previously reported constructs using oxygen releasing materials are hydrogels, but not cells. In other words, no one constructs thick living 3D tissue with high cell density even with oxygen releasing materials. To overcome these limitations, 3D tissues were constructed using C2C12 cells and LbL-HAp-CaO_2 (2 cycle LbL) that was presoaked in fibronectin solution to improve cell adhesion **(Figure 3-8a)**. HE staining images of 3D tissue without LbL-HAp-CaO_2 showed collapsed structures in which cells were separated from each other, suggesting cell death due to oxygen shortage (**Figure 3-8b**). On the other hand, a stable 3D tissue with a thickness of around 400 μm was observed in

the presence of LbL-HAp-CaO_2 (**Figure 3-8c**). In this HE staining images, some gap structures were observed. However, according to the gap shape and size, these are probably derived from the falling out HAp-CaO_2 during the fabrication process of HE staining cross-section because HAp-CaO_2 cannot be crosslinked by formaldehyde. The author also performed TUNEL staining to detect apoptosis cells in 3D tissues. Without LbL-HAp-CaO_2, many apoptotic cells with brown stained nuclei were observed (**Figure 3-8d**), suggesting cell apoptosis due to oxygen shortage. Importantly, these apoptosis cells were rarely observed in the presence of LbL-HAp-CaO_2 (**Figure 3-8e**). The percentage of apoptotic cells was also calculated by image analysis. In the control tissue, approximately half of the cells showed apoptotic cell death, whereas this number was reduced to 10% in the tissue including LbL-HAp-CaO_2 (**Figure 3-8f**). In addition, cell density of 3D tissue including LbL-HAp-CaO_2 was approximately 2 to 3 x 10^8 cells cm^{-3} estimated from the thickness of tissue and seeding cell numbers. Although the size of the cells may vary depending on the culture and fixation conditions, cell density of the author's tissue was close to that of spheroid (around 3 x 10^8 cells cm^{-3}). According to these results, oxygen supply from LbL-HAp-CaO_2 enabled the construction of thick living 3D tissue with high cell density. Actually, calculated from the oxygen release behavior in **Figure 3-6c,d** using Fick's First law, oxygen supply from 10 mg of LbL-HAp-CaO_2 was 25, 10 and 5 pmol s^{-1} after 6, 24 and 48 hours incubation in DMEM, respectively. In addition, oxygen is also supplied from the cell culture medium to tissue by diffusion. On the other hand, oxygen consumption amount of 4 x 10^6 cells of C2C12 in constructed 3D tissue was calculated as 15 pmol s^{-1}.[22] Thus, oxygen supply from the LbL-HAp-CaO_2 inside the 3D tissue is comparable to oxygen consumption of cells, which suppressed cell death due to oxygen shortage.

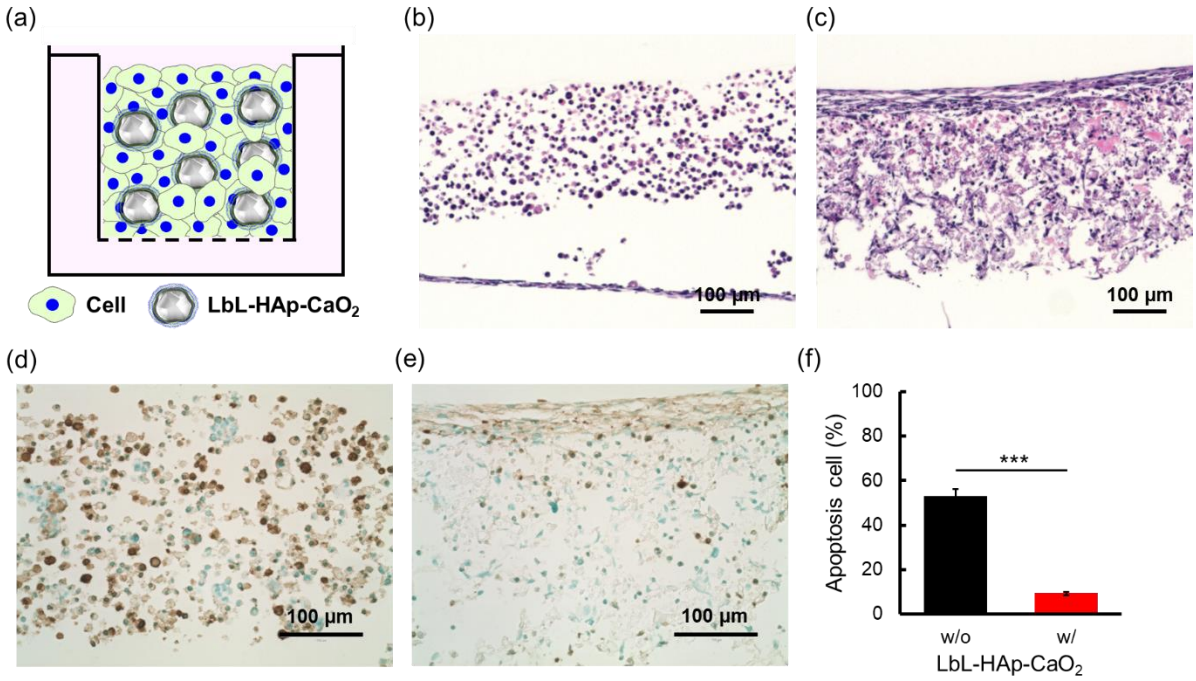

Figure 3-8. (a) Schematic illustration of the construction of 3D tissue using LbL-HAp-CaO_2. Histological images of the 3D tissue constructed using 4 x 10^6 cells of C2C12 (b,d) in the absence and (c,e) in the presence of LbL-HAp-CaO_2 (2 cycle LbL, 10 mg). Samples were stained with (b,c) hematoxylin (purple) and eosin (pink) (HE staining) and (d,e) TdT-mediated dUTP nick end labeling (TUNEL staining). 3D tissue was cultured in 5 % CO_2 incubator for 2 days. (f) Apoptosis cell ratio in 3D tissue with and without LbL-HAp-CaO_2 analyzed from TUNEL staining images using ImageJ. All data are representative of three independent experiments, mean ± SD. ***$p < 0.001$.

3.4 Conclusion

In chapter 3, the author fabricated oxygen releasing micro-cell scaffold by LbL nanofilm assembly on HAp-CaO_2. LbL nanofilm was constructed by electrostatic interaction between anionic catalase and cationic PLL. Since catalase in LbL nanofilm decomposed toxic hydrogen peroxide into oxygen, hydrogen peroxide release from LbL-HAp-CaO_2 was not observed after 2 cycle LbL. On the other hand, it is well known that PLL improve cell attachment on the substrate because of the absorption of cell adhesion proteins. Therefore, fabricated LbL-HAp-CaO_2 was successfully incorporated in 3D tissue. In control 3D tissue using only C2C12 cells, half of cells showed cell death by apoptosis due to oxygen shortage. On the other hand,

incorporation of LbL-HAp-CaO_2 dramatically suppressed cell death and provided stable 3D tissue with thickness around 400 μm because oxygen comparable to the oxygen consumption of total 3D tissue was supplied from LbL-HAp-CaO_2. In addition, cell density of constructed 3D tissue using LbL-HAp-CaO_2 was close to that of spheroid. These results confirmed that sufficient oxygen supply from LbL-HAp-CaO_2 enabled the construction of thick living 3D tissue with high cell density. To the best of the author's knowledge, no one has ever reported such a dense, living, thick, 3D tissues like the actual tissue in our body. LbL-HAp-CaO_2 therefore represent a great potential toward the development of clinically sized tissues for the application in regenerative medicines.

3.5 References

[1] T. Agarwal, S. Kazemi, M. Costantini, F. Perfeito, C. R. Correia, V. Gaspa, L. Montazeri, C. D. Maria, J. F. Mano, M. Vosough, P. Makvandi, T. K. Maiti, *Mater. Sci. Eng. C* **2021**, *122*, 111896.

[2] N. G. A. Willemen, S. Hassan, M. Gurian, J. Li, I. E. Allijn, S. R. Shin, J. Leijten, *Trends Biotechnol*. **2021**, *39*, 1144.

[3] N. Noor, A. Shapira, R. Edri, I. Gal, L. Wertheim, T. Dvir, *Adv. Sci.* **2019**, *6*, 1900344.

[4] C. Kim, J. Wong, J. Wen, S. Wang, C. Wang, S. Spiering, N. G. Kan, S. Forcales, P. L. Puri, T. C. Leone, J. E. Marine, H. Calkins, D. P. Kelly, D. P. Judge, H. S. V. Chen, *Nature* **2013**, *494*, 105.

[5] M. A. Prieto, X. Biarnés, P. Vidossich, C. Rovira, *J. Am. Chem. Soc.* **2009**, *131*, 11751.

[6] D. Tomioka, S. Fujita, J. Groll, M. Matsusaki, *Chem. Mater.* **2023**, *35*, 5378.

[7] A. Mirtič, J. Grdadolnik, *Biophys. Chem.* **2013**, *175*, 47.

[8] Z. Zhang, J. Zeng, J. Groll, M. Matsusaki, *Biomater. Sci.* **2022**, *10*, 4077.

[9] A. S. Karanfil, F. Louis, Y. Sowa, M. Matsusaki, *Biomater. Sci.* **2023**, *11*, 7623.

[10] G. Sauerbrey, *Z. Für Phys.* **1959**, *155*, 206.

[11] H. Furusawa, T. Ozeki, M. Morita, Y. Okahata, *Anal. Chem.* **2009**, *81*, 2268.

[12] T. Ozeki, M. Morita, H. Yoshimine, H. Furusawa, Y. Okahata, *Anal. Chem.* **2007**, *79*, 79.

[13] K. Noba, M. Ishikawa, A. Uyeda, T. Watanabe, T. Hohsaka, S. Yoshimoto, T. Matsuura, K. Hori, *J. Am. Chem. Soc.* **2019**, *141*, 19058.

[14] Y. Lvov, K. Ariga, I. Ichinose, T. Kunitake, *J. Am. Chem. Soc.* **1995**, *117*, 6117.

[15] Z. Zhang, J. Zeng, W. Li, M. Matsusaki, *Chem. Mater.* **2024**, *36*, 1947.

[16] A. Yu, Y. Wang, E. Barlow, F. Caruso, *Adv. Mater.* **2005**, *17*, 1737.

[17] X. Fan, R. Hussien, G. A. Brooks, *Free Radic. Biol. Med.* **2010**, *49*, 1646.

[18] F. Xu, C. Dawson, M. Lamb, E. Mueller, E. Stefanek, M. Akbari, T. Hoare, *Front. Bioeng. Biotechnol.* **2022**, *10*, 849831.

[19] S. Suvarnapathaki, M. A. Nguyen, A. A. Goulopoulos, D. Lantigua, G. C. Unal, *Biomater. Sci.* **2021**, *9*, 2519.

[20] N. G. A. Willemen, S. Hassan, M. Gurian, M. F. J. Salazar, K. Fan, H. Wang, M. Becker, I. E. Allijn, A. B. Öztürk, J. Leijten, S. R. Shin, *Adv. Healthcare Mater.* **2022**, *11*, 2102697.
[21] C. Chaweewannakorn, K. T. N. Aye, J. N. Ferreira, *SLAS Discov.* **2024**, *29*, 100190.
[22] B. A. Wagner, S. Venkataraman, G. R. Buettner, *Free Radic. Biol. Med.* **2011**, *51*, 700.

Chapter 4

Microfluidic Synthesis of Oxygen Releasing Microgels

4.1 Introduction

Micrometer-sized hydrogels, microgels, have attracted much attention in the tissue engineering field in recent years because microgel assemblies can be used for cell scaffolds, injectable materials, and 3D bioprinting.[1-3] Scaffold properties such as stiffness, microporosity and degradability are controllable at the micro-scale by modulating individual microgels. Unlike the 3D cell culture in bulk hydrogels, 3D cell culture in microgel assembly improves cell infiltration and nutrient diffusion by its tunable microporous structure, which improves long term cell survival, tissue repair and regeneration.[2] By taking advantage of oxygen-releasing materials and microgels, oxygen-releasing microgels are expected to be a very useful biomaterial for tissue engineering applications. However, to the best of the author's knowledge, no one has yet reported oxygen-releasing microgels using CaO_2 as an oxygen source.

In chapter 4, the author reports the fabrication of oxygen-releasing microgels using a droplet-based microfluidic system. A microfluidic system is suitable for the reproducible and controlled fabrication of uniform microgels based on its highly tuned channel in the micrometer range.[2-4] Herein, a water-in-oil emulsion with two aqueous phases and one oil phase was used for microgel fabrication (**Figure 4-1**). In one of the aqueous phases, dextran methacrylate (Dex-MA) was used for the polymer network of the microgel.[5] Since dextran is a biocompatible and biodegradable natural polysaccharide, dextran-based materials are suitable for tissue engineering applications.[6,7] In addition, synthesized CaO_2 nanoparticles were dispersed in the Dex-MA aqueous phase as an oxygen source. The Dex-MA aqueous phase containing CaO_2 nanoparticles was mixed with another aqueous phase containing a photoinitiator at the junction point and then droplets were formed by the continuous phase. After the photo-crosslinking of droplets, homogeneous, monodisperse and stable oxygen-releasing microgels were successfully obtained. Furthermore, the author also applied this microfluidic system for the controlled release of oxygen from the microgel. Herein, in situ amorphous calcium carbonate (ACC)

formation was also performed to incorporate CaO_2 nanoparticles in ACC in the microgel (**Figure 4-1**). In chapter 2, the author has reported controlled release of oxygen from CaO_2 microparticles in a weak acidic condition by stabilized ACC coating for biomedical applications.[8] Based on the results in chapter 2, sodium hydrogen carbonate ($NaHCO_3$) and sodium dihydrogen phosphate (NaH_2PO_4) were used for the aqueous phase including a photoinitiator in this microfluidic system. Since $Ca(OH)_2$ is already released from CaO_2 nanoparticles in the Dex-MA aqueous phase, stabilized ACC formation by mixing these two aqueous phases is expected as shown in **Figure 4-1**. Although the microgel containing CaO_2 released oxygen quickly in a neutral cell culture medium, oxygen release from the ACC-CaO_2 microgel was suppressed because incorporation of CaO_2 in ACC suppressed the reaction between CaO_2 and water. On the other hand, oxygen release from the ACC-CaO_2 microgel was observed in the weak acidic acetate buffer because the dissolution of ACC due to lower pH and the lack of calcium and carbonate ions triggered the CaO_2 reaction.[9] It is well known that the environment in ischemic tissue is weakly acidic.[10] Thus, this controlled oxygen release property of an ACC-CaO_2 microgel based on $CaCO_3$ chemistry is expected to provide selective oxygen supply in hypoxic environments. The developed oxygen releasing microgels by microfluidic system therefore show great potential for solving the oxygen shortage problem in tissue engineering field.

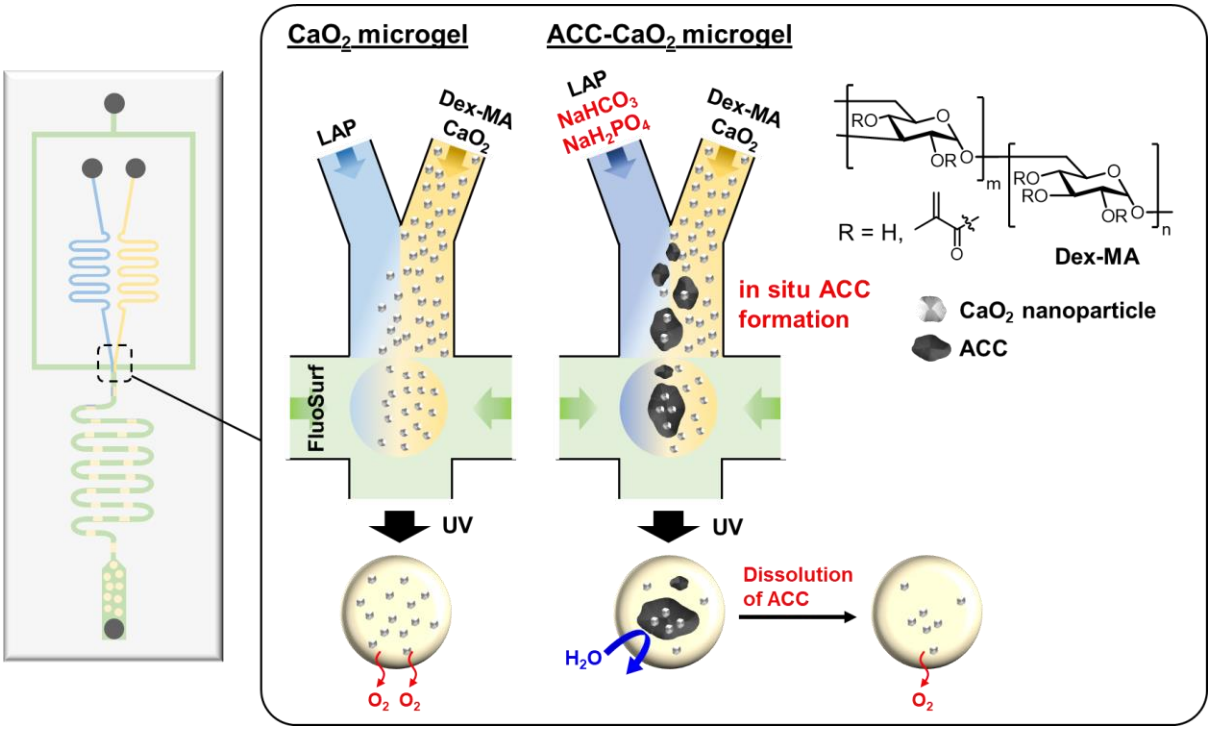

Figure 4-1. Schematic illustration of oxygen-releasing microgel synthesis and in situ ACC formation via a droplet-based microfluidic system.

4.2 Experiments

4.2.1 Materials

Glycidyl methacrylate, dimethyl sulfoxide, 4-dimethylaminopyridine, lithium phenyl-2,4,6-trimethylbenzoylphosphinate (LAP) and catalase from bovine liver and calcium peroxide (CaO_2) (particle size < 200 mesh) were purchased from Sigma Aldrich. Dextran 150 kDa and pure HPLC water were purchased from VWR International. Sodium hydrogen carbonate ($NaHCO_3$) and Dulbecco's modified Eagle's medium (DMEM) were purchased from Nacalai Tesque. Sodium dihydrogen phosphate (NaH_2PO_4) and sodium acetate were purchased from FUJIFILM Wako Pure Chemical Corporation. Sodium hydroxide (NaOH) and aluminum oxide were purchased from Honeywell International Inc. Aquapel was purchased from PWG Auto Glass, LLC. FluoSurf was purchased from Emulseo. Novec oil (Novec 7500) was purchased from 3M. Hexane was purchased from Fisher Scientific International, Inc. Acetic acid was purchased from Kishida Chemical Co., Ltd. Calcium chloride ($CaCl_2$) was purchased from Sigma Aldrich and Nacalai Tesque. Ammonium hydroxide solution (28-30%) was purchased

from Sigma Aldrich and Kishida Chemical Co., Ltd. Poly(ethylene glycol)-average mol wt 200 (PEG200) was purchased from Sigma Aldrich and FUJIFILM Wako Pure Chemical Corporation. Hydrogen peroxide was purchased from Carl Roth and Kishida Chemical Co., Ltd.

4.2.2 Synthesis of CaO_2 nanoparticles

CaO_2 nanoparticles were synthesized using a previously reported method with slight modifications.[11] 3 mL of 0.9 M $CaCl_2$ solution, 12 mL of PEG200 and 100 µL of ammonium hydroxide solution were mixed at room temperature. Then, 1.5 mL of hydrogen peroxide (30%) was added at a speed of 1 drop per 5 sec while stirring the solution. After 2 h stirring, 0.1 M NaOH was added until the pH value of the solution reached 11.5. The obtained white suspension was centrifuged for 5 min at 14,000 rpm, and sequentially washed with NaOH (0.1 M), water, and ethanol. Then, obtained CaO_2 nanoparticles were dispersed in ethanol. After 3 h incubation, CaO_2 nanoparticles dispersed in supernatants were collected. Collected CaO_2 nanoparticles were kept in ethanol until use. CaO_2 nanoparticle concentration in ethanol was calculated by measuring the dry mass of CaO_2 nanoparticle suspension. Scanning electron microscope (SEM) images of dried CaO_2 nanoparticles were taken using an Ultra-high Resolution Scanning Electron Microscope SU9000 (Hitachi-High Technologies). For the SEM, samples were sputter coated with carbon (Leica EM ACE600 sputter coater). The crystal structure of dried CaO_2 nanoparticles was measured by X-ray powder diffraction using a Nano-inXider SW/L Xenocs diffractometer equipped with two PILATUS3 hybrid detector arrays.

4.2.3 Synthesis of Dex-MA

The Dex-MA was synthesized according to a previously reported method.[7,12,13] In brief, glycidyl methacrylate was passed through glass wool (Carl Roth) containing aluminum oxide for the activation. Under an inert atmosphere, dextran (10.01 g, 0.062 mol glucose unit, 1 eq.) was dissolved in dimethyl sulfoxide (70 mL) and then 4-dimethylaminopyridine (2.00 g, 0.016mol, 0.3 eq.) was added. The reaction was initiated by adding glycidyl methacrylate (10 mL, 10.7 g, 0.075 mol, 1.2 eq.). The solution was stirred at room temperature for 48 h. The reaction solution was dialyzed for 5 days at 4 °C. The product was obtained through lyophilization and yielded a white powder. ^{1}H-NMR spectra of dextran and the modified dextran were recorded with a Bruker DPX-400 FT-NMR spectrometer at a frequency of 400 MHz. All measurements were conducted in D_2O as a solvent. The data analysis was carried out by MestReNova software. The compositions of dextran and modified dextran were

characterized by an FTIR machine Spectrum 3 from Perkin Elmer with a GladiATR accessory.

4.2.4 Fabrication of the microfluidic device

A master mold for the microfluidic device was fabricated via photolithography as previously reported.[14-16] The master mold was then used to fabricate microfluidic devices as previously reported.[5] In brief, a two-component system of siloxane and a cross-linker/curing agent Sylgard 184 Elastomer Kit was mixed. The master molds filled with the polydimethylsiloxane (PDMS)/cross-linker mixture was then placed in an oven at 60 °C overnight. The hardened PDMS device was removed from the master mold and inlets and outlets for the connection of tubes were generated with a biopsy puncher (0.75 mm). The PDMS device and a glass slide were then washed three times with isopropyl alcohol and water and then placed into an oven at 60 °C for drying. After treating the PDMS chip and glass slide with oxygen plasma (PVA TePla 100 plasma system), they were adhered by pressing together. Finally, Aquapel solution was filled into the channels and flushed out with air.

4.2.5 Microfluidic synthesis of oxygen-releasing microgels

Microfluidic experiments were conducted on a microfluidic station consisting of three syringe pumps (Harvard Apparatus, Holliston, MA, USA), to control the flow rates of the different phases. The microfluidic synthesis was observed using a microscope (Motic AE2000, TED PELLA, INC., Redding, CA) equipped with a camera (Flea3, Point Grey, Richmond, CA). The PDMS microfluidic device was connected to the syringe containing aqueous phases and a continuous phase (fluorinated oil with 2% surfactant) using fine bore polyethylene tubing. The microchannels had a rectangular cross-junction with a uniform height of 80 μm. The CaO_2 nanoparticle suspension of ethanol was centrifuged at 14,000 rpm for 5 min and then dispersed in 15 wt% Dex-MA in deionized water so that the final concentrations of CaO_2 nanoparticles were 0, 10 and 20 mg mL^{-1}. For monodisperse droplet formation, one aqueous phase containing Dex-MA and CaO_2 nanoparticles was injected into the inlet of the PDMS device at a flow rate of 150 μL h^{-1}. Another aqueous phase containing 20 mg mL^{-1} LAP in deionized water was also injected at a same flow rate. For in situ ACC formation, one aqueous phase containing 15 wt% Dex-MA and 20 mg mL^{-1} CaO_2 nanoparticles in deionized water and another aqueous phase containing 20 mg mL^{-1} LAP in 88 mM $NaHCO_3$ solution with 0.2 mg mL^{-1} NaH_2PO_4 were injected in the same way. The continuous phase containing a fluorinated oil with surfactant (FluoSurf) was injected into the third inlet at a flow rate of 600 μL h^{-1}. Two aqueous phases

were mixed at the joint point initially, then an immiscible continuous phase provided water-in-oil droplets (**Figure 4-2**). Droplets were collected from the outlet connected to the sample tube using fine bore polyethylene tubing. Collected droplets were exposed to UV light (365 nm) for 1 min to initiate cross-linking of the precursor solution and yielded monodisperse microgels. The obtained microgels were washed by Novec oil and hexane and their sizes were determined with ImageJ (average diameter of 50 microgels). Purified microgels were freeze-dried for storage. Morphology of purified and freeze-dried microgels were observed in deionized water by microscopy. Surface morphology of freeze-dried microgels was investigated by SEM (Hitachi-High Technologies) after sputter coated with carbon. Crystal structures of microgels were evaluated by XRD (AERIS, Malvern Panalytical, Malvern, U.K.). To clarify the structure of CaO_2 nanoparticles and ACC-CaO_2 in the microgels, microgels were crashed by a spatula. Microgels were sputter-coated with osmium using an HPC-30 Plasma Coater (Vacuum Device, Ibaraki, Japan) and then SEM and energy dispersive X-ray spectrometry (EDX) measurements were performed by Phenom ProX Desktop SEM (Thermo Fisher Scientific, MA) for the morphology and elemental analysis.

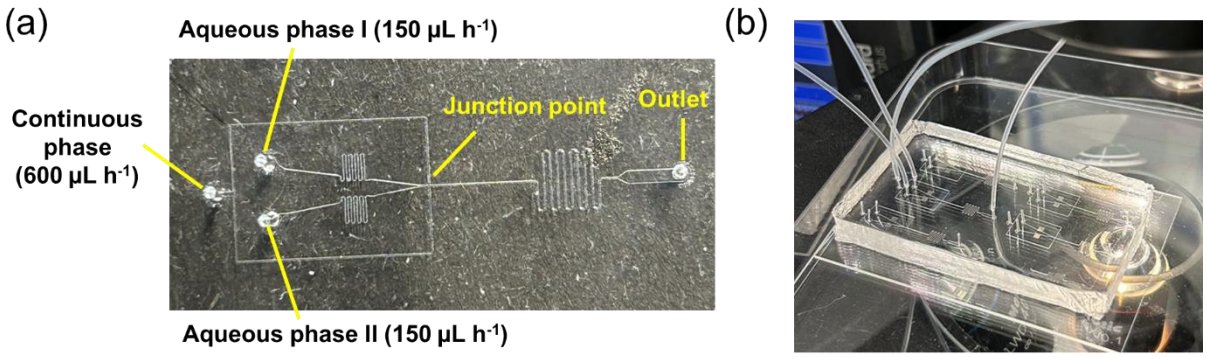

Figure 4-2. Pictures of (a) microfluidic device and (b) microgel fabrication process.

4.2.6 Oxygen and hydrogen peroxide release behaviors of microgels

Oxygen release behaviors of microgels were evaluated by measuring the dissolved oxygen amount in a solution containing microgels under a hypoxic condition as previously reported.[17] An SDRSensor Dish Reader (SDRSensor Dish Reader, PreSens, Regensburg, Germany) was placed in a hypoxia cell culture airtight bag (6-8669-03, As one, Osaka, Japan). 15 mg mL^{-1} microgels were dispersed in DMEM containing 100 U mL^{-1} catalase and then 500 μL of microgel suspension was added into a 24-well sensor dish. As a control, a DMEM solution

containing 100 U mL^{-1} catalase was also added into a 24-well sensor dish. Soon after the sample preparation, the 24-well sensor dish was placed on the Sensor Dish Reader. To create a hypoxic condition, three AnaeroPack O_2 absorbers (MITSUBISHI GAS CHEMICAL COMPANY INC., Tokyo, Japan) were placed in the bag and it was then completely sealed using parafilm. In this system, the oxygen concentration in the air went down below 1% at around 2 h. The dissolved oxygen amount in DMEM was then monitored at 37 °C. For the ACC-CaO_2 microgel, 15 mg mL^{-1} ACC-CaO_2 microgel was dispersed in DMEM and 100 mM acetate buffer (pH 5.0) containing 100 U mL^{-1} catalase. Then, the dissolved oxygen amount in the solution including microgels was measured under a hypoxic condition as mentioned above. For the morphology changes of the ACC-CaO_2 microgel, 1 mg mL^{-1} ACC-CaO_2 microgel was dispersed in DMEM and 100 mM acetate buffer (pH 5.0). After 1 h incubation at 37 °C, phase contrast images of microgels were taken with a microscope. 100 mM acetate buffer (pH 5.0) was prepared by mixing 100 mM acetic acid solution and 100 mM sodium acetate solution so that the final pH was 5.0.

Hydrogen peroxide release from microgels was evaluated in a DMEM model solution (44 mM $NaHCO_3$ solution containing 0.1 mg mL^{-1} NaH_2PO_4) and 100 mM acetate buffer (pH 5.0). 1.5 mg mL^{-1} microgels were dispersed in solution. After 60 min incubation at room temperature, the hydrogen peroxide concentration in each solution was measured using an Oxiselect Hydrogen Peroxide/Peroxidase Assay Kit (Fluorometric) (STA-344, Cell Biolabs Inc., San Diego, USA) as previously reported.[17] Due to the limitation of the detection range for this assay kit, sample solutions of microgels containing 5 and 10 mg mL^{-1} CaO_2 nanoparticles were diluted 10 times.

4.3 Results and discussion

4.3.1 Synthesis of CaO_2 nanoparticles and Dex-MA

As commercially available CaO_2 microparticles (Size < 74 μm) are too large for the microfluidic system, leading to clogging of the channels, CaO_2 nanoparticles with smaller sizes were synthesized using a previously reported method with slight modifications.[11] Synthesized CaO_2 nanoparticles were analyzed by X-ray diffraction (XRD) for crystal structure and SEM for the morphology. **Figure 4-3a** shows the XRD spectrum of synthesized CaO_2 nanoparticles. The peaks at 30, 36, 48, and 53° were observed, which were assigned to the (002), (110), (112) and (103) reflections of CaO_2.[18,19] SEM images showed aggregates composed of nanoparticles with a size around tens of nm (**Figure 4-3b**). These aggregates were formed probably during drying of aqueous dispersion on the microscopy grid.

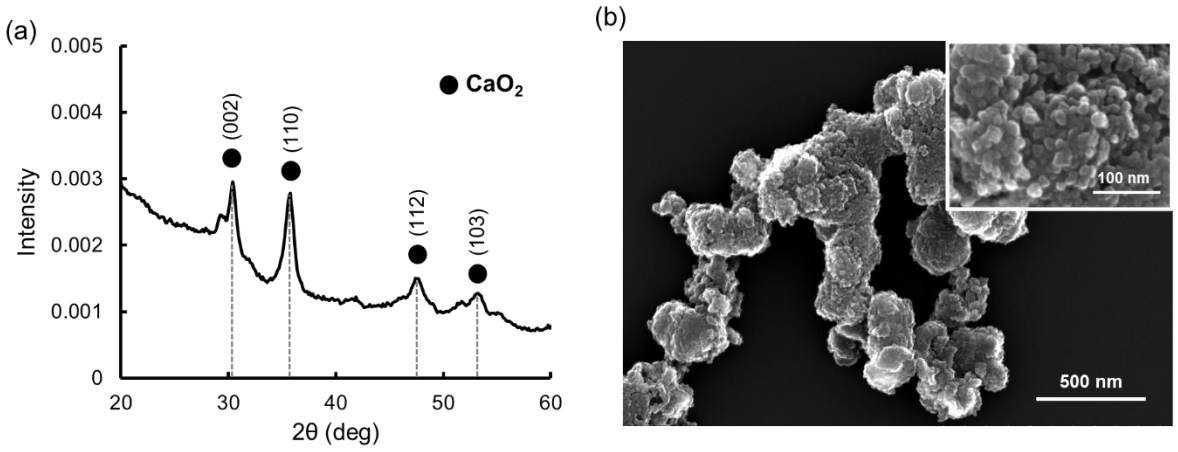

Figure 4-3. (a) XRD spectrum and (b) SEM image of synthesized CaO_2 nanoparticles.

Dex-MA was synthesized by coupling glycidyl methacrylate to dextran (Mw=150 kDa) in dimethylsulfoxide. [7,12,13] The grafting degree of the methacrylate group was 48 mol% according to the integration of relevant protons in the ^{1}H-NMR analysis (**Figure 4-4a**). The chemical composition of Dex-MA was also evaluated by Fourier transform infrared spectroscopy (FT-IR) measurement (**Figure 4-4b**). Dex-MA showed bands derived from C=C stretching vibration (blue line) at around 1,630 cm^{-1} and C=O stretching vibration (red line) at around 1,710 cm^{-1}, suggesting the successful coupling of glycidyl methacrylate to dextran.

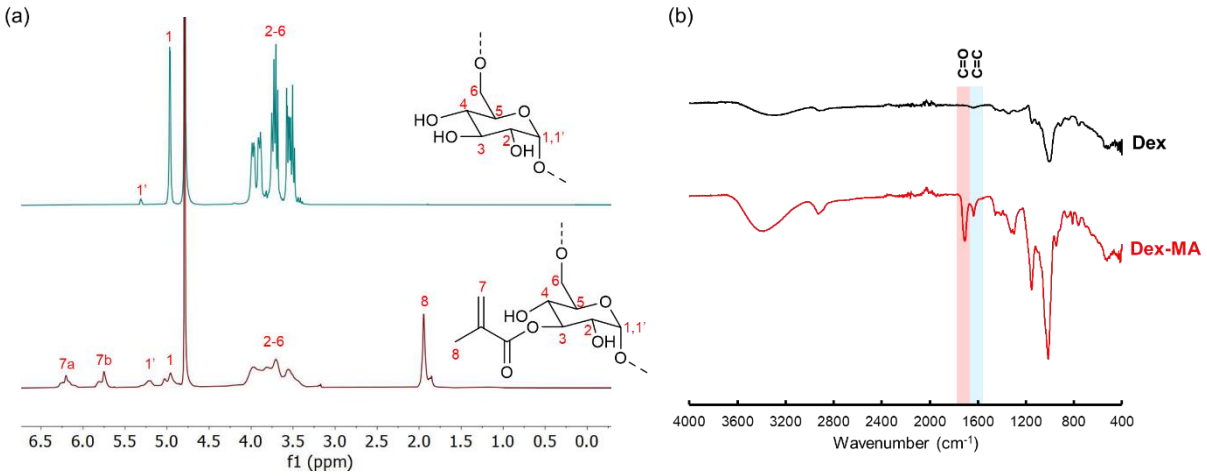

Figure 4-4. (a) ^{1}H-NMR of dextran (top) and Dex-MA (bottom) in D_2O. (b) FT-IR spectra of dextran and Dex-MA.

4.3.2 Microfluidic synthesis of Dex-MA microgel containing CaO_2 nanoparticles

Microgels were fabricated by free radical cross-linking reaction of droplets containing Dex-MA, CaO_2 nanoparticles and a photoinitiator (LAP) initiated through UV-light exposure after the microfluidic production of uniform aqueous droplets. LAP is known as a biocompatible photoinitiator and is often used for the fabrication of hydrogels in the tissue engineering field.[6,20] **Figure 4-5a** shows microfluidic synthesis of Dex-MA microgels containing 0, 5 and 10 mg mL^{-1} CaO_2 nanoparticles at the junction point. An aqueous phase containing 15 wt% Dex-MA and 0, 10 and 20 mg mL^{-1} CaO_2 nanoparticles was mixed with an aqueous phase containing 20 mg mL^{-1} LAP. Subsequently, monodisperse droplets were fabricated in a continuous phase consisting of the inert fluorinated oil "FluoSurf". A flow rate of 150 µL h^{-1} was used for both of the aqueous phases and 600 µL h^{-1} was used for the continuous phase to generate monodisperse droplets. As shown in **Figure 4-5b**, homogeneous droplets of black suspension were obtained using CaO_2 nanoparticles while transparent droplets were obtained without CaO_2. This result suggests the encapsulation of CaO_2 nanoparticles in the droplets in this system. After the droplet formation, collected droplets were exposed to UV light for 1 min and subsequently purified and redispersed in water (**Figure 4-5c**). In all conditions, homogeneous and monodisperse microgels with a size of 114.2 ± 4.1 µm for 0 mg mL^{-1} CaO_2, 111.4 ± 4.1 µm for 5 mg mL^{-1} CaO_2 and 110.5 ± 5.3 µm for 10 mg mL^{-1} CaO_2

were obtained. The amount of CaO_2 nanoparticles in the microgel derived from 5 mg mL^{-1} CaO_2 was much smaller than that before UV crosslinking. This is probably because many CaO_2 nanoparticles were decomposed by UV irradiation.[21] In the case of 10 mg mL^{-1} CaO_2, CaO_2 remained in the microgel even after UV crosslinking. According to these results, fabrication of the Dex-MA microgel containing CaO_2 nanoparticles was confirmed especially for the higher concentration of CaO_2 nanoparticles.

For the storage of oxygen-releasing microgels, the obtained microgels were freeze-dried. **Figure 4-5d,e** show SEM images of a freeze-dried Dex-MA microgel containing 0, 5 and 10 mg mL^{-1} CaO_2 nanoparticles taken at lower and higher magnifications. Freeze-dried microgels without CaO_2 showed a smooth surface structure, suggesting that the crosslinking degree of the polymer network is high. On the other hand, the freeze-dried microgel containing 5 mg mL^{-1} CaO_2 nanoparticles showed a porous structure compared to the case without CaO_2. This is probably because oxygen and hydrogen peroxide released from CaO_2 interfered with the free radical cross-linking reaction in the droplet, which provided the microgel with a lower crosslinking degree. Furthermore, the freeze-dried microgel containing 10 mg mL^{-1} CaO_2 nanoparticles showed a larger porous structure compared to the case of 5 mg mL^{-1} CaO_2 nanoparticles. This is probably because higher concentrations of CaO_2 released a greater amount of oxygen and hydrogen peroxide, which interfered more greatly with the radical cross-linking reaction.

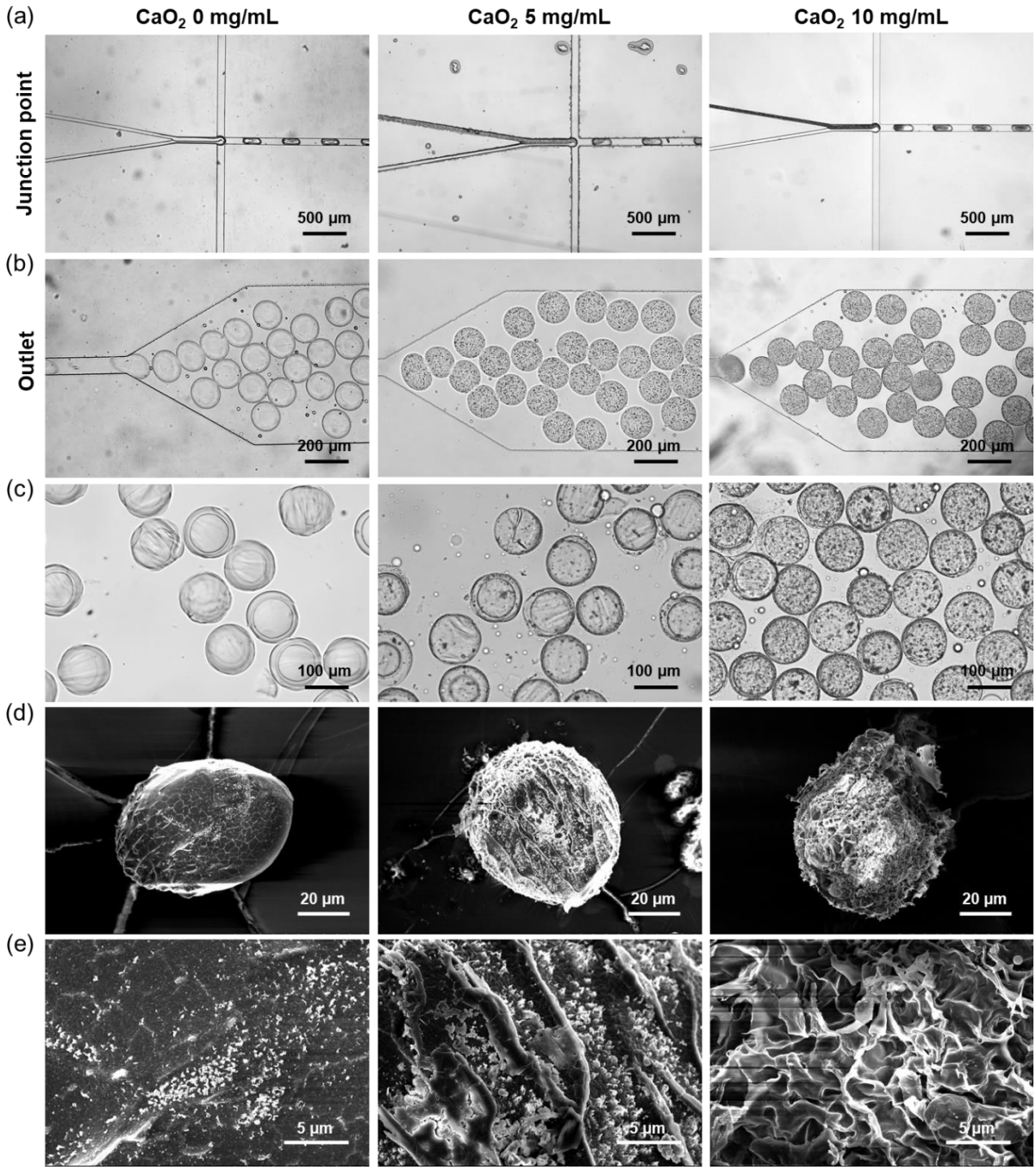

Figure 4-5. Bright field images of microfluidic synthesis of Dex-MA microgels containing 0, 5 and 10 mg mL^{-1} CaO_2 nanoparticles at (a) junction point and (b) outlet. (c) Bright field images of a purified Dex-MA microgel containing 0, 5 and 10 mg mL^{-1} CaO_2 nanoparticles. SEM images of a freeze-dried Dex-MA microgel containing 0, 5 and 10 mg mL^{-1} CaO_2 nanoparticles at (d) lower and (e) higher magnification.

To evaluate the stability of the freeze-dried microgels, they were dispersed in water. As shown in **Figure 4-6a**, all freeze-dried microgels retained their spherical morphology in water. Furthermore, after 7 days incubation in water, none of the freeze-dried microgels changed their spherical morphologies compared to soon after the dispersion in water, suggesting that microgels were not decomposed by hydrogen peroxide and oxygen released from CaO_2 (**Figure 4-6b**). These results suggested that oxygen-releasing microgels were stable even after freeze-drying. Therefore, these freeze-dried microgels are storable in a dry state until their use.

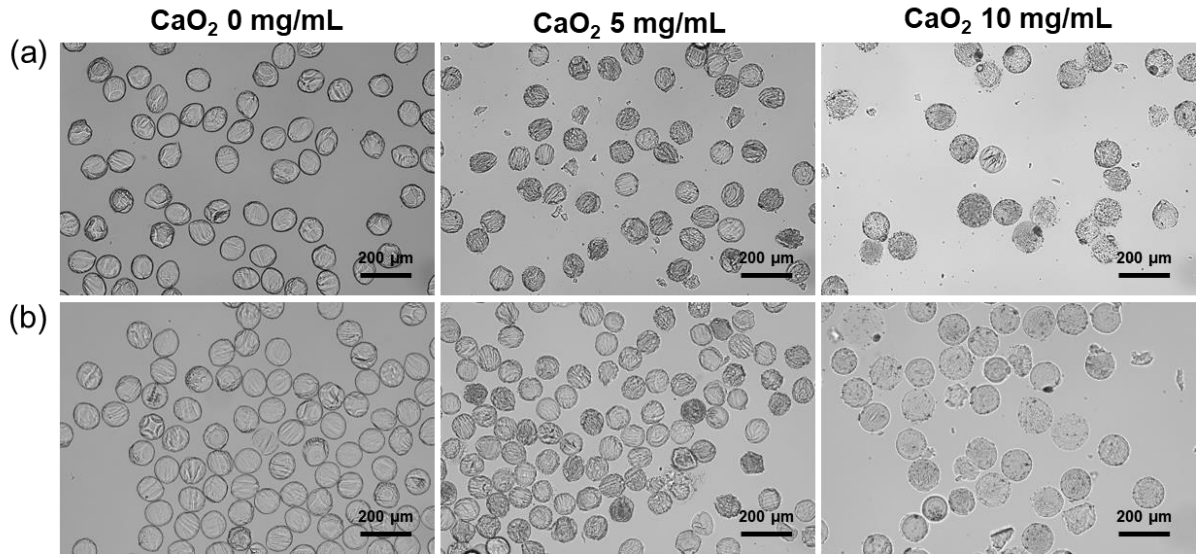

Figure 4-6. Bright field images of freeze-dried Dex-MA microgels containing 0, 5 and 10 mg mL^{-1} CaO_2 nanoparticles after (a) the dispersion in water and (b) 7 days incubation in water.

Oxygen release behaviors of freeze-dried microgels in a cell culture medium (DMEM) containing 100 U mL^{-1} catalase were evaluated by measuring dissolved oxygen concentration in the solution after the dispersion of microgels under a hypoxic condition as previously reported (**Figure 4-7a**).[17] Catalase is an enzyme which decomposes hydrogen peroxide into oxygen.[22] Thus, larger amounts of oxygen release from microgels containing CaO_2 nanoparticles can be observed since CaO_2 releases not only oxygen but also hydrogen peroxide.[23] Herein, 100% indicates equilibrium with oxygen in the atmosphere. Without microgels, dissolved oxygen concentration decreased rapidly because of the hypoxic condition (black line). On the other hand, dissolved oxygen concentration in the solution containing a microgel with 5 mg mL^{-1} CaO_2 nanoparticles increased to 108% and showed a higher value until 200 min compared to without a microgel (yellow line). Furthermore, dissolved oxygen

concentration in the solution containing a microgel with 10 mg mL^{-1} CaO_2 nanoparticles increased over 250% (detection limit of the oxygen measuring machine) and showed a higher value until 300 min compared to without a microgel (red line). These results confirm oxygen release from microgels containing CaO_2 nanoparticles. The author also evaluated hydrogen peroxide release from microgels. Since the components of DMEM such as methionine decompose hydrogen peroxide,[17,24] 44 mM $NaHCO_3$ solution including 0.1 mg mL^{-1} NaH_2PO_4 was used as a model solution for DMEM to evaluate the detailed hydrogen peroxide release behavior. As expected, the microgel without CaO_2 nanoparticles did not release hydrogen peroxide (below 1 μM), as shown in **Figure 4-7b**. The microgel containing 5 mg mL^{-1} CaO_2 nanoparticles released 33.9 ± 1.2 μM hydrogen peroxide while the microgel containing 10 mg mL^{-1} CaO_2 nanoparticles released 213.2 ± 3.3 μM hydrogen peroxide in a DMEM model solution for 60 min. The value of oxygen and hydrogen peroxide release from the microgel containing 5 mg mL^{-1} CaO_2 nanoparticles was much smaller than that of 10 mg mL^{-1} CaO_2 nanoparticles. As explained earlier, this is probably because many CaO_2 nanoparticles decomposed in the microgel containing 5 mg mL^{-1} CaO_2 nanoparticles during the radical cross-linking reaction. Thus, when enough CaO_2 nanoparticles were contained in the microgel, larger amounts of oxygen and hydrogen peroxide release can be seen.

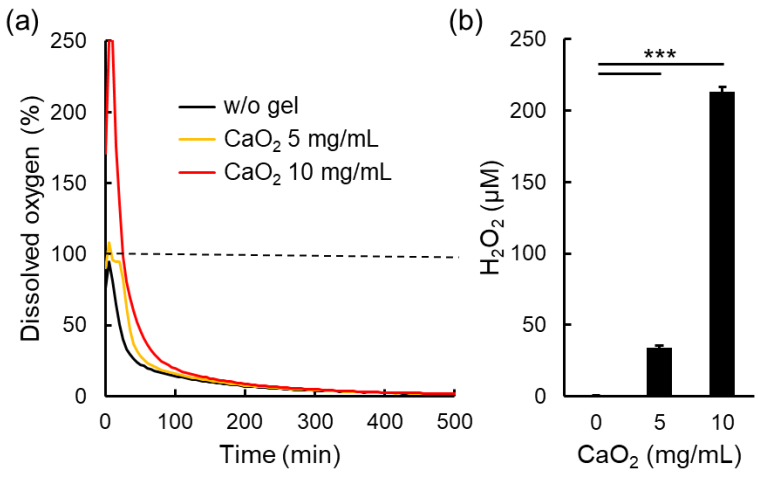

Figure 4-7. (a) Dissolved oxygen concentration changes in 500 μL of DMEM containing 100 U mL^{-1} catalase and 15 mg mL^{-1} Dex-MA microgel encapsulating 5 and 10 mg mL^{-1} CaO_2 nanoparticles under a hypoxic condition. (b) Hydrogen peroxide concentration in a DMEM model solution (44 mM $NaHCO_3$ solution containing 0.1 mg mL^{-1} NaH_2PO_4) after the dispersion of 1.5 mg mL^{-1} microgels containing 0, 5 and 10 mg mL^{-1} CaO_2 nanoparticles for 60 min. Data presented as mean ± SD, n=3. ***$p < 0.001$.

4.3.3 Microfluidic synthesis of a Dex-MA microgel containing ACC-CaO_2 by in situ ACC formation

For the in-situ ACC formation in the microfluidic system, an aqueous phase containing 15 wt% Dex-MA and 20 mg mL^{-1} CaO_2 nanoparticles was mixed with another aqueous phase containing 20 mg mL^{-1} LAP, 88 mM $NaHCO_3$ and 0.2 mg mL^{-1} NaH_2PO_4. The concentrations of $NaHCO_3$ and NaH_2PO_4 were derived from previous report about ACC coating on CaO_2 microparticles.[8] As shown in **Figure 4-8a**, aggregates were formed at the interfaces of two aqueous phases probably because of ACC formation by the reaction between $Ca(OH)_2$ derived from CaO_2 nanoparticles in the Dex-MA aqueous phase and $NaHCO_3$ containing NaH_2PO_4 in the other aqueous phase. After the droplet formation (**Figure 4-8b**), collected droplets were exposed to UV light for 1 min and subsequently purified and redispersed in water (**Figure 4-8c**). Interestingly, purified microgels showed aggregates inside, suggesting the formation of ACC in the microgel. As with the microgel containing CaO_2 nanoparticles, SEM images of the freeze-dried ACC-CaO_2 microgel showed a porous structure (**Figure 4-8d**). In addition, the freeze-dried ACC-CaO_2 microgel was stable even after dispersion in water and 7 days incubation in water (**Figure 4-8e,f**).

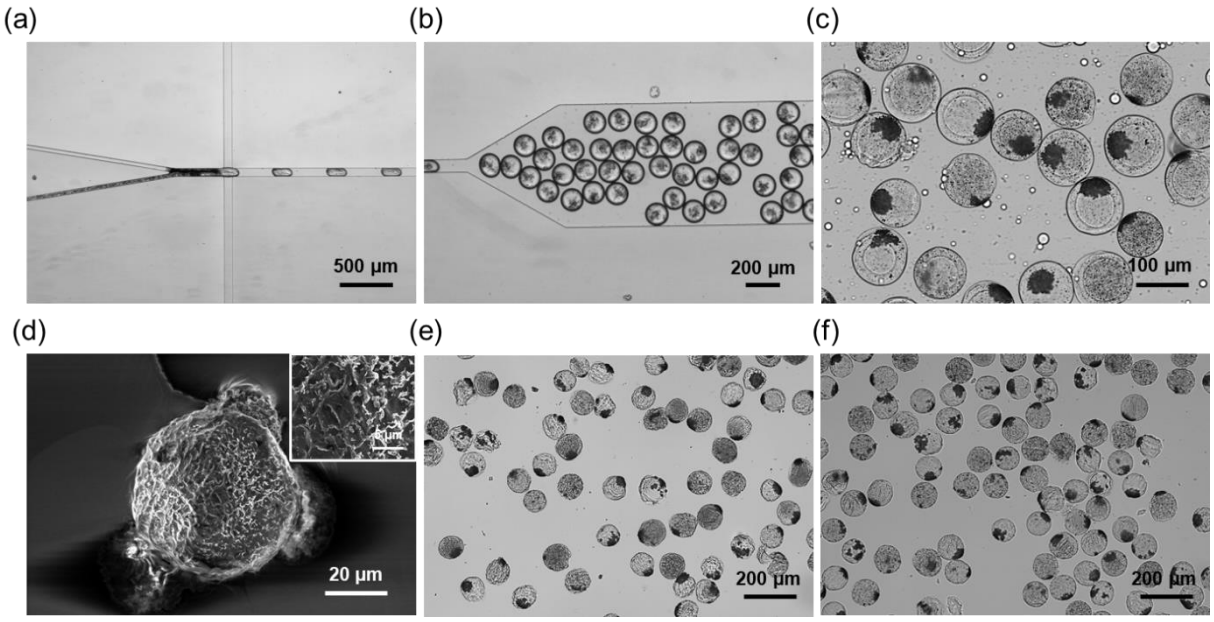

Figure 4-8. Bright field images of microfluidic synthesis of an ACC-CaO_2 microgel at (a) junction point and (b) outlet. (c) Bright field image of a purified ACC-CaO_2 microgel. (d) SEM images of a freeze-dried ACC-CaO_2 microgel. Bright field images of a freeze-dried ACC-CaO_2 microgel after (e) the dispersion in water and (f) 7 days incubation in water.

For the elemental analysis on the microgels, SEM-EDX measurements were performed. To clarify the structure of CaO_2 nanoparticles and ACC-CaO_2 in the microgels, microgels were crashed by a spatula before sputter-coating with osmium. The elemental mapping of microgels containing 10 mg mL^{-1} CaO_2 nanoparticles showed calcium throughout the cross section of microgels, suggesting that CaO_2 nanoparticles were distributed homogeneously in the microgel (**Figure 4-9a, b**). From a high magnification SEM image, CaO_2 nanoparticles with a size below 1 μm were observed (**Figure 4-9c**). On the other hand, the elemental mapping of microgels containing ACC-CaO_2 showed calcium locally, suggesting the formation of aggregates composed of CaO_2 and ACC (**Figure 4-9d,e**). This result is consistent with the observation of aggregates in **Figure 4-8**. High magnification SEM image of these aggregates showed small particles of around 1 μm in size (**Figure 4-9f**). To clarify the crystal structure of inorganic compound in microgels, XRD measurements was performed. Microgel containing 10 mg mL^{-1} CaO_2 nanoparticles showed small peaks at 30 and 36°, which were assigned to the (002) and (110) reflections of CaO_2 (**Figure 4-9g**). On the other hand, ACC-CaO_2 microgel showed peaks at 30, 36, 40, 43, 48 and 49°, which were assigned to the (104), (110), (113), (202), (024), and (116) reflections of calcite, one of the crystal structures of calcium carbonate (**Figure 4-9h**). Due to the overlap of peaks, the peaks derived from CaO_2 could not be identified at ACC-CaO_2 microgel. XRD results suggested the existence of calcite at the aggregates in ACC-CaO_2 microgel. It is well known that typical calcite shows cubic structure [8,25-28]. However, cubic structure was not clearly observed in ACC-CaO_2 microgel in the SEM image (**Figure 4-9f**). Therefore, it was suggested that most of the aggregates in microgels were ACC.

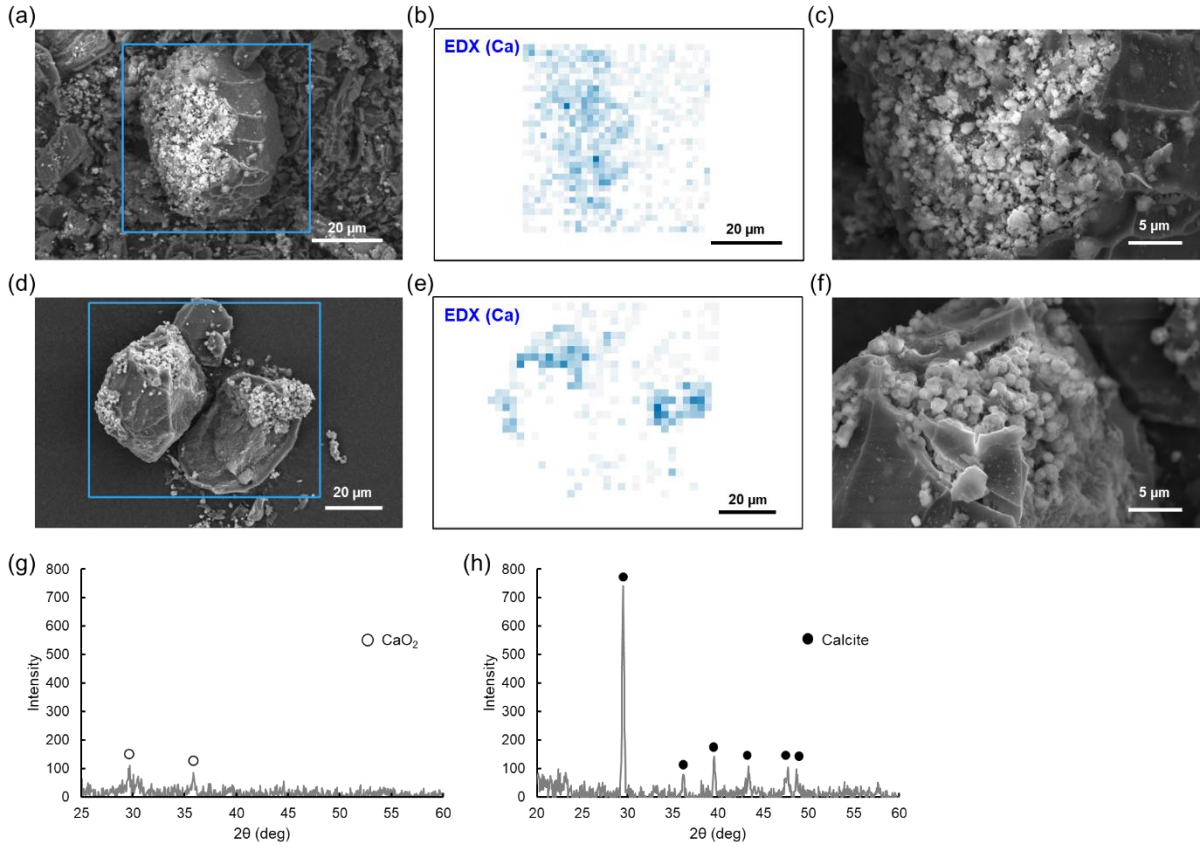

Figure 4-9. (a) SEM image, (b) elemental mapping of calcium at the blue square area in (a) by EDX and (c) high magnification SEM image of the cross section at the crashed microgels containing 10 mg mL^{-1} CaO_2 nanoparticles. (d) SEM image, (e) elemental mapping of calcium at the blue square area in (d) by EDX and (f) high magnification SEM image of the cross section at the crashed ACC-CaO_2 microgels. XRD spectra of (g) microgel containing 10 mg mL^{-1} CaO_2 nanoparticles and (h) ACC-CaO_2 microgel.

4.3.4 Controlled release of oxygen and hydrogen peroxide from an ACC-CaO_2 microgel

In chapter 2, CaO_2 microparticles coated with ACC did not release oxygen in a neutral cell culture medium because ACC suppressed the reaction between CaO_2 and water. On the other hand, ACC-CaO_2 released oxygen in a weak acidic condition because dissolution of ACC started the CaO_2 reaction. To evaluate such a controlled release of oxygen derived from the dissolution of ACC, the oxygen release behavior of the ACC-CaO_2 microgel was measured in neutral DMEM and acetate buffer (pH 5.0) containing 100 U mL^{-1} catalase under a hypoxic condition. **Figure 4-10a** shows dissolved oxygen concentration in DMEM after the addition of

the ACC-CaO_2 microgel. Unlike the microgels containing CaO_2 nanoparticles (**Figure 4-7**), the time dependent changes of dissolved oxygen concentration in DMEM containing the ACC-CaO_2 microgel showed a similar trend to the case without a microgel, suggesting that oxygen release from the ACC-CaO_2 microgel was suppressed. On the other hand, dissolved oxygen concentration in a weakly acidic acetate buffer (pH 5.0) containing the ACC-CaO_2 microgel increased until 150 min compared to the case without a microgel, suggesting oxygen release from the ACC-CaO_2 microgel (**Figure 4-10b**). Compared to the microgel containing 10 mg mL^{-1} CaO_2 nanoparticles (**Figure 4-7**), the increase value of dissolved oxygen concentration was much smaller for the ACC-CaO_2 microgel. It has been reported that CaO_2 is stable in a basic condition while it dissolves quickly in acidic and neutral conditions.[29] For the fabrication process of a microgel containing CaO_2 nanoparticles, the pH in water used for aqueous phases increased because basic $Ca(OH)_2$ was released from CaO_2. Thus, it is considered that further CaO_2 reaction was suppressed in this basic aqueous phase. For 10 mg mL^{-1} CaO_2 microparticles in water, the pH value in water reached 12.0 after 1 hour incubation. As a result, the weight loss of CaO_2 was below 1 % as expected. On the other hand, in the fabrication process of the ACC-CaO_2 microgel, $NaHCO_3$ solution was used for one aqueous phase. Since $NaHCO_3$ has a buffering effect, the pH change in the aqueous phase was suppressed compared to water. Therefore, it is considered that many CaO_2 nanoparticles were consumed during the in-situ ACC formation process. The author also evaluated hydrogen peroxide release from the ACC-CaO_2 microgel in a DMEM model solution (44 mM $NaHCO_3$ and 0.1 mg mL^{-1} NaH_2PO_4) and acetate buffer (pH 5.0). In chapter 2, the author reported that the buffer component of DMEM (44 mM $NaHCO_3$ and 0.1 mg mL^{-1} NaH_2PO_4) played an important role in the stabilization of ACC. As shown in **Figure 4-10c**, the ACC-CaO_2 microgel released around a 7-times higher concentration of hydrogen peroxide in a weakly acidic acetate buffer (pH 5.0) compared to the DMEM model solution. To understand these oxygen and hydrogen peroxide release behaviors of the ACC-CaO_2 microgel, the microgel morphologies were observed after immersing in DMEM and a weakly acidic acetate buffer (pH 5.0). In DMEM, the aggregates derived from ACC were observed inside the microgels (**Figure 4-10d**), suggesting that incorporation of CaO_2 nanoparticles in ACC suppressed the reaction with water. On the other hand, in the weakly acidic acetate buffer (pH 5.0), aggregates inside the microgel had disappeared (**Figure 4-10e**). These results suggest that the dissolution of ACC triggered the CaO_2 reaction with water, which started oxygen and hydrogen peroxide release from the ACC-CaO_2 microgel.

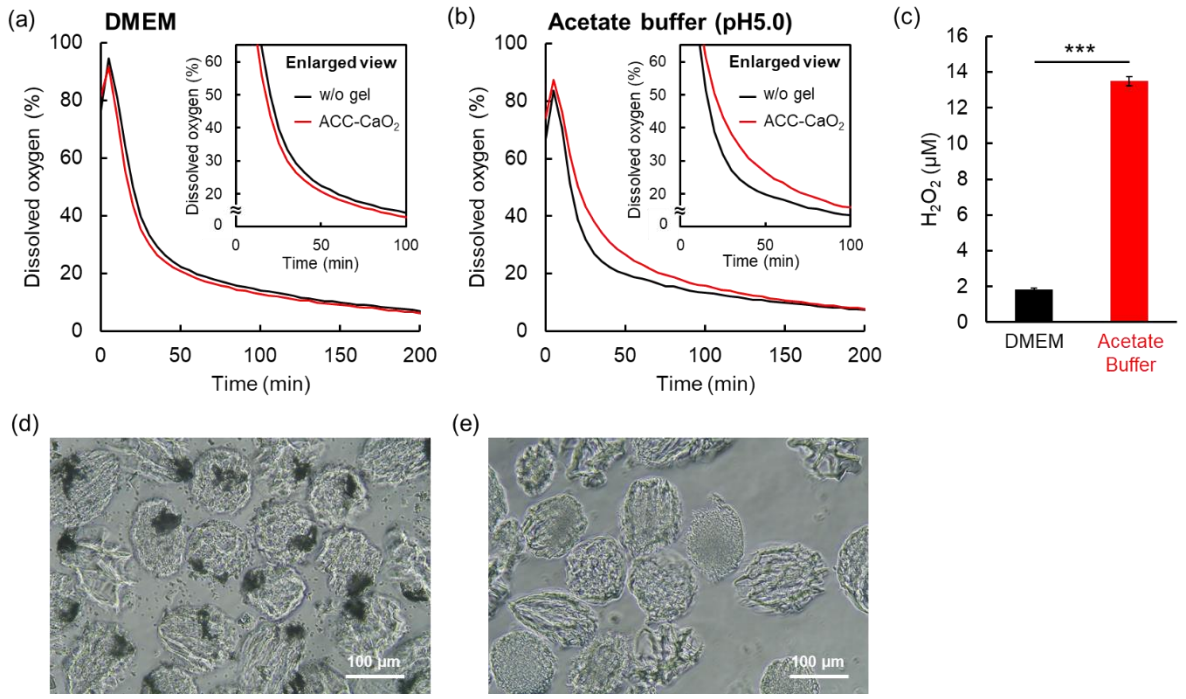

Figure 4-10. Variation of the dissolved oxygen concentration with time in 500 μL of (a) DMEM and (b) 100 mM acetate buffer (pH 5.0) containing 100 U mL^{-1} catalase and 15 mg mL^{-1} ACC-CaO_2 microgel under a hypoxic condition. (c) Hydrogen peroxide concentration in a DMEM model solution (44 mM $NaHCO_3$ solution containing 0.1 mg mL^{-1} NaH_2PO_4) and 100 mM acetate buffer (pH 5.0) after the dispersion of 1.5 mg mL^{-1} ACC-CaO_2 microgel for 60 min. Data presented as mean ± SD, n=3. ***$p < 0.001$. Phase contrast images of a freeze-dried ACC-CaO_2 microgel dispersed in (d) DMEM and (e) 100 mM acetate buffer (pH 5.0) for 60 min.

4.4 Conclusion

In chapter 4, the author reported the fabrication of oxygen-releasing microgels using a droplet-based microfluidic system. Homogeneous and monodisperse microgels containing CaO_2 nanoparticles as an oxygen source were obtained by photo-crosslinking of Dex-MA in aqueous droplets. Under optimized synthesis conditions, the author was able to vary the loading of CaO_2 nanoparticles into microgels. Obtained oxygen-releasing microgels were stable even after freeze drying, suggesting that they are storable in a dry condition. Since oxygen release from the microgel containing CaO_2 nanoparticles was observed, application of this new class of biomaterials for tissue engineering is highly expected. Furthermore, in situ ACC formation in the microfluidic system was also performed for the controlled release of oxygen from the

microgel. The obtained ACC-CaO_2 microgel did not release oxygen in neutral DMEM because incorporation of CaO_2 in ACC suppressed the reaction with water. However, the ACC-CaO_2 microgel released oxygen in a weakly acidic acetate buffer because the dissolution of ACC started the reaction between CaO_2 and water. Since the environment in ischemic tissue is weakly acidic[10] and the solubility of ACC increases in an acidic condition,[9] this controlled oxygen release property of the ACC-CaO_2 microgel based on $CaCO_3$ chemistry would be an attractive function. The author believes that application of this new class of biomaterials for tissue engineering are greatly anticipated.

4.5 References

[1] M. Xie, J. Wang, S. Wu, S. Yan, Y. He, *Biomater. Sci*. **2024**, *12*, 1950.
[2] Q. Feng, D. Li, Q. Li, X. Cao, H. Dong, *Bioact. Mater*. **2022**, *9*, 105.
[3] Z. Wei, S. Wang, J. Hirvonen, H. A. Santos, W. Li, *Adv. Healthcare Mater*. **2022**, *11*, 2200846.
[4] K. O. Rojek, M. Ćwiklińska, J. Kuczak, J. Guzowski, *Chem. Rev*. **2022**, *122*, 16839.
[5] S. Bulut, S. H. Jung, T. Bissing, F. Schmitt, M. Bund, S. Braun, A. Pich, *Small* **2023**, 2303783.
[6] S. Bulut, D. Günther, M. Bund, C. Haats, T. Bissing, C. Bastard, M. Wessling, L. De Laporte, A. Pich, *Adv. Healthcare Mater*. **2023**, 2302957.
[7] S. A. Jung, H. Malyaran, D. E. Demco, A. Manukanc, L. S. Häser, V. Kučikas, M. V. Zandvoort, S. Neuss, A. Pich, *Biomacromolecules* **2023**, *24*, 3972.
[8] D. Tomioka, S. Fujita, M. Matsusaki, *ACS Omega* **2024**, *9*, 5903.
[9] M. Wang, B. Zhou, L. Wang, F. Zhou, N. Smith, D. Saunders, R. A. Towner, J. Song, J. Qu, W. R. Chen, *J. Mater. Chem. B* **2020**, *8*, 8261.
[10] G. X. Yan, A. G. Kléber, *Circ. Res*. **1992**, *71*, 460.
[11] Y. Hu, X. Wang, P. Zhao, H. Wang, W. Gu, L. Ye, *Biomater. Sci.* **2020**, *8*, 2931.
[12] W. N. E. van Dijk-Wolthuis, O. Franssen, H. Talsma, M. J. van Steenbergen, J. J. Kettenes-van den Bosch, W. E. Hennink, *Macromolecules* **1995**, *28*, 6317.
[13] W. N. E. van Dijk-Wolthuis, J. J. Kettenes-van den Bosch, A. van der Kern Hoof, W. E. Hennink, *Macromolecules* **1997**, *30*, 3411.
[14] S. H. Jung, F. Meyer, S. Hörnig, M. Bund, B. Häßel, L. P. B. Guerzoni, L. D. Laporte, G. B. Messaoud, S. P. Centeno, A. Pich, *Small* **2024**, *20*, 2303444.
[15] S. H. Jung, S. Bulut, L. P. B. B. Guerzoni, D. Günther, S. Braun, L. D. Laporte, A. Pich, *J. Colloid Interface Sci*. **2022**, *617*, 409.
[16] L. P. B. Guerzoni, J. C. Rose, D. B. Gehlen, A. Jans, T. Haraszti, M. Wessling, A. J. C. Kuehne, L. D. Laporte, *Small* **2019**, *15*, 1900692.
[17] D. Tomioka, S. Fujita, J. Groll, M. Matsusaki, *Chem. Mater.* **2023**, *35*, 5378.

[18] D. M. D. Santos, L. M. Dias, A. K. Surur, D. A. D. Moraes, A. C. Pavarina, C. R. Fontana, D. S. Correa, *ACS Appl. Nano Mater.* **2022**, *5*, 14425.
[19] X. Zhao, M. C. Nguyen, C. Z. Wang, K. M. Ho, *RSC Adv.* **2013**, *3*, 22135.
[20] N. Monteiro, G. Thrivikraman, A. Athirasala, A. Tahayeri, C. M. França, J. L. Ferracane, L. E. Bertassoni, *Dent. Mater.* **2018**, *34*, 389.
[21] S. Zhang, B. Song, R. Wang, Z. Zhan, M. Saakes, R. D. van der Weijden, C. J. N. Buisman, Y. Lei, *ACS EST Water* **2023**, *3*, 866.
[22] M. A. Prieto, X. Biarnes, P. Vidossich, C. Rovira, *J. Am. Chem. Soc.* **2009**, *131*, 11751.
[23] H. Wang, Y. Zhao, T. Li, Z. Chen, Y. Wang, C. Qin, *Chem. Eng. J.* **2016**, *303*, 450.
[24] S. Boonvisut, A. Aksnes, L. R. Njaa, *Food Chem*. **1982**, *9*, 183.
[25] Y. Q. Niu, J. H. Liu, C. Aymonier, S. Fermani, D. Kralj, G. Falini, C. H. Zhou, *Chem. Soc. Rev.* **2022**, *51*, 7883.
[26] M. H. Nielsen, S. Aloni, J. J. D. Yoreo, *Science* **2014**, *345*, 1158.
[27] Z. Liu, Z. Zhang, Z. Wang, B. Jin, D. Li, J. Tao, R. Tang, J. J. D. Yoreo, *Proc. Natl. Acad. Sci. U. S. A.* **2020**, *117*, 3397.
[28] Z. Zou, J. Xie, E. M. Sanchez, Z. Fu, *Cryst. Growth Des.* **2021**, *21*, 414.
[29] A. Northup, D. Cassidy, *J. Hazard. Mater.* **2008**, *152*, 1164.

Concluding Remarks

In this thesis, surface modification of CaO_2 was performed for the controlled release of oxygen and oxygen releasing materials using surface modified CaO_2 were fabricated for tissue engineering applications.

In chapter 1, HAp coating on CaO_2 was performed by simple immersion of CaO_2 in PB. Since the HAp formation on CaO_2 delays the reaction with water, sustained oxygen release behavior was achieved. The author demonstrated the tissue engineering application of HAp-CaO_2 at the example of oxygen releasing gelatin hydrogels. Sustained oxygen release around 10 days from gelatin hydrogel including HAp-CaO_2 improved cell proliferation under hypoxic environments. HAp-CaO_2 therefore has great potential for use in a broad range of biomaterials as a new oxygen source capable of sustained oxygen release.

In chapter 2, stabilized ACC coating on CaO_2 was reported, which suppressed the reaction between CaO_2 and water. Stabilized ACC was produced by the reaction between $Ca(OH)_2$ derived from CaO_2 and $NaHCO_3$ including NaH_2PO_4. In contrast, surface modification of CaO_2 by calcium carbonate crystals was difficult due to the crystallization process via dissolution-reprecipitation. Interestingly, pH-dependent oxygen release from ACC-CaO_2 was observed in a cell culture medium probably because ACC on CaO_2 dissolved in a weak acidic condition. Since the environment in cancer and ischemetic tissues are known as weakly acidic, controlled release of oxygen from ACC-CaO_2 at these environments are highly expected.

In chapter 3, oxygen releasing micro-cell scaffold was fabricated by catalase/PLL LbL nanofilm assembly on HAp-CaO_2. Since catalase in LbL nanofilm decomposed toxic hydrogen peroxide into oxygen, hydrogen peroxide release from LbL-HAp-CaO_2 was not observed after 2 cycle LbL nanofilm assembly. Importantly, incorporation of LbL-HAp-CaO_2 in 3D tissue dramatically suppressed cell death due to oxygen shortage and provided stable 3D tissue with thickness around 400 μm because of sufficient oxygen supply from LbL-HAp-CaO_2. To the best of the author's knowledge, no one has ever reported the construction of such a thick living 3D tissue with high cell density. LbL-HAp-CaO_2 therefore represent a great potential toward the development of clinically sized tissues for the application in regenerative medicines.

In chapter 4, oxygen-releasing microgels were fabricated using a droplet-based microfluidic system. Homogeneous and monodisperse microgels containing CaO_2 nanoparticles as an oxygen source were obtained by photo-crosslinking of Dex-MA in aqueous droplets. Furthermore, in situ ACC formation in the microfluidic system was also performed for the controlled release of oxygen from the microgel. As with the case in chapter 2, the obtained ACC-CaO_2 microgel showed pH dependent oxygen release behavior. By taking advantage of oxygen-releasing materials and microgels, application of this new class of biomaterials for tissue engineering is highly expected.

List of Publications

Chapter 1

Hydroxyapatite Nanocoating on Calcium Peroxide Microparticles for Sustained Oxygen Release

Daisuke Tomioka, Satoshi Fujita, Jürgen Groll, and Michiya Matsusaki

Chem. Mater. **2023**, *35*, 5378-5391.

Chapter 2

Controlled Release of Oxygen from Calcium Peroxide in a Weak Acidic Condition by Stabilized Amorphous Calcium Carbonate Nanocoating for Biomedical Applications

Daisuke Tomioka, Satoshi Fujita, and Michiya Matsusaki

ACS Omega **2024**, *9*, 5903-5910.

Chapter 3

Construction of thick living 3D tissue with high cell density using calcium peroxide-based oxygen releasing micro-cell scaffold

Daisuke Tomioka, Naoko Sasaki, Satoshi Fujita, and Michiya Matsusaki

Manuscript in preparation

Chapter 4

Fabrication of oxygen-releasing dextran microgels by droplet-based microfluidic method

Daisuke Tomioka, Shannon Anna Jung, Andrij Pich, and Michiya Matsusaki

RSC Adv. **2024**, *14*, 26544-26555.

Supplementary publication

1. Development of temperature dependent oxygen releasable nanofilm by modulating oxidation state of myoglobin

   Daisuke Tomioka, Hirotaka Nakatsuji, Shigeru Miyagawa, Yoshiki Sawa, and Michiya Matsusaki

   Chem. Commun. **2021**, *57*, 5131-5134.

2. Ultra-Rapid and Specific Gelation of Collagen Molecules for Transparent and Tough Gels

by Transition Metal Complexation

Tomoyuki Suezawa, Naoko Sasaki, Yuichi Yukawa, Nazgul Assan, Yuta Uetake, Kunishige Onuma, Rino Kamada, **Daisuke Tomioka**, Hidehiro Sakurai, Ryohei Katayama, Masahiro Inoue, and Michiya Matsusaki

Adv. Sci. **2023**, *10*, 2302637.

Acknowledgements

This study was carried out from 2019 to 2025 at Department of Applied Chemistry, Graduate School of Engineering, Osaka University. In the past six years, I have received a lot of assistance and support during my research. Upon the completion of this thesis, I would like to express my gratitude to all those who have helped me.

Foremost, I am extremely grateful to my supervisor, Prof. Michiya Matsusaki for his invaluable advice, continuous support, and encouragement during this work. I also appreciate that Prof. Matsusaki gave me an opportunity to study abroad at RWTH Aachen University. These absolutely broaden my horizon and enrich my life experience.

I am deeply grateful to the thesis committee: Prof. Toshiyuki Kida and Prof. Kazuya Kikuchi, for their insightful comments and their donation of time.

I would like to extend my sincere thanks to Prof. Andrij Pich and Ms. Shannon Anna Jung in RWTH Aachen University for their kind supports of my research in Aachen and article writing. I also thanks to all the member in Prof. Pich's research group for their kind support in both research and daily life in Aachen.

I am deeply grateful to Dr. Satoshi Fujita in National Institute of Advanced Industrial Science and Technology for his insightful comments and suggestions in the experiment, data discussion and article writing. Thanks to Prof. Toshiyuki Kida and Associate Prof. Hajime Shigemitsu for their assistance in XRD measurement. Thanks to Prof. Hiroshi Uyama and Associate Prof. Hsu Yu-I for their assistance in SEM-EDX measurements. Thanks to Prof. Jürgen Groll in University of Würzburg for his help in the project.

Besides my supervisor, I am deeply grateful to Dr. Naoko Sasaki and Dr. Hirotaka Nakatsuji for the continuous and very patient help in my research. Thanks to Associate Prof. Masahiko Nakamoto and Assistant Prof. Kenta Homma for the comments and suggestions. Thanks to Dr. Fiona Louis, Dr. Dong Hee Kang, Dr. Agathe Figarol, Dr. Zhengtian Xie, Dr. Zeng Jinfeng, Dr. Marie Piantino, Dr. Abdul Sisak Muhammad Asri, Dr. Quentin Muller, Dr. Yucheng Shang, Dr. Zhang Zhuying and Dr. Asli Sena Karanfil for their comments and guidance to my experiments.

I would like to offer my special thanks to Ms. Eri Enomoto and Ms. Chika Sugiki for their kind

support and help in the laboratory affairs, scholarships application and daily life.

My appreciation also goes to the previous and current fellows in the laboratory: Thanks to Guest Associate Prof. Shiro Kitano, Guest Associate Prof. Shinji Irie, Visiting researcher Yoshihiro Kodama, Asuka Kato, Yasuyuki Naito, Koichi Hattori, Yuka Yoshinouchi and Mizuho Suzuki. Thanks to Ms. Yukiko Sorayama, Ms. Lisa Thibes, Ms. Mizue Onishi, Mr. Yasuhiro Naka, Mr. Yuichi Yukawa, Mr. Hao Liu, Ms. Jinyu Li, Mr. Kazuma Ishiguro, Mr. Noboru Hiraoka, Mr. Tomoyuki Suezawa, Mr. Shogo Shimada, Mr. Ryo Mitsuyasu, Mr. Rei Miyata, Ms. Yuning Zhang, Ms. Lingyu Pei, Mr. Yuki Koba, Mr. Tomoya Matsuo, Mr. Kazuki Moroishi, Mr. Kazuki Yoshida, Ms. Nozomi Kasahara, Mr. Tamaki Kumauchi, Ms. Misa Miyamoto, Mr. Ryosuke Isobe, Mr. Yusuke Kajiura, Ms. Kaori Hayazaki, Mr. Kazuki Odake, Ms. Chika Nakadozono, Ms. Sukulya Bunuasunthon, Ms. Panitporn Laowpanitchakorn, Ms. Li He, Mr. Rentaro Sakamoto, Ms. Wu Chun-Yi, Ms. Riko Akehi, Mr. Ryoto Itani, Mr. Kanta Iwamoto, Ms. Aya Nagura, Ms. Itsuki Miyaguni, Ms. Hong Young Kyoung, Ms. Tomoka Iida, Mr. Kanta Ogura, Ms. Rino Kamada, Ms. Ryo Sekiya, Mr. Takuro Kawamoto, Mr. Tomoya Ushiroda, Mr. Kohei Uno, Ms. Sayaka Oshitani, Ms. Reina Funatomi, Mr. Kakeru Yasumoto and so on. Thanks to their accompany and kind support for both research and daily life.

I would like to thank the research support from Japan Society for the Promotion of Science (JSPS, DC1, 22J20533).

I would like to express my deep appreciate to my parents and friends who endured this long process with me, always offer support. And finally, thanks to my fiancée, Yuki Higashino who have been my greatest supporters throughout the completion of my thesis and helping me overcome every challenge.

January 2025

Daisuke Tomioka